Norwegian University of Life Sciences
Faculty of Environmental Science and Technology
Department of Mathematical Sciences and Technology (IMT)

Master Thesis 2015
30 credits

Experimental study of soiling on photovoltaic modules in a Nordic climate

Helene Berg Pedersen

Preface

The study performed throughout these last months was based on an initiative taken by the Institute for Energy Technology (IFE), to determine the effect of soiling on glass covering photovoltaic (PV) modules in a Nordic climate.

Some other studies on the area do exist. However, most have been conducted at locations where factors like geographic characterization, climate and weather conditions, soil composition and the optimal PV-module settings differ from what is seen in a Nordic climate.

Writing a master thesis has been a process with all its joys and frustrations. This master thesis is the result of hard work and countless hours spend in the laboratory. It is a true joy to see the results within these next pages. Still, it is bizarre to realize that I end my studies at NMBU with this thesis.

It is with gratitude that I finalize this study and thesis - it would not have been possible without the experience and knowledge from people in the academic environment. I want to thank everybody who have helped and supported me in this process.

First and foremost, I want to thank Josefine Helene Selj, my supervisor at IFE, for dedicated and enthusiastic guidance. Your knowledge in physics and experience with equipment has been essential. Further, I would like to thank Arne Auen Grimenes, my supervisor at NMBU, for optimism, time and valuable advices.

I want to thank Erik Stensrud Marstein at IFE, for enthusiasm regarding my research and results, and for guidance on the thesis structure. I am also grateful to Trygve Furuseth for help with the Scanning Electron Microscope, and to Ørnulf Nordseth for instructions and time regarding the Ocean Optics equipment.

Throughout my education, my parents have supported and encouraged me. Thank you so much for all your love and backing.

Finally, I want to thank my very good friend Reidun Marie Romundstad, for reading and commenting this master thesis.

Kjeller, May 13 2015.

Helene Berg Pedersen

Sammendrag

Formålet med denne masteroppgaven er å undersøke hvor mye støv og andre avsetninger akkumulerer på og påvirker optiske verdier på overflaten av glassplater som dekker fotovoltaiske (PV) solcellepaneler i et nordisk klima, representert ved Kjeller (Akershus). Elektrisk solenergi har sett stor økning og satsning i Europa de senere årene, og fra januar 2015 fikk også norske innbyggere økonomiske insentiver for privat utbygging av solceller. Det har blitt gjennomført en rekke forskningsprosjekter tilknyttet støv på solceller, men disse er hovedsakelig gjennomført i områder rundt Midtøsten eller ved andre geografiske områder preget av ulike karakteristikker og forhold enn dem vi ser i et nordisk klima.

Det første steget for å vurdere hvordan støv akkumulerer på glassflater brukt i solcellemoduler var å sette opp et test-anlegg på et tak tilknyttet Institutt For Energiteknikk (IFE) på Kjeller. Anlegget bestod av både normale glassplater og glass belagt med et anti-støvbelegg (TripleO), med en helningsvinkel på 45˚. Målinger ble foretatt hver uke, gjennom en periode fra 17. februar til 14. april, på glassprøver eksponert for naturlig støv.

Resultater viser at det samler seg omtrent 29 % mer støv på anti-støvglassene enn på normalglassene etter en uke med naturlig støvakkumulering, men at støvmengden på begge glassene er svært avhengig av nedbør. Regn bidrar til å vaske glasset, men selv kraftig nedbør var ikke nok til å vaske glassplatene helt rene for støv. Det er observert en støvtetthet på 37 mg/m^2 og 50 mg/m^2 etter en uke med mye regn for henholdsvis normale og anti-støvglassplater. For uker uten regn er det målt en støvtetthet på opptil 102 mg/m^2 og 125 mg/m^2 for henholdsvis normal og anti-støvglassene. Dette svarer til en økning på henholdsvis 176 % og 150 %.

Ukentlige optiske målinger viser at transmittansen gjennomsnittlig reduseres fra 91,5 % til 90,3 % for normalglasset, og fra 90,8 % til 89,9 % for anti-støvglasset. Transmittansen er mest påvirket ved korte bølgelengder. Den reduserte transmittansen for normalglassplatene svarer til en reduksjon i effektiviteten til en standard c-Si solcelle på 0,2-0,3%.

Det er en tilnærmet lineær sammenhengen mellom redusert transmisjon og akkumulert støvtetthet. Det forventes en reduksjon i transmittansen på 0,09 % og 0,11 % per 10 mg/m^2 for henholdsvis normal og anti-støvglassene.

Støvanalyser viser at oksygen, silisium og karbon dominerer. Dette er vanlige partiklene i naturlig støv. Bilder av glassflatene tyder på at støvpartiklene har en diameter i størrelsesorden $d < 10^1$. Det er da grunn til å anta at Mie- og Rayleigh spredning forekommer.

Abstract

The purpose of this study is to investigate how dust and soil accumulate and affect optical values of glass surfaces used in photovoltaic solar modules, in a Nordic climate. Investments in and utilization of electrical solar energy has increased substantially in Europe during the recent years. As from January 2015, Norwegian inhabitants can receive public subsidies for installing solar panels at home. A wide range of research has been conducted to investigate the effect of soiling on photovoltaic modules, but these are mainly focused around the Middle East or other geographical areas with environmental characteristics that differs from a Nordic climate.

The first step in evaluating how dust and soil accumulate on glass was to establish a test-setup at a rooftop of the Institute for Energy Technology (IFE) at Kjeller. The setup consists of both normal glass samples and glass samples coated with an anti-soiling coating (TripleO), with a tilt angle of 45˚. Measurements are conducted every week, from February 17 to April 14, on glass samples exposed to natural soiling.

Results show that approximately 29 % more soil accumulates on the anti-soiling coated glass samples than on the normal glass samples after one week of soiling, but both soil densities are strongly dependent on precipitation. Rainfall helps clean the glass samples, but no recorded level of precipitation was high enough to clean the glass samples completely. Soil densities after one week of 37 mg/m^2 and 50 mg/m^2, for the normal and anti-soiling coated glass samples respectively, were recorded after periods with much rain. Soil densities as high as 102 mg/m^2 and 125 mg/m^2 for the normal and anti-soiling coated glass respectively, were measured after weeks with no rain. This equals an increase of about 176 % and 150 %, for the normal and anti-soiling coated glass samples, respectively.

Mean weekly optical measurements show that the transmittance reduced from 91.5 % to 90.3 % for the normal glass samples, and from 90.8 % to 89.9 % for the anti-soiling coated glass. The transmittance seems to be most affected at shorter wavelengths. The reduced transmittance for the normal glass samples corresponds to a decrease in efficiency for a standard c-Si solar cell of about 0.2-0.3 %.

An approximately linear connection between the increase in soil density and the reduced transmittance is observed. This gives an expected reduced transmittance of 0.09 % and 0.11 % per 10 mg/m^2 for the normal and anti-soiling coated glass samples, respectively.

Soil analyses show that oxygen, silicon and carbon dominates, which are common dust elements. Pictures of the glass surfaces indicate that the diameters of the dust particles are in the order of $d < 10^1$ μm. This provides reason to believe that Mie and Rayleigh scattering occur.

List of symbols

Symbols	Exploration	Unity
A	Area	m^2
c	The speed of light in vacuum	m/s
e^-	Electron	-
E_g	Band gap energy, also called “the forbidden zone”	eV
E_{photon}	Photon energy	eV
f	Frequency	Hz
h^+	Hole	-
h	Planck’s constant	eV*s
I	Intensity of radiation	W/m^2
$I_{AM1.5G}$	Standard solar spectral irradiation on a plane at 37° tilt toward the equator, facing the sun	W/m^2
K	Absorption coefficient	m^{-1}
L	Length / thickness	m
n	Refractive index	-
$N_{photons}$	Number of photons per square meter and per second	$\#photons/m^2*s$
M	Mass	mg
M_c	Measured signal for the calibration measurement	-
M_s	Measures signal for the glazing sample	-
$\overline{\Delta M}$	Mean mass change	mg
ΔM_C	Change in mass due to cleaning	mg
ΔM_{OM}	Change in mass due to optical measurements	mg
ΔM_{total}	Total accumulated soil	mg
MD	Soil density	mg/m^2
MD_C	Soil density which is cleaned off	mg/m^2
MD_{OM}	Soil density which falls off due to optical measurements	mg/m^2
MD_{total}	Total accumulated soil density	mg/m^2
$\overline{MD}$	Mean soil density	mg/m^2
P_i	Incoming available power at the PV-module surface	W/m^2
P_{el}	Electrical generated power	W/m^2
r	Reflectance at a smooth interface	%
S_c	Measured calibration signal	-
S_s	Measured signal for the glazing sample	-
V	Fraction of incoming photons	-
α	Absorptance	%
α_s	Solar altitude angle	°

β	Panel tilt angle	°
γ	Panel orientation	°
γ_s	Solar azimuth angle	°
η	Efficiency	%
θ	Angle of incidence	°
θ_z	Zenith angle	°
λ	Wavelength	nm
μ	Cosin of the angle of incidence	-
ρ	Reflectance	%
τ	Transmittance	%
τ_r	Transmittance when only reflection losses are considered	%
τ_a	Transmittance when only absorption losses are considered	%
φ	Azimuth angle	°
ω	Latitude	°

Subscripts

a	Absorption
AS	Anti-soiling glass
i	Incoming
N	Normal glass
r	Reflected
t	Transmitted
λ	At a specified wavelength
θ	At a specified angle of incidence

Contents

1 Introduction

1.1 Background and motivation

The way humans live today makes it difficult to imagine a world without electrical energy. With a growing population and increasing consumption, our need for energy is expected to grow. Scientists all over the World agree: human activity is the cause of the climate changes, and the emission of climate gases is the mainspring [1]. In 2012, 67 % of the electrical energy produced in the World was generated from fossil fuels [2]. This includes coal, gas and oil, which releases climate gases into the atmosphere.

This gives rise for the need to control human emission. One promising solution is to replace electricity generated from fossil fuels with renewable energy, a topic given great attention over the last years. A branch of the renewable energy sector is the photovoltaic (PV) solar energy. This technology utilizes solar radiation and converts it to electrical energy. During the past years, a number of governments (especially in leading European countries) implemented economic incentives for installation of photovoltaic panels. Production increased and prices fell, leading to an exponential growth of installed PV-panels worldwide [3]. Figure 1 illustrates the cumulative development in PV capacity since 1992.

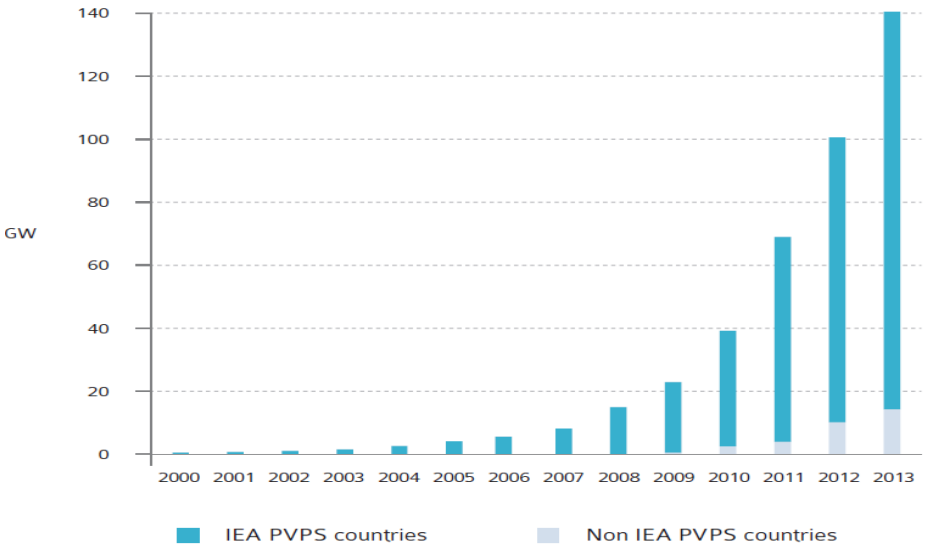

Figure 1: Evolution of cumulative photovoltaic (PV) installations (GW) [4].

Germany is currently the country with the highest level of installed PV capacity in terms of total capacity. The German insolation potential is approximately the same as in the south of Norway, about 1100 kWh/m^2 per year [5]. Solar electrical energy has not yet been able to compete with electrical energy prices in Norway, however this might be about to change. As from January 2015, Norwegian inhabitants can receive public subsidies for installing solar panels at home, through the governmental agency ENOVA [6].

Incoming solar radiation is the most essential factor for energy production utilizing photovoltaic panels. Accumulation of sediments, dust, bird droppings, snow and other impurities on the surface of the panels reduces transmission of solar radiation, thereby causing a lower power output for the panels. Transmission, reflection and absorption depend on factors like the surface characteristics, incoming wavelength and the angle of incidence from the incoming solar beam, which changes as the sun crosses the sky during the day. The presence of soil on PV-panels affects the optical values. Extensive research has been conducted to quantify the reduced efficiency due to soiling, but the results vary greatly with location. This is because soiling depends on many factors, including: climate, human activity, environmental differences, soil composition and so on. The change in transmission and reflection as a function of accumulated soil density has not been given much attention yet. However, a better understanding of this relation, and more information about the expected soil deposition, can help predict production losses due to soiling and give a basis for evaluating the need for physical cleaning of the PV-modules.

Local variations make soiling on photovoltaic panels a challenging, but very important field of research. With more information with respect to soiling in a northern climate, it is possible to give a more accurate and reasonable estimate for the production losses and efficiency reductions due to soiling.

1.2 Research definition

This study aims to investigate the accumulation of soil on photovoltaic panels in a Nordic climate, represented by Kjeller. It seeks to answer the following questions:

- How much soil accumulates on tilted glass covers?
- How does soil deposition affect the transmittance? Is this change in transmittance affected differently at different wavelengths?
- What is the effect of anti-soiling coating?
- What important elements occur in the soil at Kjeller?

The study aims to give an expected accumulation of soil and a change in transmittance due to one week of soiling. It seeks to suggest a pattern between the accumulated soil density and the reduced transmittance. The connection between reduced transmittance and wavelength is studied in more details. Weather data is investigate to see if there is an effect from precipitation. The laboratory equipment used throughout the different experiments are owned and frequently in use at Institute for Energy Technology (IFE).

1.4 Thesis structure

Chapter 1 addresses the background and motivation for this study, and defines the research goals.

Chapter 2 presents relevant theory within this field of research. This includes basic background information about the incoming solar radiation and the operation of photovoltaic modules, as well as important calculations for the interaction between beam radiation and glazing materials. It establishes a basic understanding of soiling associated with PV-modules and how this varies with different factors. This chapter presents results from previous studies conducted in this area of research.

Chapter 3 presents the different measurement equipment used during the research. This includes the Angular Dependent Reflection and Transmission Measurement (ADRTM), the ellipsometer, the Mettler Toledo Excellence Plus weight, the Scanning Electron Microscope (SEM) and finally the Ocean Optics setup.

Chapter 4 provides the methodology applied during the research. First, it describes the setup for the glass samples at the rooftop. Then is presents the methods used to investigate the accumulation of soil and how this soil affects optical values. Then, the method for soil analyses is presents, before the chapter gives the methodology applied to investigate artificial dust on glass samples.

Chapter 5 presents and discusses the results obtained from the methodology described in chapter 4. This includes theoretical calculations for BK7-glass, initial optical measurements on clean glass samples, weekly mass and optical measurements, the soil analyses and results from the experiment with artificial dust.

Chapter 6 summarizes the most important conclusions and provides some suggestions for further work.

2 Theoretical prerequisites

This chapter addresses the theoretical background required for understanding the work presented in this study. It provides information about solar radiation, a basic introduction to photovoltaic solar cells, how radiation interacts with glazing samples and results from previous studies regarding soiling on photovoltaic modules.

The theory in the following chapter is based on *Solar Engineering of Thermal Processes* [7] and *Physics of Solar Energy* [8], with other sources presented.

2.1 Solar radiation

2.1.1 Resource base

The sun is a sphere of intensely hot gases that constantly emits energy as electromagnetic waves at a very high rate. This energy is spread as a sphere with an increasing diameter as the distance from the sun increases. Therefore, only a small portion of this energy reaches Earth. The solar constant, S_0, is the mean solar radiation flux density outside the atmosphere, and is approximately:

$$S_0 = 1367 \text{ W/m}^2$$

The earth orbits the sun in an elliptical path. This means that the distance between the earth and the sun varies over the year, with roughly 1.7 %, resulting in variations in solar radiation outside the atmosphere, at about ± 3.3 %.

Because of atmospheric effects, the amount of incoming energy is further reduced before reaching Earth's surface. The incoming radiation at a given location varies with factors like: latitude, time of the day and year, cloud cover, aerosols and so on.

The incoming solar radiation that reaches Earth's surface is usually expressed as power density of the radiation (W/m^2), called irradiance. It is estimated to about 1000 W/m^2 in clear conditions when the sun is near the zenith (directly overhead) [9].

2.1.2 Relevant angles for tilted panels

The irradiation of photovoltaic modules on Earth's surface depends upon several factors, including the geographic position, and the orientation of the module. Photovoltaic modules are tilted and oriented to receive maximum beam radiation per area and optimize the power production. Figure 2 and 3 show relevant angles for both geographical location and module setup, respectively. The angles are defined on the following page.

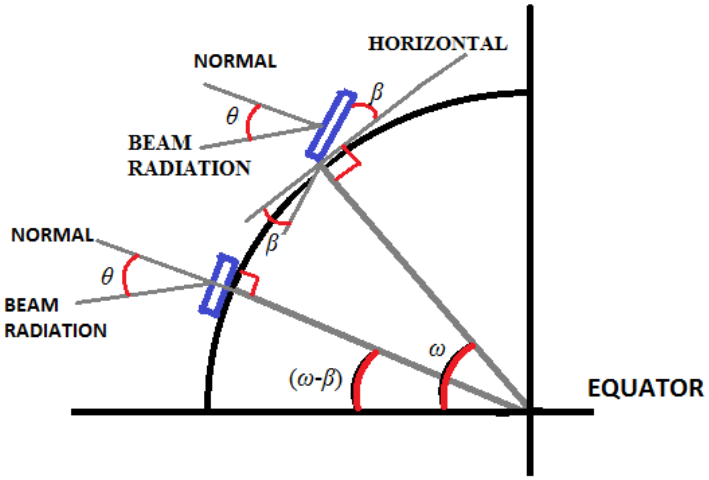

Figure 2: Relevant angles for irradiation of PV-modules on Earth's surface. ω is the latitude, θ is the angle of incidence and β is the tilt angle of the panel. From: [7].

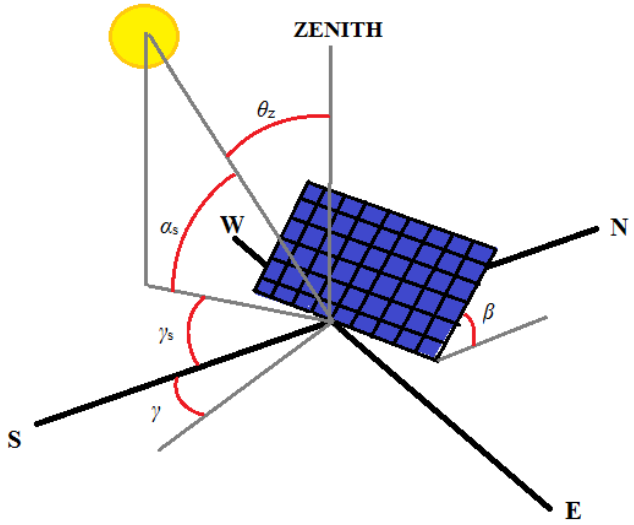

Figure 3: Relevant angles for irradiation on a PV-module setup. γ is the panel orientation, γ_s is the solar azimuth angle, α_s is the solar altitude angle and θ_z is the zenith angle. From: [10].

Important angles that relate a panel to the earth and beam radiation are given below and shown in figure 2 and 3. The horizontal plane is oriented orthogonal to the zenith-line for the given location.

- ω **Latitude:** the angle north or south of equator, with north defined as positive ($-90^\circ \leq \omega \leq 90^\circ$).
- β **Tilted angle:** the angle between the back of the panel and the horizontal ($0^\circ \leq \beta \leq 180^\circ$), with 180° meaning that the panel faces down.
- γ **Panel orientation:** the angle between the line that point straight out of the PV-panel and south. It is measured in the horizontal plan. By definition, east is negative and west is positive ($-180^\circ \leq \gamma \leq 180^\circ$). (Also referred to as: panel azimuth angle).
- θ **Angle of incidence:** the angle between the solar position and the normal to the panel. (Also referred to as: polar angle).
- ϕ **Azimuth angle:** the angle between the normal line and the angle of the projection of the beam on the horizontal.

Angles that describe the position of the sun in the sky are:

- θ_z **Zenith angle:** the angle between the vertical and the line to the sun.
- α_s **Solar altitude angle:** the angle between the horizontal and the line to the sun.
- γ_s **Solar azimuth angle:** the angle between the horizontal south and the solar position. It is measured in the horizontal plane ($180^\circ \leq \gamma_s \leq 180^\circ$).

2.1.3 Factors of variations

2.1.3.1 Atmospheric effects

The solar radiation attenuates as it penetrates the atmosphere due to reflection, scattering and absorption.

Reflection occurs when radiation interacts with atmospheric particles and is redirected. This means that all the radiation is potentially lost. Reflection in the atmosphere is mainly caused by clouds, and will therefore vary with location and time.

Scattering is caused by interaction with air molecules, water vapor and droplets and dust in the atmosphere. It depends on the number of particles the radiation must pass, the size of the particles and the wavelength of the radiation. When sunlight scatters at particles with diameters less than approximately 10 % of the wavelength, it is called Rayleigh scattering. This scatters the radiation forwards and backwards. Mie scattering occurs if the particles are larger than the wavelength, and produces a pattern with a sharper and more intense forward lobe for larger particles. Both scatter patterns affect and scatter more in the shorter wavelength spectrum.

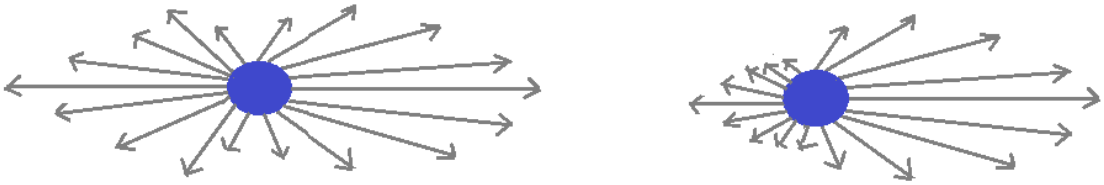

Figure 4: Mie (left) and Rayleigh (right) scattering. From: [11].

Atmospheric absorption is largely due to ozone, water vapor and carbon dioxide. They absorb different wavelengths, displayed in figure 5 as the characteristic notches in the solar radiation at sea level. The areas of the radiation spectrum that are absorbed are known as the absorption bands.

The largest portion (about 50 %) of the incoming radiation penetrates the atmosphere and is absorbed by Earth. Approximately 30 % of solar radiation is reflected or scattered from the atmosphere back to space immediately, 20 % is absorbed by the atmosphere and clouds [8].

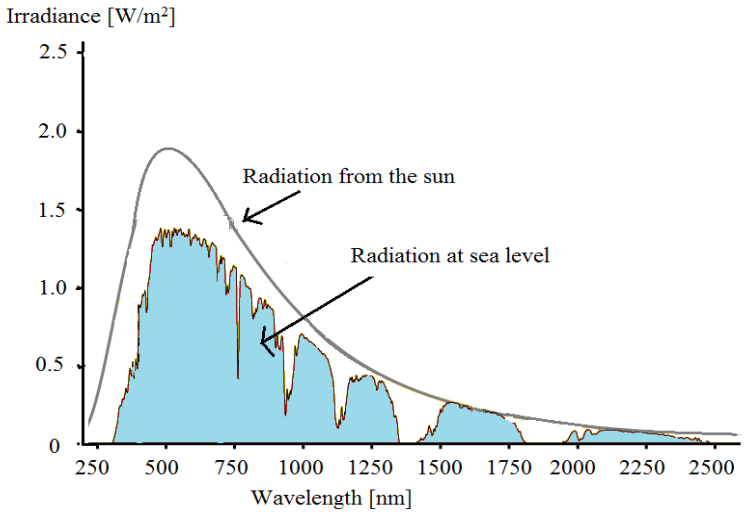

Figure 5: The solar radiation spectrum. From [12].

Beam radiation is the amount of radiation that passes straight through the atmosphere, while diffuse radiation is the scattered solar radiation that reaches Earth. Global solar radiation (GR) is the sum of direct and diffuse radiation at a horizontal surface, while total radiation is the sum at any arbitrary surface.

2.1.3.2 Insolation variations at different locations

The maximum amount of incoming solar radiation during a year decreases with increasing latitude. This is because the angle between the horizontal and the sun's position (called solar altitude angle) is lower. and because the incoming radiation is spread over a larger surface area. The last is illustrated in figure 6 below.

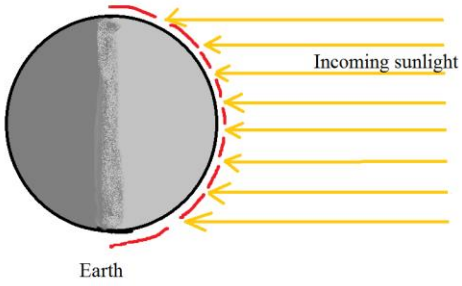

Figure 6: Incoming solar radiation is spread over a larger surface area at higher latitudes. From: [13].

At higher latitudes, seasons are characterized by many hours of sun during summer time and a short number of solar hours during winter. This results in more insolation per day during summer.

The intensity of incoming radiation also varies during the day. With lower solar heights, the radiation is spread over a larger area, reducing the intensity. In addition, the path length of the radiation in the atmosphere increases, meaning that it penetrates more atmosphere and can experience more scattering and absorption. Air mass (AM) defines the actual path length light travels through the atmosphere to the shortest possible length.

The amount and composition of solar radiation reaching Earth's surface differ with location due to variations in the atmospheric composition. Human and natural activities, like pollution, farming, sea salt, volcanoes or dust, affect the concentration and composition of aerosols. Aerosols can scatter or absorb incoming radiation, or they can act as condensation cores and lead to cloud formation. Water at different states has a high impact on the transmission of radiation through the atmosphere. Examples like clouds, fog and water droplets can reflect, scatter or absorb solar radiation. This varies with location, but can also change during the day or with season.

2.1.4 Polarization

Solar radiation is electromagnetic (EM) radiation, meaning that is consists of both electrical and magnetical fields perpendicular to one another. It is a transverse wave, and its properties do not change as is propagates vacuum.

Polarization denotes the direction of the electrical field vector as the EM-wave penetrates space. It is easy to determine the direction of the magnetic field, since it is perpendicular to the electric field. There are two different polarization states. They are either perpendicular to, or parallel to, the plan spanned by the incident beam and the surface normal. These are denoted as s- and p-polarization, respectively (originally from Germany, with s: senkrecht = vertically and p: parallel).

Unpolarized EM-waves consists of both polarization directions. The different polarization components can be extracted by sending unpolarized radiation through polarization filters. Different filters let different components through, while blocking others. For instance: a vertical filter lets the vertical components (s-fields) through, while blocking all others. The same applies to horizontal filters. The use of polarization filters is illustrated in figure 7.

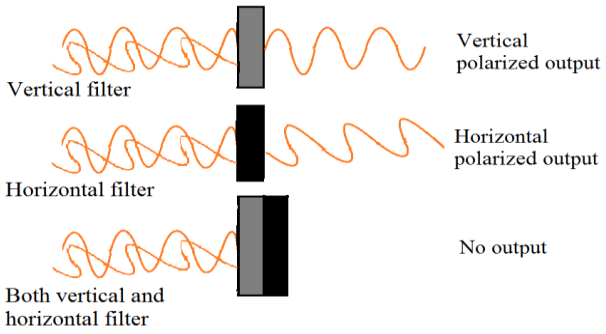

Figure 7: Polarization filters let different components of the radiation through, while blocking others. From: [14].

Solar radiation is unpolarized, meaning that it contains both polarization components. It consists of a random mixture of waves having different spatial characteristics, wavelengths, phases, and polarization states.

2.2 Photovoltaic solar cell technology

Photovoltaic (PV) solar cells convert energy from incoming solar radiation into electrical energy, using the photovoltaic effect. This subchapter first addresses the basics of solar cells and the absorption of solar energy. Then, a simple explanation of the electricity generation is given, before the structure of a solar module is presented.

2.2.1 Solar cells

The solar cell industry is currently dominated (over 80 %) by wafer based crystalline silicon (c-Si) [15]. Silicon (Si) is a semiconductor, meaning that it conducts electricity poorly at room temperature, but with a potential for increasing conductivity. It is characterized by a filled valence band and an empty conduction band at 0 K, but with a narrow band gap (E_g), also called "the forbidden zone". When electrons are given sufficient amount of energy (more than E_g), they can excite from the valence band to the conduction band. This results in two different energy carriers: an electron (e^-) and a hole (h^+). They participate in conduction. This can occur at higher temperatures (more energy) or by absorption of photons with energy greater than the band gap. The last case is further explained in chapter 2.2.2.

The valence band, conduction band and band gap (E_g) for a semiconductor is illustrated in figure 8 below. It also shows the excited electron and the hole. The band gap for silicon is: 1.12 eV.

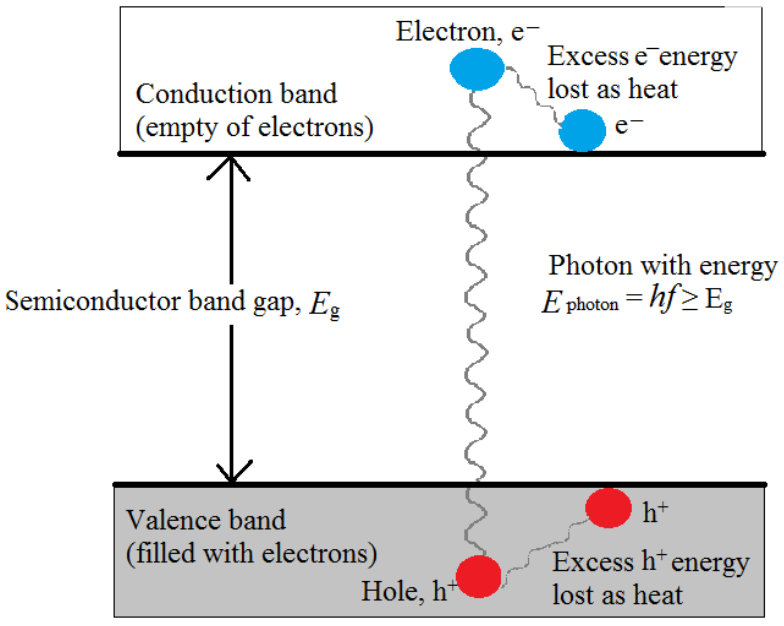

Figure 8: Generation of an electron-hole (e^- and h^+) pair, by a photon with energy greater than the band gap (E_g) of the semiconductor. From: [8].

2.2.2. Absorption

The photon energy (E_{photon}) is determined by the wavelength of the radiation. When solar energy irradiates a PV-module, photons can be reflected from the surface or transmitted. If the energy of the transmitted photon is equal to or greater than the band gap (E_{g}) of the semiconductor, the photon can be absorbed and excite an electron from the valence to the conduction band, thereby forming an electron-hole pair. This is expressed as:

$$E_{\text{photon}} = hf = \frac{hc}{\lambda} \geq E_{\text{g}} \tag{1}$$

Where *h* is the Planck constant, *c* is the speed of light in vacuum, *f* is the frequency of the incoming light and λ is the associated wavelength.

Photons with energy greater than the band gap will not be able to create more than one electron-hole pair. The extra amount of energy is transferred to the electron, as kinetic energy. This energy is wasted, as the electron quickly thermalizes back down to the conduction band edges.

2.2.3 Generation of electrical energy

When semiconductors are used in photovoltaic cells, they are combined with atoms consisting of either one extra (n-doped) or one less (p-doped) electron in the valence band. This is called doping. Phosphorus (n-doping) and boron (p-doping) are commonly used with silicon. Doping increases the conductivity of the semiconductor, and gives rise to an inner electrical field when a p- and n-doped material is brought together, forming a p-n junction. This electrical field is also called “built-in electrical field”. It points from the n- towards the p-doped material, shown as *E* in figure 9.

As a photon with sufficient energy is absorbed in the semiconducting material of the solar cell, it creates an electron-hole pair. However, electrons are minority carriers in the p-doped material, as holes are in the n-doped material, and can recombine. This results in losses of electrical energy. Nevertheless, because of the built-in electrical field, the electrons can drift into the n-doped material and the holes into the p-doped material, if the light-generated minority carrier reaches the p-n junction.

By connecting the two terminals of the solar cell together, electron from the n-doped material can pass through the external load, creating electricity, before recombining in the p-doped material. This is illustrated in figure 9.

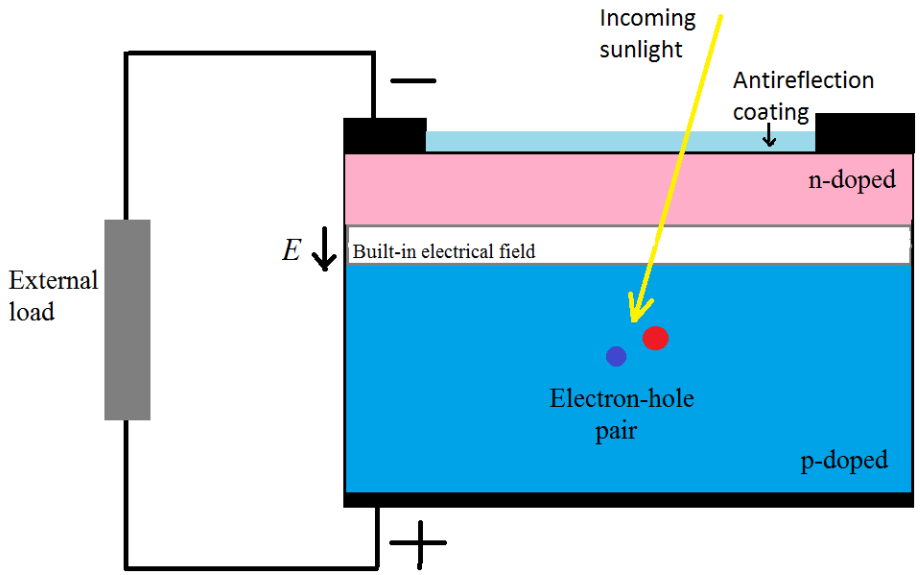

Figure 9: A basic solar cell with n- and p-doped material. It shows how sunlight can create an electron-hole pair. The letter *E* refers to the built-in electrical field. From: [16].

The External Quantum Efficiency (EQE_λ) indicates the amount of current that the PV-cell will produce when irradiated by photons of a particular wavelength. It includes losses that may occur, and has to be calculated for each PV-panel [17]. If all photons of a certain wavelength are absorbed and the resulting minority carriers are collected, then the EQE at that particular wavelength is unity. The quantum efficiency for photons with energy below the band gap is zero.

$$\mathrm{EQE}_\lambda = \frac{\text{electrons/second}}{\text{photons/second}} \tag{2}$$

The electrical current produced by a PV-cell when exposed to sunlight is calculated by integrating the cell's quantum efficiency over the complete solar electromagnetic spectrum.

The efficiency of a PV-solar cell (η) is determined by the amount of electrical power generated, to the incoming solar power available at the surface:

$$\eta = \frac{P_{\mathrm{el}}}{P_{\mathrm{i}}} \tag{3}$$

Where P_{el} is the electrical generated power and P_{i} is the incoming available power at the surface.

Because of the great variations in incoming radiation at Earth's surface, discussed in chapter 2.1.3, a set of standard conditions are established for uniform comparisons of photovoltaic modules. The standard test conditions (STC) are:

- An ambient temperature of 25˚C
- Irradiance of 1000 W/m^2
- An air mass equal to AM1.5

The air mass is a representation of the path length of the sunlight through Earth's atmosphere, relative to the path length at zenith (when the sun is directly overhead).

A standard c-Si solar cell has efficiency around 15-20 % [18].

2.2.4 Solar cell and module design

A fraction of the incoming radiation fails to generate electron-hole pairs, even though the energy is sufficient, because it is reflected. This is called optical losses. Bare silicon has a surface reflection of about 30 %. To reduce the surface reflection, the wafers are coated with an anti-refection coating. The efficiency of the anti-reflection coating depends on the thickness of the coating, and of the refractive index (explained in chapter 2.3.1). These parameters differ with wavelength and are therefore chosen to minimize the reflection for wavelengths at 0.6 µm, which corresponds to the peak power of the solar radiation (as seen in figure 5). The percentage of incoming radiation that is reflected at different wavelengths, for bare silicon, silicon under a glass cover (as in a PV-module) and under an optimal anti-reflection cover is illustrated in figure 10.

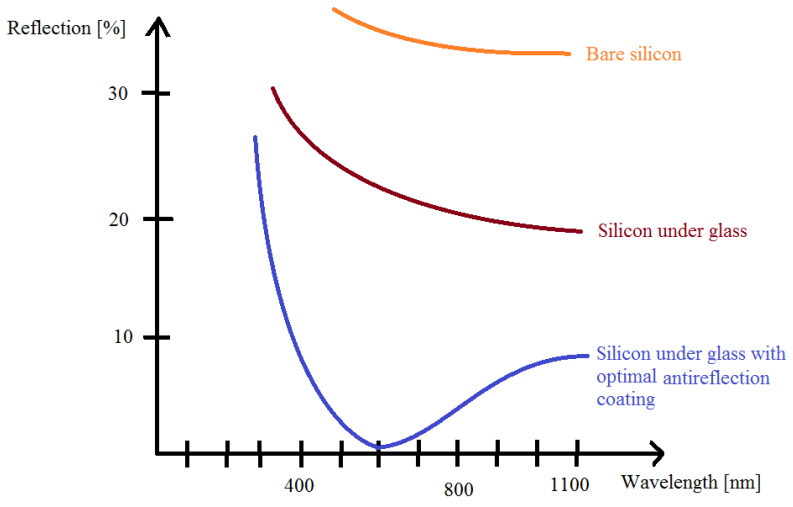

Figure 10: Different reflections for silicon under different conditions. From: [19].

Because silicon solar cells are fragile, they are framed to achieve better mechanical strength and to protect them from external effects. A typical solar module consists of a glass cover at the top, which transmits most solar radiation, two sheets of ethylene vinyl acetate (EVA) film for encapsulation, solar cells and a back plate, all framed by a metal structure. This is shown in figure 11 below.

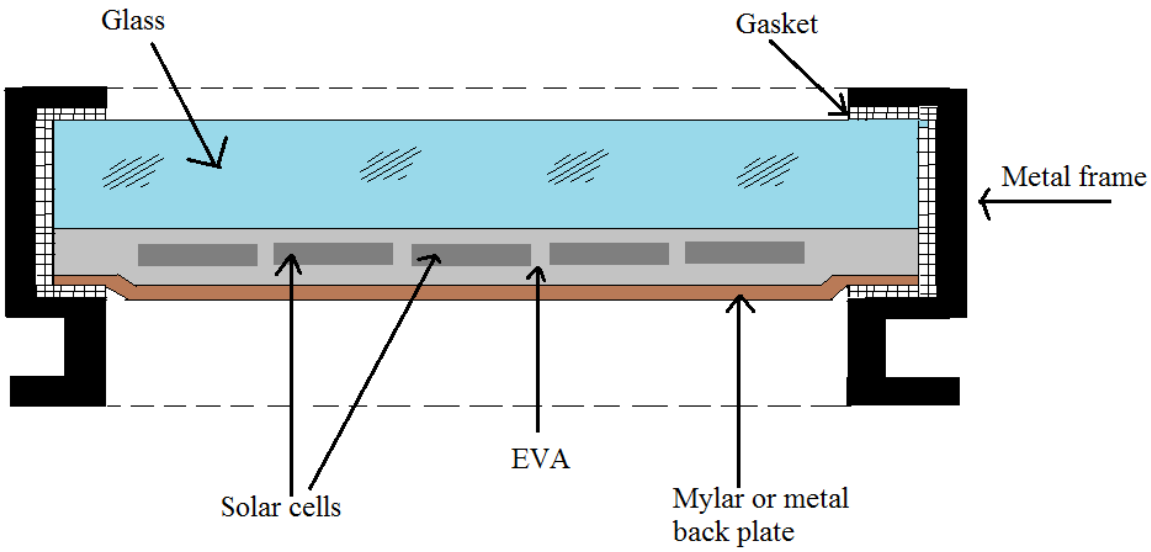

Figure 11: Cross section of typical solar module. Note that thicknesses and sizes may vary. From: [8].

2.3 Optical properties of materials

Photovoltaic solar modules should maximize the absorption of solar radiation in the photovoltaic cells. This implies a maximum amount of transmitted light through the glass covering the cell. Some of the main properties of the glass material are therefore: the absorptance (α), reflectance (ρ) and transmittance (τ), of shortwave radiation (higher photon energy). In addition to being properties of the surface material, the absorptance, reflectance and transmittance also depend on the wavelength (λ) and the direction of the incoming radiation as well as surface conditions like: temperature, roughness, cleanliness etc.

This chapter first gives relevant definitions used throughout this thesis. It then addresses radiation at an interface, which is needed to understand radiation of glazing materials. The chapter explains the methodology used to calculate transmittance, reflectance and absorptance of materials, at different surfaces and incoming radiation characteristics.

2.3.1 Definitions

Some important definitions are:

μ	**The cosin of the angle of incidence:** cos(θ), with θ being the angle between the solar position and the normal to the panel, as explained in chapter 2.1.2.
φ	**The azimuth angle:** the angle between the line that point straight out of the panel and the angle of the projection of the beam on the horizontal, as explained in chapter 2.1.2.
τ	**Transmittance:** the fraction of transmitted to incoming radiation intensity (I_t/I_i). It depends on wavelength and on the direction of incoming radiation $\tau_\lambda(\mu, \varphi)$.
ρ	**Reflectance:** the fraction of reflected to incoming radiation intensity ($I_{r\lambda}/I_{i\lambda}$). It depends on the wavelength and on the direction of incoming radiation $\rho_\lambda(\mu, \varphi)$.
α	**Absorptance:** the fraction of absorbed to incoming radiation intensity ($I_{a\lambda}/I_{i\lambda}$). It depends on the wavelength and on the direction of incoming radiation, $\alpha_\lambda(\mu, \varphi)$.
n	**Refractive index:** is characteristic for a medium. It is defined as the speed of radiation in a vacuum compared to the speed in the medium (c/v).
K	**Absorption coefficient:** is characteristic for a medium. Is describes how far into material light of a particular wavelength can penetrate before it is absorbed.

2.3.2 Radiation at an interface

Radiation of opaque materials is either reflected from the surface or absorbed in the material. The different portions depend on the angle of the incoming radiation and its wavelength.

2.3.2.1 Absorptance

The monochromatic directional absorptance is a property of the surface. It is defined as the fraction of incoming radiation intensity at a given wavelength (λ) from a defined direction (μ, ϕ) that is absorbed:

$$\alpha_\lambda(\mu, \varphi) = \frac{I_{\lambda,a}(\mu, \varphi)}{I_{\lambda,i}(\mu, \varphi)} \qquad (4)$$

I indicates the intensity of the incoming (i) and absorbed (a) radiation. Absorptance at a defined wavelength is calculated by integrating over the respective angles of incidence, while absorptance at a defined angle of incidence is calculated by integrating over the respective wavelengths.

2.3.2.2 Reflectance and reflection

Reflectance in defined as the amount of reflected radiation to the amount of incoming radiation intensity. Further specifications are based on direction and/ or the wavelength of the radiation.

The reflected radiation from a surface consists of two different distribution components: specular and diffuse reflection. In most practical cases, the reflected radiation consists of both forms of reflection, and is called global reflection.

The specular reflection reflects the incoming radiation like a mirror, meaning that the incoming and reflected angles (θ) are equal, and the azimuthal angles (ϕ) differ by 180˚, referring to figure 12. This is the main component of the global reflection for smooth surfaces. The diffuse reflection on the other hand, is distributed uniformly in all directions. The general case will include both specular and diffuse reflection, as illustrated in figure 12.

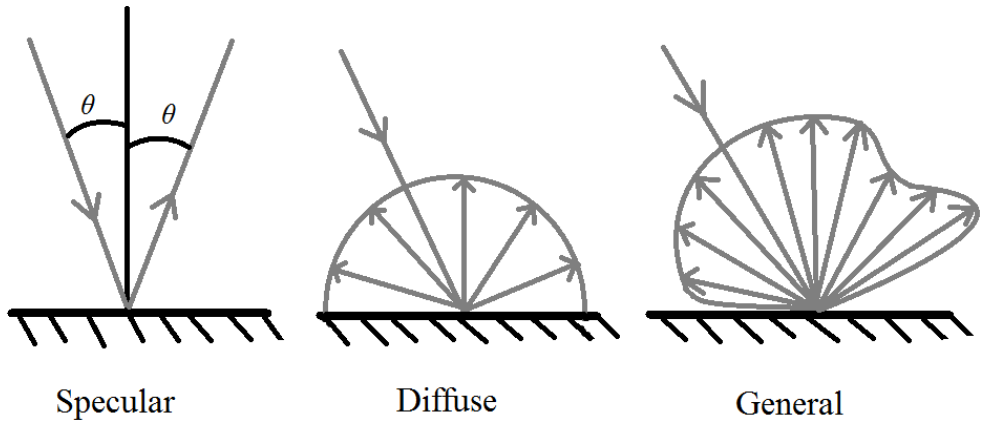

Figure 12: Reflection from surfaces. From: [7].

The magnitude of the reflected intensity for a given surface in a specified direction is a function of the wavelength and the spatial distribution of the incident radiation. This is called the biangular reflectance, and is expressed as:

$$\rho_\lambda(\mu_\mathrm{r}, \varphi_\mathrm{r}, \mu_\mathrm{i}, \varphi_\mathrm{i}) = \lim_{\Delta\omega_\mathrm{i}\to 0} \frac{\pi I_{\lambda,\mathrm{r}}(\mu_\mathrm{r}, \varphi_\mathrm{r})}{I_{\lambda,\mathrm{i}}\mu_\mathrm{i}\Delta\omega_\mathrm{i}} \tag{5}$$

The subscripts r and i refer to reflected and incident respectively, μ and ϕ are direction angles and ω_i is the arc length measured in radians of the incoming radiation. This relationship is illustrated in figure 13.

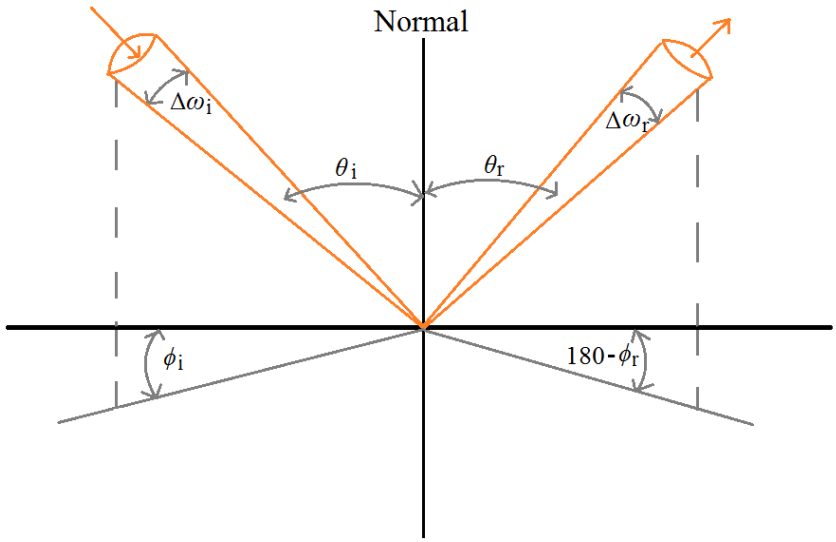

Figure 13: Coordinate system for the reflection. From [7].

By integrating over all wavelengths or/and all angles of incoming and/or reflected angled, different relations between the reflected and incoming radiation intensity is obtained.

2.3.3 Radiation through glazing materials

As explained in chapter 2.2.4, glass covers the photovoltaic modules. When evaluating the performance of a photovoltaic panel, three properties of the glass cover are highly important: the reflectance, transmittance and absorptance. The reflectance, transmittance and absorptance are functions of the incoming radiation, as well as thickness, refractive index (n) and absorption coefficient (K) of the material. The refractive index and the absorption coefficient of a material depend on the wavelength of the incoming radiation.

2.3.3.1 Reflectance and reflection

The reflection of radiation at an interface of two mediums is the amount of radiation that is reflected. The reflectance is the proportion of reflected radiation to the incoming radiation (I_r/I_i).

Fresnel's equations apply to smooth surfaces, and describe the specular reflection of unpolarized radiation as it interacts between mediums of different refractive indexes. Recall that solar radiation is initially unpolarized. It becomes partially polarized when interacting with a medium at an angle different from zero. This is because the radiation reflected at an interface is different for each component of polarization. Polarization is taken into account by defining the plan

spanned by the incident beam and the surface normal, and the two components parallel (r_p) and perpendicular (r_s) to the plan. These are called p- and s-polarization respectively, and r is the reflectance at a smooth surface (specular reflectance).

Fresnel's equations are expressed as:

$$r_\mathrm{s} = \frac{\sin^2(\theta_2 - \theta_1)}{\sin^2(\theta_2 + \theta_1)} \tag{6}$$

$$r_\mathrm{p} = \frac{\tan^2(\theta_2 - \theta_1)}{\tan^2(\theta_2 + \theta_1)} \tag{7}$$

$$r = \frac{I_\mathrm{r}}{I_\mathrm{i}} = \frac{1}{2}(r_\mathrm{s} + r_\mathrm{p}) \tag{8}$$

Here the angles θ_1 and θ_2 are the angles of incidence and refraction, as illustrated in figure 14. r_s and r_p give the perpendicular and parallel component of unpolarized radiation respectively, and *r* gives the specular reflectance of unpolarized radiation as it interacts with a smooth surface. *I* is the radiation intensity, while the subscripts i and r refer to incident and reflected, respectively.

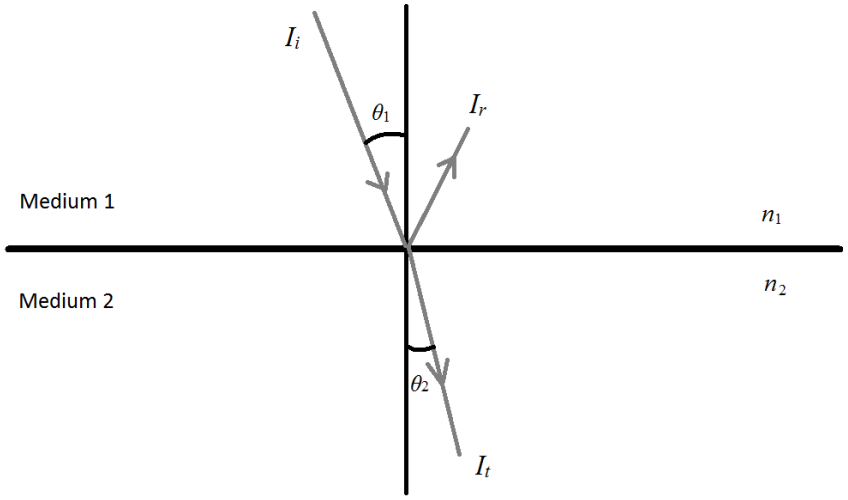

Figure 14: Radiation at the interface between two mediums of different refractive indexes. *I* refers to radiation intensity, while the subscripts i, r and t refer to incident, reflected and transmitted, respectively. From: [7].

The connections between the incoming and refractive angles depend on the refractive indexes (n_1 and n_2) of the two mediums. This is illustrated in figure 14, and described by Snell's law:

$$\frac{n_1}{n_2} = \frac{\sin\theta_2}{\sin\theta_1} \tag{9}$$

Both incoming (θ_1) and reflected (θ_2) angles are zero at normal incidence, and both reflection polarization components are equal. Then, the specular reflection, given by equation (8), reduces to:

$$r(0) = \frac{I_\mathrm{r}}{I_\mathrm{i}} = \left(\frac{n_1 - n_2}{n_1 + n_2}\right)^2 \tag{10}$$

Here $r(0)$ refers to the specular reflectance at zero degrees of incidence, while n_1 and n_2 are the refractive indexes for the two different mediums. I is the intensity of the incoming (i) and reflected (r) radiation.

2.3.3.2 Transmittance and transmission

The transmission through a medium is the radiation that passes through without being reflected at the interface or absorbed in the media. The transmittance is the proportion of transmitted radiation to the incoming radiation intensity ($I_\mathrm{t}/I_\mathrm{i}$). To calculate the total transmittance, it is necessary to know the transmittance when only reflection losses and when only absorption losses are considered.

When only reflection losses are considered (neglecting absorption) the transmittance (τ_r) of initially unpolarized radiation is the fraction of incoming radiation remaining after refraction is considered. Solar cells are covered with a glass cover. This cover consists of two interfaces per surface which can cause reflection losses. This is illustrated in figure 15.

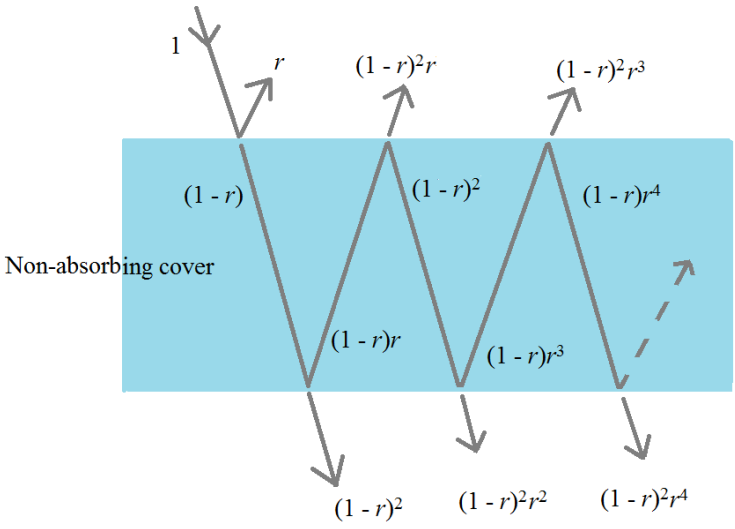

Figure 15: A non-absorbing cover with two interfaces for reflection losses. From: [7].

When polarization is taken into account, the transmittance (when only reflection losses are considered) through a single cover is:

$$\tau_{rs} = (1 - r_s)^2 \sum_{n=0}^{\infty} r_s^{2n} = \frac{1 - r_s}{1 + r_s} \tag{11}$$

$$\tau_{rp} = (1 - r_p)^2 \sum_{n=0}^{\infty} r_p^{2n} = \frac{1 - r_p}{1 + r_p} \tag{12}$$

$$\tau_r = \frac{1}{2}\left(\frac{1 - r_p}{1 + r_p} + \frac{1 - r_s}{1 + r_s}\right) \tag{13}$$

The subscript *r* means that only reflection losses are considered, p refers to the parallel and s to the perpendicular component of the unpolarized radiation. These values vary with the incidence and reflected angle, as described by equations 6 to 8.

Figure 16 shows the transmitted radiation, when only absorption losses are considered (τ_a).

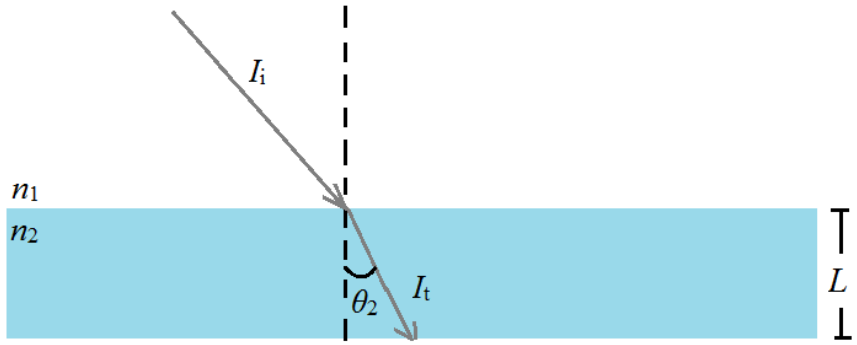

Figure 16: Some radiation is absorbed as radiation penetrate a partially transparent material. This figure does not show the reflected radiation, to illustrate how Bouguer's law describe the transmittance when only absorption losses are considered. L is the thickness of the glazing sample and θ_2 is the angle of refraction. From [7].

As radiation penetrates a partially transparent material, some portion will be absorbed. Looking at the total distance the radiation has traveled in the medium (from zero to $L/\cos\theta_2$, with L referring to the thickness of the material), Bouguer's law describes the transmittance of radiation when only absorption losses are considered (τ_a) as:

$$\tau_a = \frac{I_{\text{transmitted}}}{I_{\text{incident}}} = e^{-\frac{KL}{\cos\theta_2}} \tag{14}$$

The index a means that only absorption losses are considered. The value of the absorption coefficient (K) varies with wavelength. The angle θ_2 is the angle of refraction to the normal of the surface (given by Snell's low), and L is the thickness of the medium.

Because the absorption coefficient (K) for glass is in the order of 10^{-1} m^{-1} (see Appendix A) the transmittance when only absorption losses are considered (τ_a) is rarely less than 0.9.

2.3.3.3 Optical properties of a single cover

The transmittance (τ), reflectance (ρ) and absorptance (α) of a single cover is the average of the two polarization components. When both reflection and absorption losses of the incoming radiation are taken into account, combined with the simplification noted for glass covers above ($\tau_a \geq 0{,}9$), the transmittance, absorptance and reflectance are approximately:

$$\tau \cong \tau_a \tau_r \tag{15}$$

$$\alpha \cong 1 - \tau_a \tag{16}$$

$$\rho \cong \tau_a - \tau \tag{17}$$

This is a simplified calculation for glass covering PV-cells. Here τ_a is the transmittance when only absorption losses are accounted for, while τ_r is the transmittance when only looking at reflection losses and τ is the total transmittance of the material. α is the absorptance and ρ is the reflectance.

2.4 Soiling on photovoltaic panels

Air pollution particles, pollen, dust, bird droppings, snow and other impurities are some natural and anthropogenic sources of soil that can deposit on photovoltaic (PV) panels. Soiling on PV-panels generally involves everything that covers the surface, and naturally interferes with illumination quality, by both attenuating and scattering incident light [20]. The amount of soil on PV-panels is usually measured as either:

- Soil quantity: the amount of soil accumulated on the panel, during a defined time interval.
- Soil level: the decrease in power production due to soiling, during a defined time interval.

The accumulation and effect of soil on PV-panels depends on various factors associated with the surrounding environment and the module setup. Examples are geographic and climate variations, PV-panel setups as well as soil density and particle size distribution. The next subchapters present results from previous studies on this field of research.

Figure 17: Soiling on PV-panels. Reprinted with permission © [21].

2.4.1 Effect from soiling

One of main issues with soiling on photovoltaic modules is the attenuation of the incident solar spectrum. When dust particles are illuminated, they absorb, scatter and reflect the light, which reduce the intensity of the incoming radiation, and hence the power output. These effects vary with soil density, composition, particle shape, as well as size distribution [20]. Thicker layers of snow, bird droppings and leafs are examples of soiling that causes hard shading conditions, while soft shading conditions are caused by factors like sand, dust, pollen or thin layers of snow [22].

Experiments have showed that smaller particles have a far greater effect on reducing the transmission than larger particles [23]. This is due to the very small diameter of the particles which results in a denser cover. Other studies show that smaller particles will also result in more scattering when compared to larger particles [20], and derivations from a spherical shape will increase the scattering. In addition, the particle size can affect the cleansing of the module due to rainfall. Larger particles (60 μm) seem to be more easily drained off than smaller particles (2-10 μm) [24].

The scattered and absorbed light is observed to be sensitive to the ratio between the soil density and the wavelength of the incoming radiation. Qasem [20] measured that transmission reduces more for shorter wavelengths (300-570 nm) than for longer wavelengths due to the deposition of dust on glass samples, and concluded that dust affects shorter wavelengths more severe. He also reported that the wavelength-dependence of the transmittance reduction is reduced with an increase in soil density. Some of his results are shown in figure 18 below.

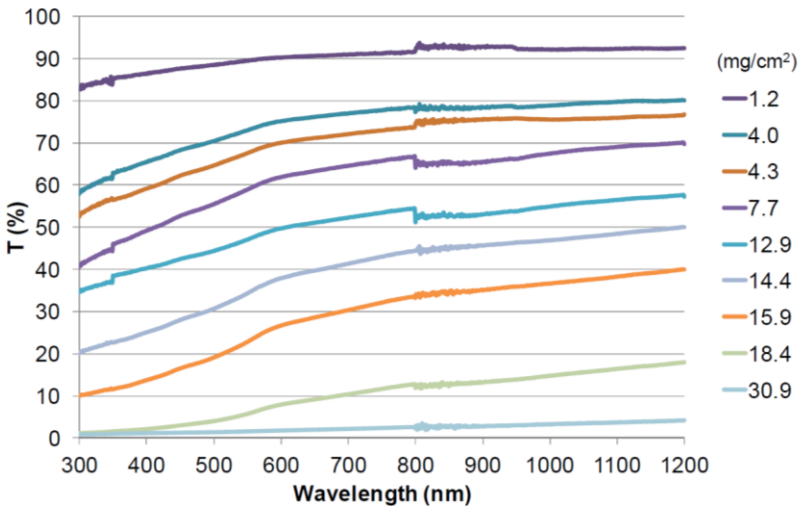

Figure 18: Measured spectral transmittance curves for different soil density samples [20]. It shows that with an increase in soil density, the wavelength-dependence of the transmittance reduction is reduced. The small discontinuity in the transmittance curve at 350 nm and 800 nm happens as the detector changes in the spectrophotometer.

2.4.2 Factors influencing the deposition of soil

As mentioned in earlier, several factors influence the accumulation of soil on photovoltaic modules. Climate and weather, the geographic characterizations of the location and the setup of the PV-modules are important variations that have been reported to affect the deposition of soil. It is essential to notice that results regarding soiling are not universal, because they are highly dependent on the particular location and measurement periods. Some important issues are discussed below.

2.4.2.1 Weather and climate

Weather is the conditions of the atmosphere at a given location over a short period of time, while climate is a long term (usually more than 30 years) average of the weather patterns at the location. Some essential atmospheric conditions that affect the accumulation of soil are: precipitation, wind speed [25] and dew [26].

A wide range of research have been conducted to detect and measure the decrease in transmission and efficiency due to the presence of soil, and many results report of a connection between efficiency and precipitation. Research conducted at the University of Malaga [27] concludes that rainfall can help clean PV-modules, if the precipitation level is high enough. The mean daily irradiation loss due to soiling was measured to about 4 %, but as high as 20 % after long periods without rainfall.

Research was conducted at Berkley University with a goal to investigate the effect of soil on energy production for PV-systems at various locations across The United States. Their results clearly state that irradiation losses increased in the absence of rain. Data show an increase in efficiency of PV-systems from 7.5 % to 12.5 % at 20 mm rainfall [28]. Suggested thresholds sufficient to clean PV-modules until a point of saturation vary from 0.5 mm for locations with lighter soiling rates [26] to 5.0 mm for more dense soiling deposition [29]. However, their results also conclude that there will be some soiling left on the modules after rainfall. Other reports state that the decrease in transmission due to soiling saturates after about five weeks, due to partial cleaning by rain [24].

Wind speed is reported to influence dust accumulation on the surface of PV modules. Generally, a low-speed wind pattern increases the dust deposition, while a high-speed wind dispel dust settlement and has a cleaning effect [30]. However, the PV panel settings in relation to the wind movement and the properties of the dust (weight, size, type etc.) affect the dust deposition.

Cold winters are often associated with snow. Only a thin layer of snow reduces the transmitted radiation due to the high albedo (0.9 for new snow), which leads to high reflection. The transmission is further reduced with increasing snow depth. At 10 cm snow cover, the transmitted radiation reduces to about 5 % for light at 550 nm, and less than 1 % for radiation at 800 nm [31]. Snow was not present during the measurements carried out in this study.

Humidity can cause formation of dew on PV-modules, which may cause partial cleaning. Caron and Littmann [26] investigated the reduction in efficiency due to soiling in California, and compared it with meteorological data. Their research shows a number of partial recoveries in efficiency when there was no recorded rainfall, but most likely a collection of dew on the front side of the modules. Other research shows a reduction in transmission on glass samples (up to 11.8 %) due to soiling, which reduced after dew simulations (6.8 %) in the laboratory [32]. Still, there is little documented information available regarding this cleaning effect.

2.4.2.2 Locational variations

A given location has properties that distinguish it from other areas. These are divided into physical and human characterizations. The physical characterizations describe the natural environment, such as topography and soil composition in the ground, while the human characterizations define the impact of human interaction with the environment, such as agriculture or city pollution.

Caron and Littmann's study from California shows that the deposition of soil tends to vary greatly with differences in locations. They measured soiling at PV-panels with a tilt angle of 25˚ over a one year period. They defined "soiling rates" as how quickly contaminations accumulated on panels, and found that soil accumulated with a rate less than 1.0 % per month in low desert areas, but as high as 11.5 % per month in heavy agricultural regions [26].

The soil composition and particle distribution varies with location. As noticed in the previous subchapter, these differences seem to have different effects on the transmission of radiation. By investigating five kinds of dust (three sorts of limestone particulates with different classes, carboe and cement) having different physical properties, Mohammad and Farmy show that carbon particulates result in the worst deterioration of performance of PV-cells, and a higher loss in power output, among the different dusts used [23].

2.4.2.3 Module setup

A PV-system has setup specifications, usually set to maximize the amount of incoming radiation. The tilt angle of the PV-modules is one specification that has a documented effect on the accumulation of soil. Steeper angles cause less soil to attach, due to gravitational forces, and will therefore result in a reduced soil density on the module surface. A study carried out in Egypt [33], used 100 glass panels with different tilt angles to measure the monthly average dust deposition over a seven month period. The results indicate that as tilt angle increases, dust particles tend to roll from the surface. The study measured a dust deposition of 15.84 g/m^2 (0˚) and 4.48 g/m^2 (90˚), corresponding to a diminishing transmittance of approximately 52 % and 12 %, respectively. Similar investigations have been conducted in Kuwait, where glass plates

with tilt angles of 0˚, 15˚, 30˚, 45˚ and 60˚, exposed to the environment for 38 days, measured a reduction in transmission of 64 %, 48 %, 38 %, 30 % and 17 %, respectively [34].

2.4.3 Anti-soiling coating

Glass can be treated with an anti-soiling coating, also referred to as easy-to-clean coating, or self-cleaning coating. The overall goal of the coating is to prevent efficiency losses due to the presence of soil, without affecting the transmittance through the glass.

Anti-soiling coating is based on either hydrophobic or hydrophilic properties, meaning either water repellent or water attracting, respectively. The hydrophobic material causes a minimized contact area between the surface and the water, leading to a high contact angle between the surface and the water droplets ($\alpha > 120^{\circ}$ for super-hydrophobic material), and a round shaped droplet. This gives a suitable cleaning effect. The hydrophilic coating on the other hand, maximizes the contact area, leading to a water film on the surface and a small contact angle between the surface and the water droplet ($\alpha < 10^{\circ}$ for super-hydrophilic material). This increases the transportation of dirt particles off the surface, if there is sufficient amount of water present [32]. Both coating alternatives are illustrated in figure 19, where β indicates the tilt angle of the glass.

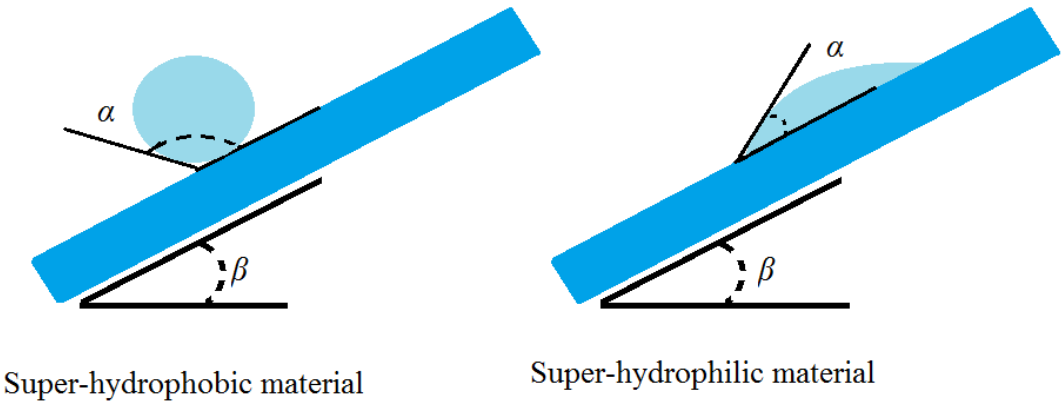

Figure 19: Water droplets form with different contact angles (α) for two different anti-soiling coating alternatives. β is the tilt angle of the glass. From: [22].

Lorenz et al. [32] have studied the increase in transmission due to simulated rain events on both hydrophilic anti-soiling coated glass and non-coated glass. Their results indicate that the coated glass has strong advantages (approximately full restoration in transmission) compared to the non-coated glass, especially regarding sticky dust (transmission loss of 5 % after rain on sticky dust), but also after small amounts of rain. Hydrophilic anti-soiling also showed a better tendency to increase transmission due to dew (reduction of 1.5 %), than non-coated glass (reduction of 6.8 %) [32]. Little information is found about the hydrophobic material.

However, Pettersen [22] conducted experiments with both normal and anti-soiling coated glass samples at Kjeller, from October to November 2014, with a tilt angle of 45˚. Her results showed that the transmittance was about 2 % lower for the anti-soiling coated glass samples after five weeks of exposure. It is unknown whether the anti-soiling coating is a hydrophilic or a hydrophobic coating.

2.4.4 Soiling in a northern climate

Generally, there is little research conducted regarding the issue of soiling in a northern climate. Available reports are often focused around areas associated with deserts and/ or high agriculture activity, often exposed to little rain. Some characterizations for a northern climate are the higher latitudes, which result in a steeper optimal tilt angle of the PV-panels, different precipitation levels during seasons and varying soil composition with geographic location.

PVsyst is an acknowledged simulation and design software, commonly used to predict the power production by a PV-system. This software suggests a power loss less than 1 % due to the accumulation of soil in a typical middle European climate [22].

A study carried out in Belgium to determine the effect of dust settlement on power output of PV-modules, with tilt angles of 35˚ and periods of regular rain, is an acceptable basis for comparison to Norwegian climate and conditions. Results show that the problem with dust deposition on the PV-modules is not as severe as in more desert-like areas. The study shows a constant power loss for the PV-modules between 3 % and 4 %. Still, these results do not reflect a one-year period, and further studies are needed.

3 Measurement equipment

Research conducted throughout the experimental period aims to investigate the phenomenon of soil deposition on the glass cover of photovoltaic modules in a northern climate. It focuses on the problem at Kjeller, by exposing glass samples at a tilt angle of 45˚ to the natural environment. Measurements are performed on the polluted glass samples to investigate the effect of soil on the transmittance and specular reflectance as a function of wavelength and angles of incidence. In addition, the accumulation of soil is measured and physical elements of the collected soil are investigated.

This subchapter presents the different measurement equipment used during the experiments and addresses some basic theory and functionality of the measurement setup. The Angular Dependent Reflection and Transmission Measurement (ADRTM) is the most central equipment, and will therefore be described in more details.

3.1 Angular Dependent Reflection and Transmission Measurement (ADRTM)

3.1.1 Basic setup

The Angular Dependent Reflection and Transmission Measurement (ADRTM) is an optical measure system used to examine transmittance, reflectance and/or absorptance as a function of incoming wavelength, angle of incidence and polarization state. The system is illustrated in figure 20 and consists of the main components:

- 100 W light source
- Monocromator
- Optical chopper
- Lenses (1 and 2)
- Polarization filter
- Integrating sphere
- TraQ software program

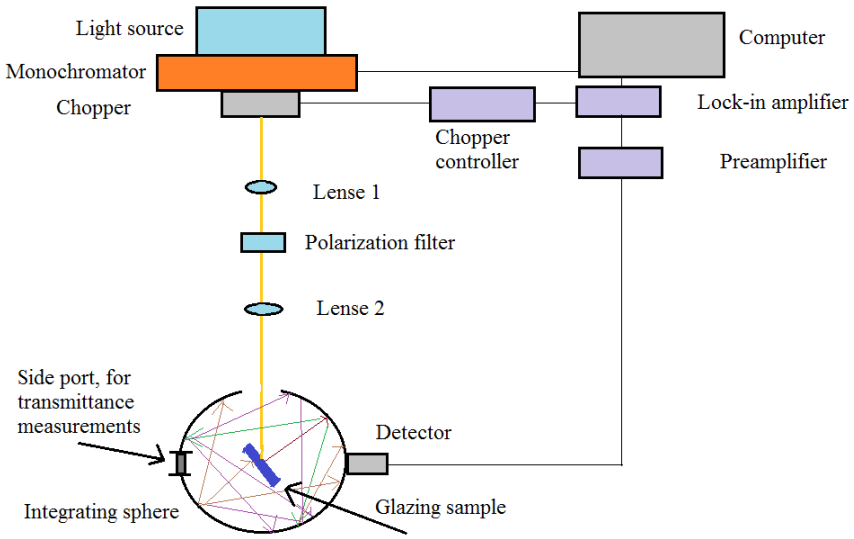

Figure 20: Schematic diagram of the measurement system ADRTM. This diagram shows the glazing sample inside the integrating sphere, for measuring the sum of transmittance and reflectance. From: [35].

Light is sent from the light source through the monochromator and optical chopper. The light beam has a diameter larger than 1 cm. The monochromator filters out undesirable wavelengths, resulting in one specific incoming wavelength at a time. The optical chopper filters out background noise like electromagnetic fields and stray light. Then, the radiation beam passes lens 1, which collimates and focuses the light before it enters the filter of specified polarization. The filter gives either s-, p- or unpolarized light. Recall from subchapter 2.1.4, that incoming sunlight is approximately unpolarized. Lens 2 collimates and focuses the beam before it enters the integrating sphere. The theory of an integrating sphere and its applications are given in more details. Experiments in this study are conducted with the settings:

- Wavelength spectrum from 350 nm to 1100 nm, with intervals of 10 nm
- Unpolarized filter
- One experiment with polarization filters

3.1.2 The integrating sphere

At an integrating sphere, the hollow inner surface is coated with a diffusely reflecting material. When a radiation beam enters the narrow hole from any direction, it is reflected diffusely at the walls until the radiation is distributed equally at the inner surface of the sphere. The radiation is detected from a limited solid angle and spatially integrated [36]. This is illustrated in figure 21. Reflection measurements give global reflection, which consists of both specular and diffuse reflection, as described in subchapter 2.3.2.

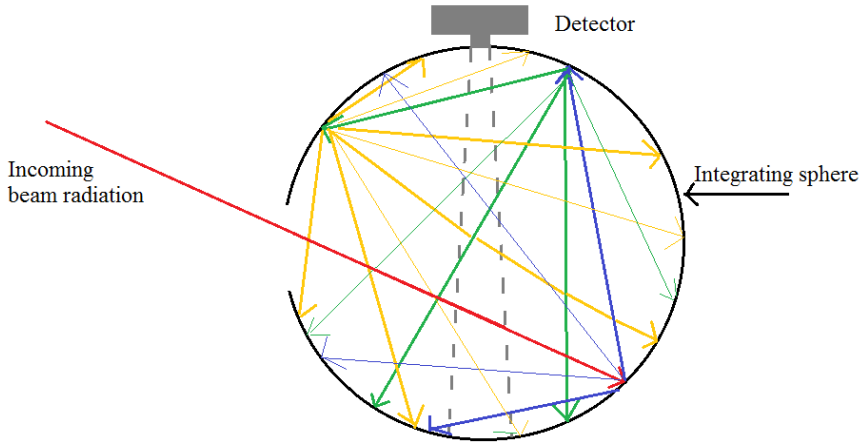

Figure 21: Diffuse reflection in an integrating sphere. From: [36].

The setup uses an integrating sphere from Labsphere with a center-mount configuration which allows samples to be placed inside the sphere. This configuration can be rotated to change the angle of incidence on the samples. Because some light is reflected back through the entrance at small angles of incidence, the rotational angle is limited to about $10^{\circ} < \theta < 75^{\circ}$. The samples inside the sphere are size limited to about 4 x 4 cm. Samples can also be placed in front of the opening of the integrating sphere. The samples mounted external to the sphere can be larger, but the angle of incidence is limited to about $0^{\circ} < \theta < 30^{\circ}$. This is because the angle is varied by rotating the sphere, and the beam will not enter the sphere at larger angles.

The integrating sphere has four entrance holes evenly spaced, where the radiation beam can enter (and exit). The holes are tactically covered when not in use. Different optical values are measured by placing the glass-sample either in front of the entrance port or inside the sphere, as illustrated in figure 22. Note that this figure views the sphere from above, meaning that the glazing samples are vertically mounted. The optical measurements are:

- Transmittance through the glazing sample
- Sum of transmittance and reflectance from the glazing sample

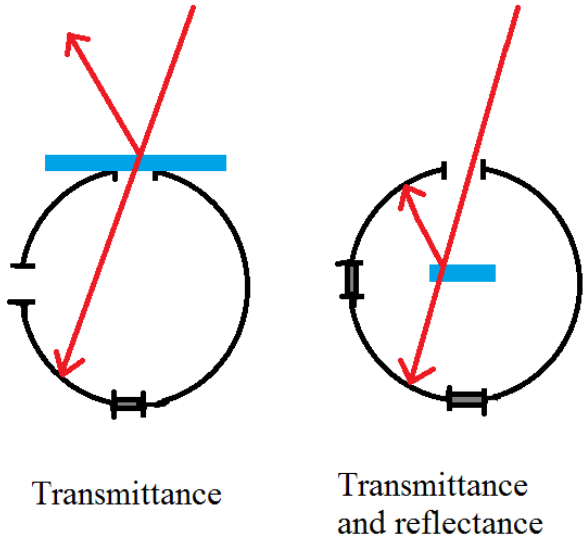

Figure 22: Mounting of the gass sample on the integrating sphere. This figure views the sphere from above.

As seen in figure 22, transmittance is measured by placing the glazing sample in front of the opening of the integrating sphere (leaving the side port open), while the sum of transmittance and reflectance is measured by using the center-mount configuration and placing the sample inside the sphere.

In integrating sphere measurements, desired values at a defined angle of incidence are found through a calibration and a sample measurement. The calibration measurement is performed without the glazing sample and with the sphere conditions as similar to the conditions during the sample measurements as possible. The desired values are calculated using the following formula:

$$M_{s,\lambda} = \frac{S_{s,\lambda}}{S_{c,\lambda}} M_{c,\lambda} \tag{18}$$

Here S is measured signal and M is the reflectance or transmittance. The subscripts s and c represents sample and calibration, respectively. The λ subscript indicates wavelength dependence. The reflectance or transmittance of the calibration ($M_{c,\lambda}$) is set to unity.

One calibration measurement is sufficient if the incidence angle is changed, but a new calibration must be performed if the glazing sample, polarization filter or optical measuring value (either transmittance and/ or reflectance) are changed. The results are logged by the software program TraQ and evaluated in Excel.

3.2 The ellipsometer

The ellipsometer used in this study is a J. A. Woollam Variable Angle Spectroscopic Ellipsometer (VASE), shown in figure 23 below. It is a precision instrument that exploits the change in polarization state of light after reflection (or transmittance) from a surface, to characterize optical and compositional properties of a sample. In this study, the ellipsometer is used to measure specular reflectance from both interfaces of the glass as a function of the radiation beam wavelength, angle of incidence and polarization state.

The incident light source is an arc lamp, mounted within a monochromator housing, seen as the black squared pillar to the right in figure 23 below. The monochromator sorts out unwanted wavelengths, before the light beam passes a polarizer that states the polarization. The diameter of the light beam is 4 mm, and the surface area of the detector is in the same order. The glass sample is mounted in a vertical position, shown in the middle of figure 23. The vertical position is possible due to vacuum suction at the backside. The reflected radiation is analyzed to resolve the polarization state after the reflection. Results are detected and given by the software program WVASE32, before being transferred to Excel for evaluation. The small diameter of the incoming radiation and the small surface area of the detector make the equipment vulnerable to surface variations on the glass sample.

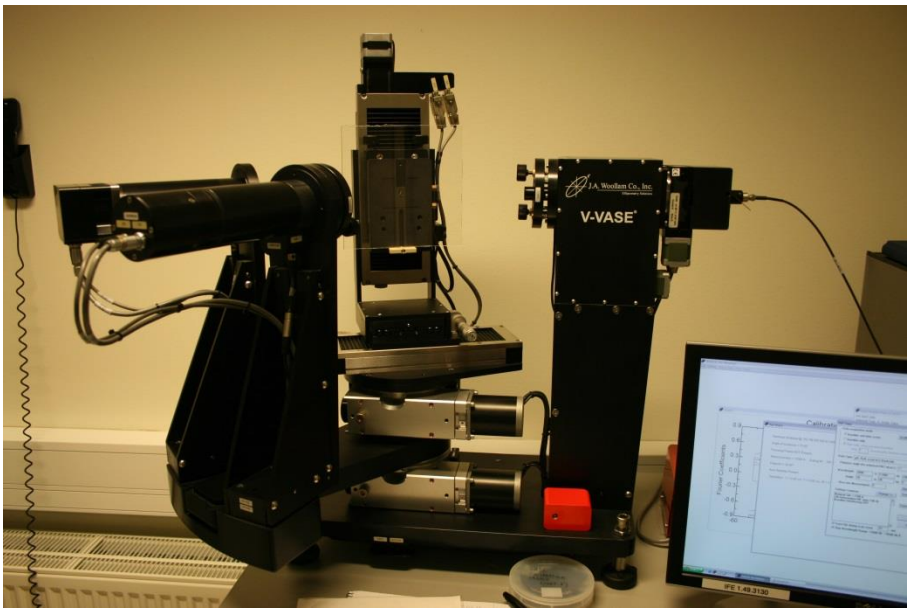

Figure 23: The ellipsometer with a glass sample, shown in the middle of the picture.

Experiments in the study are conducted with the settings:

- Both s- and p-polarized specular reflection, one at a time.
- Wavelength spectrum from 350 nm to 1100 nm, with intervals of 10 nm.
- Angle of incidence from 20˚ to 80˚, with intervals of 5˚. (Angles beyond the interval are not possible).

The linear polarization is found based on the theory from subchapter 2.1.4, which says that linear polarization is given by the mean of the two polarization states.

3.3 Mettler Toledo Excellence Plus weight

Quantification measurements are conducted using a Mettler Toledo Excellence Plus weight. The weight has a measure area encapsulated by movable glass walls and a movable roof. It has an accuracy of 0.0001 g, and a maximum capacity of 200 g. Figure 24 below shows the weight with a glass sample inside the housing.

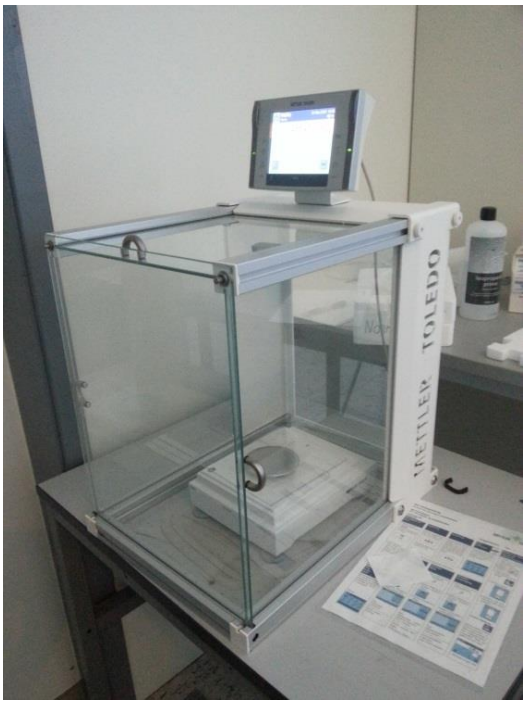

Figure 24: The Mettler Toledo Excellence Plus weight employed during research.

3.4 Scanning Electron Microscope (SEM)

A Scanning Electron Microscope (SEM) is a microscope that uses an X-ray microanalysis technique called Energy Dispersive Spectrometry (EDS), for the elemental analysis or chemical characterization of a sample. The setup is illustrated in figure 25 below. It uses a focused beam of electrons to form a 2-dimentional image of surface variations in a sample. This image has a spatial resolution of 1 nm. The electron-scan reveals information [37] about:

- The sample texture
- Chemical composition
- Crystalline structure and orientation of materials making up the sample

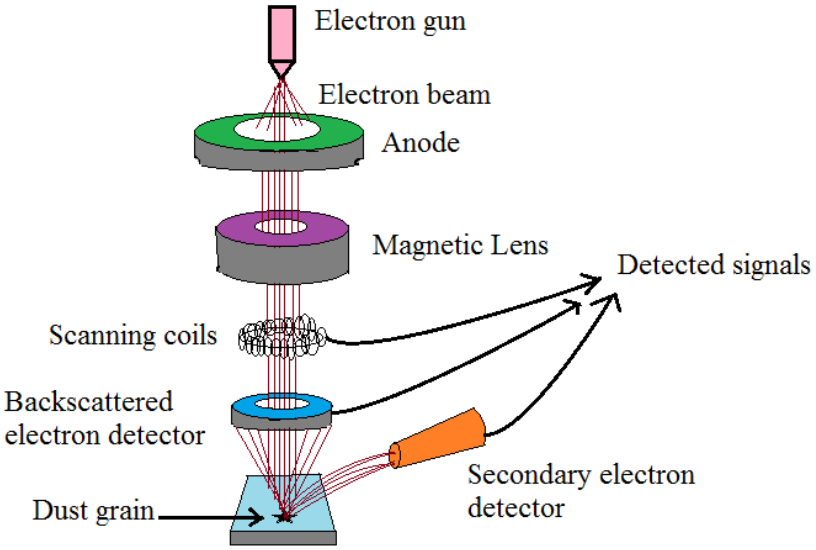

Figure 25: Schematic illustration of important components in the measurement setup for the Scanning Electron Microscope (SEM). From: [38].

An electron gun produces a focused beam of high-energy electrons. This beam is controlled and focused by electromagnetic fields and lenses, before it hits the sample. The electron beam detects a droplet shaped excitation volume, at about 5 µm deep and 5 µm wide [39]. This ejects electrons and X-rays from the sample with different energy peaks. The characterization by the EDS is largely based on principle that each element has a unique atomic structure and that energy levels in electron shells varies in discrete fashion with atomic number [40], resulting in a unique set of energy peaks on its X-ray emission spectrum. The X-rays are detected to produce a signal and an

image of the surface [38]. This signal gives information about the different detected components, and how likely they are. The accuracy of the detected EDS signal is limited by the fact that some elements will have overlapping energy peaks in the detected signal, which means that it may be difficult the detect the precise component.

Samples examined with the SEM are limited in size to about 4x4 cm. They have to be treated with a carbon coating (involving carbon gassing of the surfaces and covering the edges with carbon tape). This is to improve the contact between the electron beam and the glass surface and strengthening the signal. The carbon coating affects the surface of the glass samples.

The Scanning Electron Microscope can give a wide range of information about the surface of a sample. In this study, the SEM is used to perform:

- Surface analyses to investigate important components on the glass surface
- Point analyses to examine important components of dust grains

Information from the scans are logged and exported to Excel for further examination.

3.5 Ocean Optics

The Ocean Optics measurement equipment used during this study is an optical measure system that gives transmittance as a function of incoming wavelength and angle of incidence. It consists of two sensors that measure the wavelength spectrum from 200 nm to 1000 nm and from 900nm to 1720 nm, with intervals of 1 nm and 2 nm, respectively.

Light is sent from a deuterium-halogen light source through an optical fiber tube, with an inner diameter of 1.5 mm. This tube is inserted to a fixed semicircular device that can be moved in a vertical direction. It consists of 11 different holes that provide an angle of incidence of 0˚, 18˚, 36˚, 54˚, 72˚ and 90˚, from both sides. A glazing sample is placed on top of a cylindrical tube. The sensors are located inside the tube. The optical setup is illustrated in figure 26.

This Ocean Optics system uses the software program SpectraSuite. Transmittance measurements are conducted by first measuring all incoming radiation (without the glazing sample) at the defined angle. Then, the glazing sample is placed between the sensor and the semicircular device and the transmitted radiation is measured. The results are transferred to Excel for evaluation.

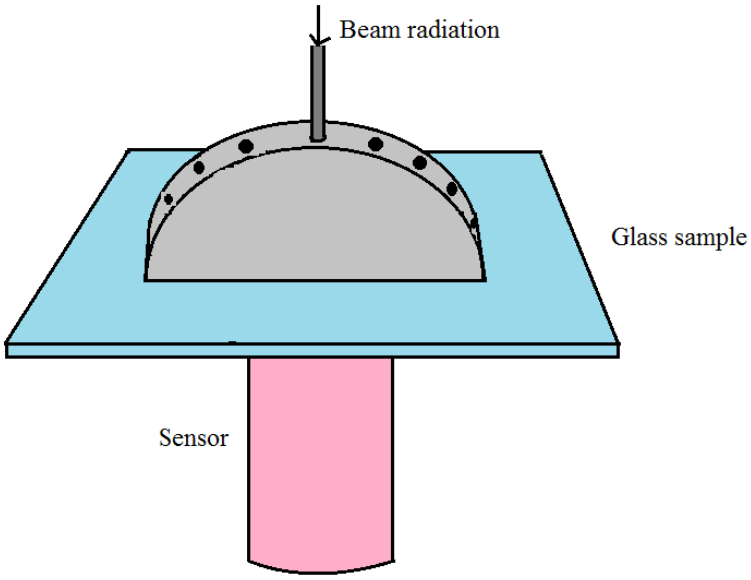

Figure 26: Basic illustration of the most important components in the Ocean Optics measurement setup.

The transmittance for glazing samples is measured in a horizontal position. This is a great benefit when glass samples are polluted with dust and other sorts of soiling. A disadvantage is the narrow diameter of the incoming beam radiation. This makes the equipment vulnerable for small surface variations, which will occur at a polluted sample.

The Ocean Optics setup is not used to measure variations in transmittance due to natural soiling. However, it is used to measure reduced transmittance due to artificial dust. This is because of the higher soil density, and the need for a horizontal position.

4 Experimental methodology

The overall purpose of this study is to establish a better understanding of how soil accumulates on the glass cover of PV-panels in a Nordic climate, and how this affects optical properties of the module glass. This is examined by exposing both standard glass for PV-modules and glass coated with an anti-soiling coating to the natural environment at Kjeller. Optical properties and mass changes due to soiling are measured, and soil analyses on the accumulated soil are performed. In addition, the relationship between artificial soil density and the reduction in transmission is investigated to identify the reduced transmission due to variations in soil density.

4.1 Experimental structure

This subchapter gives an overview of the different approaches conducted in this study to examine soiling in a northern climate. Basic characteristics for the location at Kjeller are presented, as well as the research-setup at the rooftop.

4.1.1 Basic overview of the experimental methodology

The natural accumulation of soil on glass commonly used to cover photovoltaic solar cells is investigated by exposing different glass samples to the natural environment at Kjeller. A schematic illustration of the different measurements conducted throughout this experimental period is given in figure 27. The first five boxes describe the experiments concerning natural soiling at Kjeller, while the last box refers to a separate experiment with artificial dust on glass samples. Further details are given below the figure.

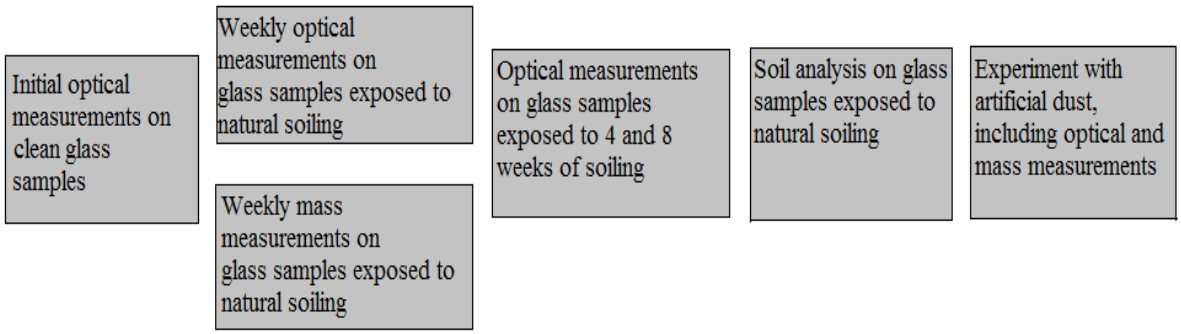

Figure 27: A schematic illustration of the different measurements conducted on glass samples throughout this experimental period. The first five boxes describe the experiments concerning natural soiling at Kjeller, while the last box refers to a separate experiment with artificial dust on glass samples.

Theoretical transmittance, reflectance and absorptance are calculated based on properties for BK7-glass. This is because properties for BK7-glass are well characterized at all wavelengths. BK7-glass is designed to have next to no absorptance, and theoretical values are therefore expected to differ slightly from the optical measurements conducted on the glass samples.

Initial optical measurements on clean glass samples, both normal glass and glass coated with an anti-soiling coating, are conducted. These involve transmittance, specular reflectance, absorptance, as well as transmittance by polarized light. The results are referred to as "initial optical measurements on clean glass samples", throughout this thesis.

The natural accumulation of soil on glass samples is investigated by exposing sixteen different glass samples to the natural environment at Kjeller. Half of the samples are treated with an anti-soiling coating (TripleO), to study the assumed reduction in soil deposition. The samples are mounted at a rooftop of the Institute for Energy Technology (IFE), with a tilt angle of 45˚.

Eight glass samples (four normal and four anti-soiling coated) are inspected in laboratories every week. They are used to investigate how one week of soiling affects the transmittance and specular reflectance, as functions of wavelength and angle of incidence. Measurements focus on the changes in these optical values. The glass samples are used to quantify the accumulation of soil, expressed as soil density. After measurements are conducted in laboratories, the glass samples are cleaned with spirit and placed back at the rooftop.

The additional eight glass samples (four normal and four anti-soiling coated) are left uncleansed during the experimental period. Optical measurements are performed after four and eight weeks of exposure.

Soil analyses are conducted on glass samples exposed to one week of soiling, at two selected dated during the experimental period. These analyses are performed to determine important elements in the natural soil at Kjeller, and to investigate the size of the soil grains. The glass samples are replaced at the rooftop due to the carbonized surface (recall subchapter 3.4).

A separate experiment is conducted with artificial dust, to examine the relation between soil density and transmittance. This is conducted by polluting glass samples with artificial dust, before transmittance and mass measurements are conducted. The dust is selected based on identified soil components from the soil analyses conducted at the glass samples from the rooftop.

4.1.2 Test site and experimental setup

Kjeller is a densely populated area outside Oslo (59.7˚N and 11.1˚E). It is characterized by a flat topography and an inland climate. This means that there are less wind, low humidity and great variations in temperature during the day and over the year. Research is conducted at the Solar Energy department, at the Institute for Energy Technology (IFE). This test site is located close to a military airport, roads and the city Lillestrøm.

To investigate the natural accumulation of soil at Kjeller, sixteen glass samples of 2 mm thickness are placed at a rooftop at IFE. The glass samples are standard glass used in the PV-industry to cover solar cells. Half the samples are coated with TripleO, an anti-soiling cover. There is no available datasheet for this specific coating, and it is unknown whether this is hydrophilic or super-hydrophobic coating. These samples are further on in this thesis denoted as “normal glass” and “anti-soiling glass”, respectively.

The samples consist of two different surface areas: 17x17 cm and 3.8x3.8 cm. These are referred to as “large samples” and “small samples”. The larger size is chosen because it collects a larger quantum of soil and will therefore give a better representation for the soil accumulation. Some samples are smaller due to size limitations in some measurement equipment (inside the integrating sphere and the SEM).

The glass samples are mounted on a rack, as an extension of an existing solar panel system, not yet operational. They are installed at tilt angle of 45˚.

Angel brackets are mounted on the rack to support the glass samples. The samples are additionally secured with a small piece of tape. This ensures that the glass samples are easy to remove and remount. The angle brackets have an edge that protrude and might influence the effect of precipitation. This is shown in figure 28. Figure 29 shows the rooftop.

Figure 28: Glass sample installation at the rooftop.

Figure 29: Existing solar panel system at the rooftop.

All experiments are conducted with great care to avoid soil from falling off and not to damage the glass samples. This is ensured by keeping the samples inside closed expanded polyester boxes during transportation and storage. Rubber gloves are worn when handling the samples. The larger glass samples are labeled at the back side, and all expanded polystyrene boxes are marked according to the related sample.

The rooftop-set consists of two base setups:

a. Eight samples are cleaned every week after measurements are conducted.
b. Eight samples are left uncleansed. They are investigated after four weeks and at the end of the experimental period.

Measurements are performed every Tuesday from February 24 to April 14. Notes regarding the glass samples are written in a research log. Measurements include transmittance, reflectance and absorptance, as well as mass measurements to quantify the accumulated soil. The experiments are duplicated to better verify the results.

Soil analyses are performed to determine the composition and size distribution of the soil. More detailed measure methods are given in the next subchapters.

Wet glass samples, due to dew, precipitation or other factors, are dried indoors in a horizontal position before measurements are carried out. This might affect the results, because of the lacking tilt angle that can lead to draining.

4.2 Quantified accumulation of soil

This subchapter addresses the methodology applied to measure and calculate the accumulation of soil on normal and anti-soiling coated glass samples, after they have been exposed to one week of soiling at Kjeller.

The experiments aim to answer:

- How much soil accumulates on a normal and an anti-soiling coated glass sample after one week of exposure?
- Are the normal and anti-soiling coated glass samples affected differently?
- How does precipitation effect the accumulation of soil?

Half the glass samples are collected every Tuesday for weekly measurements. To define the soil quantity (accumulation of soil density in a definite time interval) for the glass samples as accurately as possible, several measurements are made:

a. The large glass samples are weighted.
b. Optical measurements are conducted.
c. The large glass samples are weighted again directly after the optical measurements. This is conducted to determine the amount of soil that might fall off due to the vertical positioning during optical measurements.
d. The glass samples are cleaned with small rags and weighted once more. This is to correlate the transmittance to the dust density actually present during the optical measurements.
e. The small rags are also weighted before and after cleaning and would be expected to show the same absolute change in mass.
f. The total soil density is calculated by adding the amount of soil that falls off during optical measurements and the amount of soil that is cleaned off.

Measurements are conducted using a Mettler Toledo Excellence Plus weight, presented in chapter 3.3. Weekly measurements for one large glass sample are illustrated in figure 30 below, in subchapter 4.2.2. The same method applies to the other three glass samples.

4.2.1 Methodology test

Tests were performed prior to the experimental period to verify the technique and investigate the accuracy of the weight. This involved weighting four small rags before and after they were soaked with Isopropanol Prima spirit and dried in expanded polystyrene boxes. The two different values were compared to examine possible differences. The results are presented in table 1.

Name	Mass before spirit [mg]	Mass after spirit [mg]	Relative difference [%]
Rag 1	506.6	506.3	-0.06
Rag 2	346.1	345.9	-0.06
Rag 3	364.6	364.6	0.00
Rag 4	470.3	470.1	-0.04

Table 1: The mass of small rags before and after they were soaked with spirit and dried.

The differences between the masses of the rags are in the range from 0.0 mg to 0.3 mg. Recall that the uncertainty of the weight is ± 0.1 mg and that the surface area of the large glass samples are approximately $A = 0.0289$ m^2. This means that a measure uncertainties of 0.4 mg may occur, which gives scaled results of approximately 13.8 mg/m^2.

It is noteworthy that the rags seem to have a higher mass before they are soaked with spirit and dried. This might result in lower mass changes for the rags used to clean the large glass samples. Still, the relative difference is low, and the methodology is considered valid. Nevertheless, two large glass samples (one normal and one anti-soiling) are cleaned with spirit, while the other two are cleaned with dry rags, due to the small mass differences.

4.2.2 Natural accumulation of soil

Results from the normal and anti-soiling coated glass samples are kept separately. The methodology for weekly measurement for one glass sample is illustrated in figure 30 below.

The large samples are carefully weighted before and after optical measurements are performed, because the glass samples are vertically positioned during these measurements. This mass difference is used to determine the amount of soil that falls off due to optical measurements (ΔM_{OM}), and is expressed as:

$$\Delta M_{\mathrm{OM}} = M_{after\ OM} - M_{before\ OM} \tag{19}$$

$M_{\mathrm{before\ OM}}$ is the mass of the glass samples before the optical measurements are conducted, while $M_{\mathrm{after,\ OM}}$ is the mass after the optical measurements.

The glass samples are cleaned after the optical measurements are conducted. There is one small rag (about 3x3 cm) per glass sample. The small rags are weighted before cleaning. Two glass samples (one normal and one anti-soiling coated sample) are cleaned with Isopropanol Prima spirit, while the other two (one normal and one anti-soiling coated sample) are cleaned with dry rags. The wet samples and rags are dried in expanded polystyrene boxes. Finally, the now clean glass samples and dirty rags are weighted once more. This is to determine the amount of soil that is cleaned off. The mass differences due to cleaning (ΔM_{C}) is based on the mean value for the cleaned glass sample and the rag. The mass differences are expressed as:

$$\Delta M_{\mathrm{C,glass}} = M_{\mathrm{after\ C,glass}} - M_{\mathrm{before\ C,glass}} = M_{\mathrm{after\ C,glass}} - M_{after\ OM} \tag{20}$$

$$\Delta M_{\mathrm{C,rag}} = M_{\mathrm{after\ C,rag}} - M_{\mathrm{before\ C,rag}} \tag{21}$$

$$\Delta M_{\mathrm{C}} = \frac{1}{2}\left(\Delta M_{\mathrm{C,glass}} + \Delta M_{\mathrm{C,rag}}\right) \tag{22}$$

It is assumed that the amount of soil that falls off due to optical measurement will fall off before the measurements are conducted. The amount of soil that is cleaned off is therefore assumed to equal the soil that stays on the glass samples during the optical measurements.

The total soil deposition after one week at Kjeller ($\Delta M_{\mathrm{total}}$) is based on the mass change due to optical measurements ($\Delta \mathrm{M_{OM}}$) and cleaning (ΔM_{C}). This is to include more measure data and strengthen the results. It is expressed as:

$$\Delta M_{\mathrm{total}} = \Delta \mathrm{M_{OM}} + \Delta M_{\mathrm{C}} \tag{23}$$

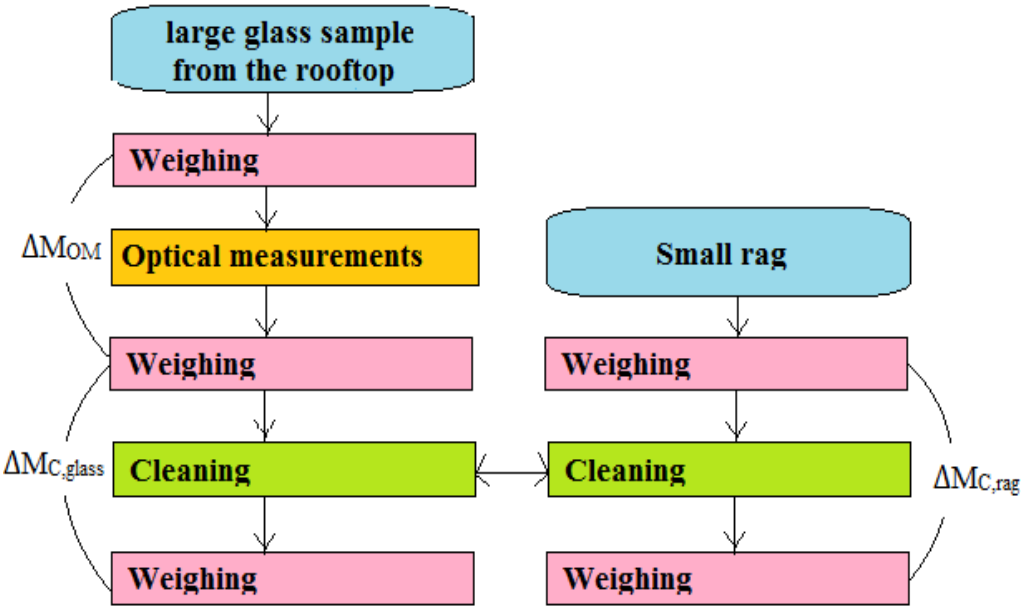

Figure 30: A schematic illustration of the methodology applied for weekly measurements on one large glass sample. The same method applies for the other three large glass samples (two normal and two anti-soiling coated samples).

The mass of the large glass samples is of the same order as the maximum capability of the Mettler Toledo Excellence Plus weight. Therefore, the weight needs time to stabilize before the correct value is given. This was not noticed during the first two weeks of measurements. The weight does not need time to stabilize for the rags, due to the smaller mass.

The mass changes due to optical measurements and cleaning measured by the large glass samples are not valid for the first two weeks, as noted above. Therefore, the mean mass change due to optical measurements for the entire experimental period excludes the first two dates. The mean mass change due to cleaning for the entire experimental period excludes the mass changes for the glass samples but includes the mass changes of the rags for the first two measure dates. The mean values are calculated based on equation 24 below, here represented by the mean mass change due to cleaning:

$$\overline{\Delta M_{\mathrm{C}}} = \frac{1}{\mathrm{n}} \sum_{\mathrm{i}=1}^{\mathrm{n}} \Delta M_{\mathrm{C,i}} \tag{24}$$

n is the number of measurements, and i defines the different weeks of measurements.

The total soil deposition for the first two measure dates are calculated based on the mean mass change due to optical measurements for the entire period and the mass change of the small rags

at the respective dates. This is because the mass changes of the large glass samples are excluded for the first two measure dates. A mean accumulation of soil ($\overline{\Delta M_{\text{total}}}$) is calculated based on equation 24 above.

Recall that the size of the large glass surfaces is approximately 17x17 cm. Soil densities (*MD*) are calculated based on the different mass changes (ΔM) and the surface area (A) of the glass surfaces. It is expressed by equation 25 below, here represented by the mass change due to cleaning:

$$MD_{\text{C}} = \frac{\Delta M_C}{A} \tag{25}$$

The subscript C refers to the cleaning event. This is replaced by the subscripts OM or total to calculate the soil density that falls off due to optical measurements or the total accumulated soil density, respectively.

Statistical uncertainties are not calculated, due to only two measurements per sample.

4.3 Optical properties of the natural soil deposition

This subchapter addresses the methodology applied to measure and calculate optical values for the normal and anti-soiling coated glass samples, after they have been exposed to natural soiling at Kjeller. The experiments focus on the changes in these optical values, due to the presence of soil.

The experiments aim to answer:

- How is the spectral reflectance affected by soiling?
- What are the transmission losses due to one week of soiling?
- Are there any noticeable relation between the change in transmittance and the accumulated soil density?
- Are there any difference between the normal and the anti-soiling coated glass samples?

4.3.1 Accuracy of the ADRTM

The sensitivity of the ADRTM equipment is investigated to examine if the system can detect small changes in transmittance due to the presence of soil at the glass samples. Measurements employing the ADRTM require a calibration measurement where the incoming beam does not hit the glazing sample, but where the sphere conditions are as similar as possible to the conditions during the sample measurements. For transmittance measurements, this calibration measurement includes a glazing sample that covers the open side port. Some portion of the globally reflected radiation in the sphere is transmitted and reflected due to the glazing sample at the side port, while some radiation leaves the front port. This is similar to the sample measurement, where the glazing sample covers the front port and the side port is kept open.

The sensitivity of the equipment is examined by applying three different methods for the calibration measurement for transmittance. The first involve a closed side port on the integrating sphere, the second having the glazing sample at the open side port and the third having a completely opened side port. This is illustrated in figure 31.

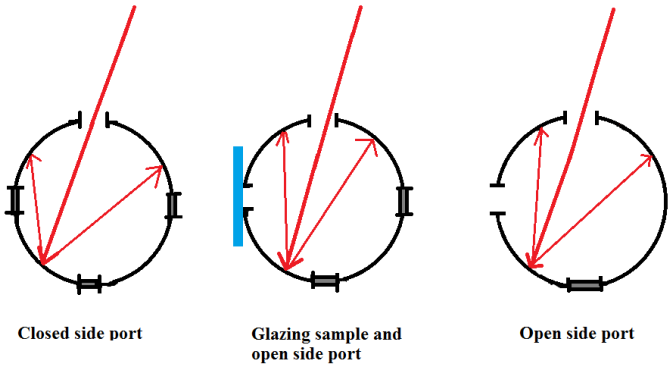

Figure 31: Three different calibration measurements for transmittance to investigate the accuracy of the ADRTM. The middle one is the correct calibration measurement.

Results from the three different calibration measurements for transmittance are plotted in graph 1. A small discontinuity in the transmittance curves at about 550 nm occurs during all initial transmittance measurement on the clean glass samples, employing the ADRTM. This happens as the monochromator changes settings. This is accounted for, and described in chapter 4.3.2. The measured transmittance is higher than expected. One possible explanation is that the calibration measurements are conducted at 0˚ angle of incidence, and some radiation can be reflected out the entrance port. Nevertheless, the inside of the sphere is coated with diffusely reflecting material and should therefore not be affected by this. This somewhat higher transmittance value is accounted for when the change in transmittance is calculated, due to subtraction.

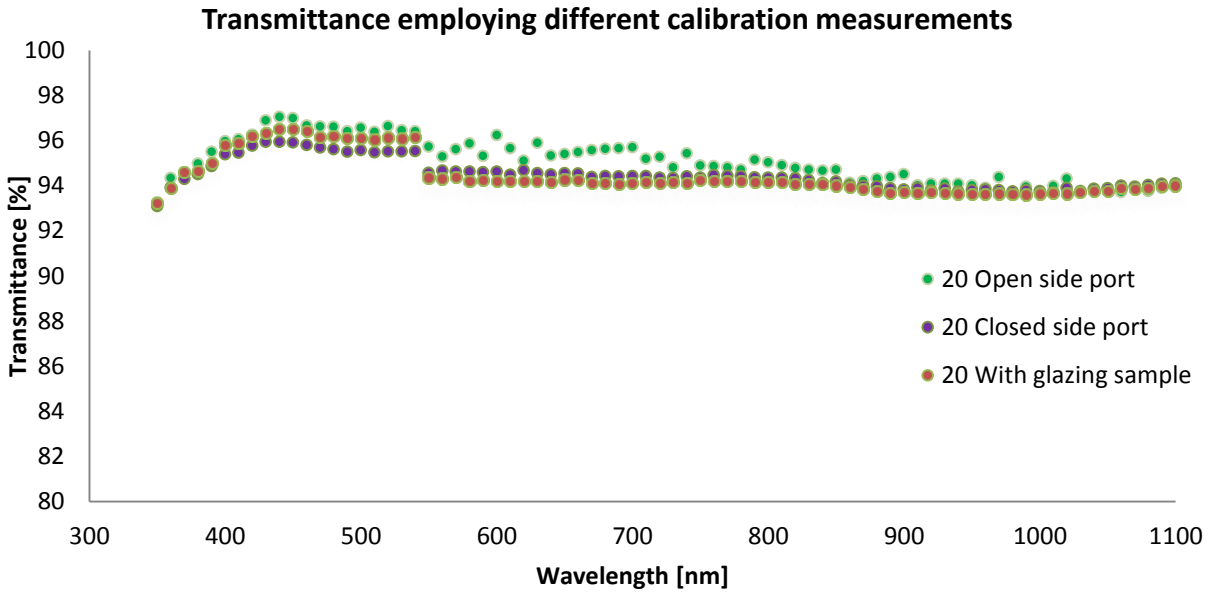

Graph 1: Transmittance measurements at 20˚ angle of incidence for a normal glass sample, employing three different calibration measurements. The curve "with glazing sample" is the correct calibration measurement.

Recall that the transmittance values are computed by dividing the sample measurement on the calibration measurement (see subchapter 3.1.2). This implies that a smaller calibration measurement would result in higher transmittance values. The transmittance values are weighted against the AM1.5G spectrum, given in subchapter 4.3.6. These show lowest transmittance values when the side port is open, higher values when the glazing sample covers the open side port and highest values when the side port is closed. The difference in transmittance between measurements conducted with closed and open side port is about 0.67 % of the transmittance measured with open side port.

This result agrees with expectations. If the side port is closed, approximately all incoming radiation are globally reflected and detected inside the sphere. If the side port is open, a portion of the globally reflected light escapes through the side port, which results in lower values for the calibration measurement, and higher transmittance values.

The results show that small changes in the condition measurement have an impact on the measured transmittance of the glass sample. This provides reasons to believe that the ADRTM are accurate, and will detect differences in transmittance due to the presence of soil on the glass samples.

4.3.2 Change in weekly transmittance

The change in transmittance due to one week of natural soiling at Kjeller is investigated by comparing weekly transmittance measurements to the initial transmittance value for clean samples. This is conducted on the large glass samples, employing the ADRTM. The angle dependence are limited to $0° < \theta < 30°$ (as noted in chapter 3), because the glass samples are placed in front of the integrating sphere.

As noticed in graph 2, the transmittance values for the initial transmittance measurement on clean glass samples make a step-like shift at approximately 550 nm, where the monochromator changes filter. This was noticed for both the normal and anti-soiling coated glass samples, at February 17. However, this step-up shift does not occur during the rest of the experimental period. There is no physical reason that would result in this step-up shift at the point where the monochromator changes filter.

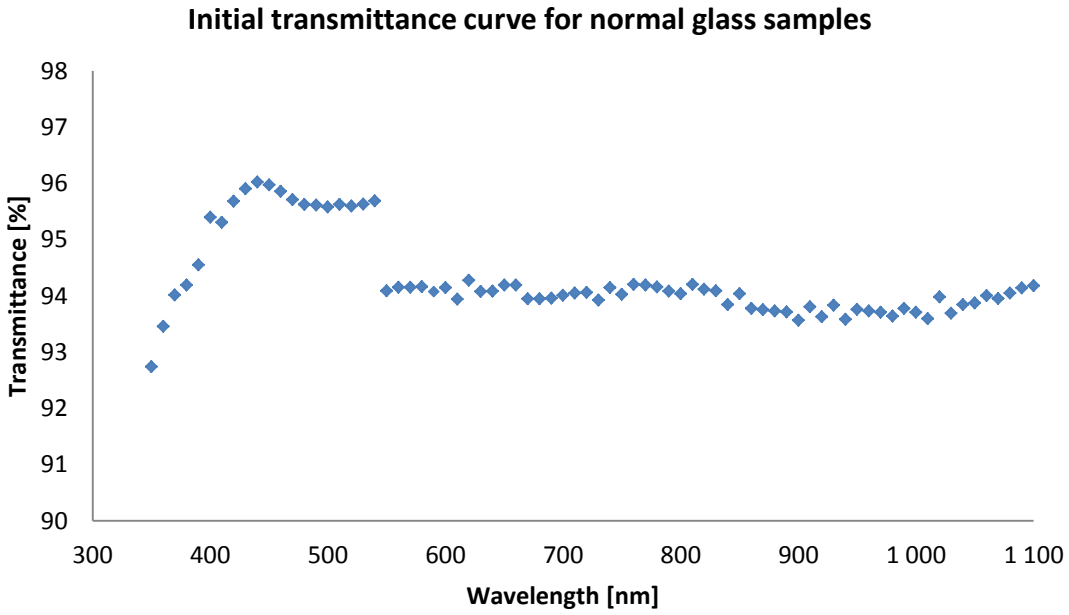

Graph 2: Initial transmittance curve at 20˚ angle of incidence for normal glass samples, showing a step-up shift.

The step-up shift is accounted for in the initial measurements. First, the difference between the transmittance at 540 nm and 550 nm is found. This is about 1.6 % and 1.1 % for normal and anti-soiling glass, respectively. Then, this value is subtracted from all transmittance values below 550 nm. This gives the adjusted initial transmittance curves for the clean glass samples. Graph 3 shows this adjusted curve for the normal glass samples.

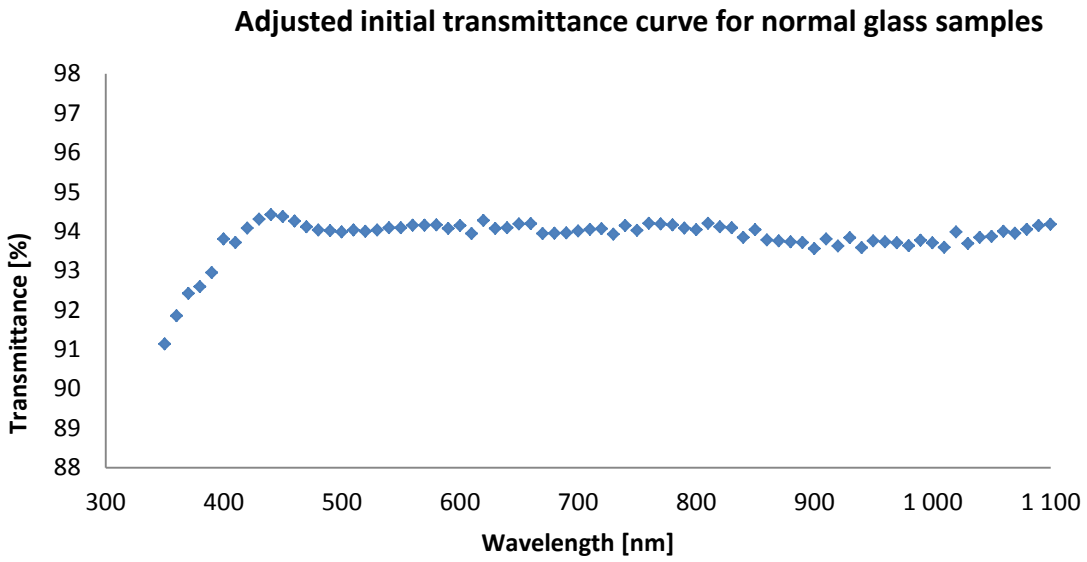

Graph 3: Adjusted initial transmittance curve for the normal glass samples. This measurement is conducted at 20˚ angle of incidence.

The weekly transmittance (from measurements employing the ADRTM) is defined as the mean value from the duplicated measurements. The change in transmittance at a specified angle of incidence and wavelength ($\Delta\tau_{\theta,\lambda}$) due to one week of soiling is calculated as:

$$\Delta\tau_{\theta,\lambda} = \tau_{\theta,\lambda,\text{ADRTM}} - \tau_{\theta,\lambda,\text{ADRTM,clean}} \tag{26}$$

$\tau_{\theta,\lambda,\text{ADRTM}}$ is the mean weekly transmittance at a specific incoming angle and $\tau_{\theta,\lambda,\text{ADRTM,clean}}$ is the initial transmittance measurement for the sample. The subscripts λ and θ refers to the specific wavelength and angle of incidence, while ADRTM refers to the measurement equipment.

The experiments focus on the change in transmittance at 20˚ angle of incidence.

4.3.3 Specular reflectance

The ellipsometer measures specular reflectance as a function of incoming wavelength and an angle of incidence from 20° to 80°. The surface structure of clean glass samples is approximately smooth, which means that the greatest part of the reflection is specular.

The ellipsometer is used to measure the specular reflectance of the glass samples exposed to natural soiling. These measurements are not duplicated, due to the long measuring time. The change in specular reflectance is calculated by replacing transmittance with reflectance from the ellipsometer in equation 26. Changes in global and internal reflectance have not been studied.

4.3.4 Transmittance

Initial transmittance for clean glass samples is calculated based on the sum of transmittance and reflectance (from glass samples inside the ADRTM) and specular reflectance (from the ellipsometer). This method is selected to view the transmittance at a wider range of angles of incidence. It gives the transmittance as a function of incoming wavelength and angle of incidence in an interval from 20° to 80°. Because the ADRTM measure global reflection, while the ellipsometer give specular reflection, the calculated transmittance is expected to be slightly higher than real values. However, the largest portion of the reflectance is likely to be specular for clean glass samples (as noted in chapter 4.3.3). The initial transmittance on clean glass samples is calculated as:

$$\tau_{\theta,\lambda,\text{clean}} = (\tau + \rho)_{\theta,\lambda,\text{ADRTM}} - \rho_{\theta,\lambda\ \text{specular}} \tag{27}$$

$(\tau + \rho)_{\theta,\lambda,\text{ADRTM}}$ is the mean sum of transmittance and reflectance from the duplicated measurements given by the ADRTM, and $\rho_{\theta,\lambda\ \text{specular}}$ is the specular reflectance from the ellipsometer.

It is not possible to detect the change in diffuse and internal reflectance during the research in this study. The change in transmittance (measured with the ADRTM) accounts for these changes. The transmittance due to soiling ($\tau_{\theta,\lambda}$) is therefore calculated based on the initial transmittance values and the change in transmittance:

$$\tau_{\theta,\lambda} = \tau_{\theta,\lambda,\text{clean}} + \Delta\tau_{\theta,\lambda} \tag{28}$$

$\tau_{\theta,\lambda,\text{clean}}$ is the initial transmittance and $\Delta\tau_{\theta,\lambda}$ is the change in transmittance.

4.3.5 Absorptance

The sum of transmittance, reflectance and absorptance equals one. The absorptance is calculated based on the measured value for the combination of transmittance and reflectance, which are measured employing the center-mount configuration in the ADRTM. The absorptance is evaluated as a function of incoming wavelength and angle of incidence in the interval from 10° to 70°. The absorptance at a defined angle of incidence ($\alpha_{\theta,\lambda}$) is calculated as:

$$\alpha_{\theta,\lambda} = 1 - (\tau + \rho)_{\theta,\lambda,\text{ADRTM}} \tag{29}$$

$(\tau + \rho)_{\theta,\lambda,\text{ADRTM}}$ is the mean sum of transmittance and reflectance measurements. The change in absorptance is calculated based on equation 26, by replacing transmittance values with absorptance.

Recall that radiation is reflected diffusely at the inner surface of the sphere. Because the small glass samples are placed inside the sphere, there is reason to believe that the measured absorptance is higher than real values.

4.3.6 Weighting against the AM1.5G spectrum

Transmittance, reflectance and absorptance, at a defined angle of incidence, are calculated by weighting the respective values at different wavelengths to the AM1.5G spectrum for Global Tilt [41]. The AM1.5G spectrum represents terrestrial solar spectral irradiation on a surface of specified orientation, as a common reference for evaluating PV-modules. Global Tilt defines the receiving surface as an inclined plane at 37° tilt toward the equator, facing the sun [41].

Recall that it is the number of photons, not the amount of incoming energy, which is interesting in photovoltaics. The transmittance, reflectance and absorptance are therefore weighted against the portion of incoming photons at the given wavelength. The number of photons from the incoming solar radiation at a defined wavelength ($N_{\text{photons},\lambda}$) is calculated by dividing the incoming irradiation at this wavelength ($I_{\text{AM1.5G},\lambda}$) given by the AM1.5G spectrum for Global Tilt, on the energy for one photon ($E_{\text{photon},\lambda}$), given by equation 1. This gives the number of incoming photons per second and area at a defined wavelength:

$$N_{\text{photons},\lambda} = \frac{I_{\text{AM1.5G},\lambda}}{E_{\text{photon},\lambda}} = \frac{I_{\text{AM1.5G},\lambda}}{hc/\lambda} \tag{30}$$

Where h is the Planck constant, c is the speed of light in vacuum and λ is the radiation wavelength.

This is conducted for the specified wavelength interval from 350 nm to 1100 nm with intervals of 10 nm. The total amount of incoming photons for the spectrum is the sum of all photons at given wavelengths:

$$N_{\text{photons},350-1100\text{nm}} = \sum_{\lambda=350}^{1100} N_{\text{photons},\lambda} \tag{31}$$

The weighted value (V_λ) for the different wavelengths equals the number of incoming photons at the specified wavelength, divided by the total number of incoming photons (from 350 nm to 1100 nm). It is expressed as:

$$V_\lambda = \frac{N_{\text{photons},\lambda}}{N_{\text{photons},350-1100\text{nm}}} \tag{32}$$

The transmittance, reflectance or absorptance at a defined angle of incidence (τ_θ, ρ_θ, α_θ) is calculated by summing the multiplied weighted value and the corresponding transmittance, reflectance or absorptance at the defined wavelength (from 350-1100 nm). This is expressed below, her represented by transmittance:

$$\tau_\theta = \sum_{\lambda=350}^{1100} V_\lambda * \tau_{\theta,\lambda} \tag{33}$$

The integrated value for AM1.5G Global Tilt for the wavelength interval from 350 nm to 1100 nm gives the total incoming irradiation ($I_{\mathrm{AM1.5G}}$). It is calculated by summing the multiplied weighted value (V_λ) with the corresponding incoming intensity ($I_{\mathrm{AM1.5G},\lambda}$). This is expressed by equation 33 above.

Chapter 2.3.4 explains how the transmittance, reflectance or absorptance are calculated based on the amount for either transmitted, reflected or absorbed radiation. By rearranging equations, the transmission, reflection or absorption at a defined angle of incidence is calculated as below, here represented by transmission ($I_{\mathrm{t},\theta}$):

$$I_{\mathrm{t},\theta} = \tau_\theta * I_{\mathrm{AM1.5G}} \tag{34}$$

τ_θ is the measured transmittance (reflectance or absorptance) at a defined angle of incidence and $I_{\mathrm{AM1.5G}}$ is the incoming irradiation for the defined wavelength interval (350 nm < λ < 1100 nm). The subscript t refers to transmission and is replaced with r and a for reflection and absorption, respectively.

4.3.7 Change in efficiency for a PV-module due to soiling, by EQE

Recall that the efficiency of a PV-module is highly dependent on the amount and energy of incoming photons. The expected reduction in efficiency is calculated based on External Quantum Efficiency (EQE) measurements (recall subchapter 2.2.3) performed at IFE for a representative c-Si solar cell, with an efficiency of η = 16.9 %.

The sum integral of the multiplied EQE_λ, the weighted value (V_λ, given by equation 32) and the change in transmittance ($\Delta\tau_{\lambda,\theta}$) is proportional to the change in efficiency, while the sum integral of the multiplied EQE_λ and weighted value is proportional to the efficiency of the PV-module. This can express the relative reduced efficiency at a specified angle of incidence ($\Delta\eta_\theta/\eta$) due to soiling, given by equation 35.

$$\frac{\Delta\eta_\theta}{\eta} = \frac{\sum_{\lambda=350}^{1100} \Delta\tau_{\lambda,\theta} * \mathrm{EQE}_\lambda * \mathrm{V}_\lambda}{\sum_{\lambda=350}^{1100} \mathrm{EQE}_\lambda * \mathrm{V}_\lambda} \quad (35)$$

The subscript λ and θ refers to the specific wavelength and angle of incidence, $\Delta\tau$ is the reduced transmittance, V is the weighted value and EQE is the defined External Quantum Efficiency for the given PV-cell.

The reduced efficiency due to soiling is calculated as:

$$\Delta\eta_\theta = \frac{\Delta\eta_\theta}{\eta} * 16.9\ \% \quad (36)$$

16.9 % is the efficiency of a representative c-Si solar cell at IFE, while $\Delta\eta$ refers to the change in efficiency due to the change in transmittance.

4.4 Soil analyses

The composition and distribution of the accumulated soil is examined employing a Scanning Electron Microscope (SEM). This subchapter describes the method used to conduct these studies. It aims to answer the following questions:

- What is the approximate size distribution of the dust grains?
- What are the main components of the accumulated soil at Kjeller?

The analyses are conducted on the small glass samples from the rooftop. The small samples are selected due to size limitations in the SEM. Soil analyses are conducted on two selected dates during the experimental period: surface scans on April 15 and point analyses on May 4.

4.4.1 Surface scans

The SEM is used to perform surface scans on the normal glass sample, to examine the soil grain size, distribution and important components. Because the surface of the glass sample is carbonized, optical measurements are conducted prior to the surface scan. This might affect the results from the SEM, due to the vertical position of the glass samples during optical measurements. Nevertheless, this is expected to represent the soil that stays on the glass sample during the optical measurements.

The surface scans are conducted at various areas and enlargements on the glass sample. This includes a scan of the entire surface, and close up scans of different dust grains. The results are exported to Excel for evaluation.

Note that results can only be used as an indication and not a representation for one week of soiling at Kjeller. This is because the surface scans are performed at one specific date during the examination period, and seasonal as well as weekly and daily variations will occur. The soil analyses were performed on April 15, a date prior to a week of little precipitation.

The glass sample is replaced at the rooftop, due to the carbonized surface.

4.4.2 Point analyses

Point analyses employing the SEM are conducted to identify important components in dust grains on normal glass samples after one week of soiling. An extra glass sample was placed at the rooftop one week prior to the measurements. This glass sample does not have to be used for optical measurements before the point analyses are conducted. Results will give an indication of important components in the soil at Kjeller.

The point analyses are performed by selecting different dust grains on the glass surface for evaluation. One point is directed at the glass sample for comparison. Different surface areas of the glass sample are investigated. Results from the point analyses are exported to Excel and analyzed.

Point analyses are conducted at May 4, a date prior to a week of little rain. Note that results can only be used as an indication and not a representation for important components after one week of soiling at Kjeller. This is because of the small data set, and seasonal as well as weekly and daily variations.

Recall that the SEM uses the X-ray microanalysis called Energy Dispersive Spectrometry (EDS) to evaluate the chemical composition. The results from the analyses are accepted, even though different components may result in overlapping energy peak (as noted in subchapter 3.4), which may result in incorrect components. The results are studied carefully to avoid these possible errors. A more likely element is selected if the EDS detects unlikely components with energy peaks overlapping with elements that are more common.

4.5 Polluting glass samples with artificial dust

The connection between dust density and reduced transmission is investigated by polluting normal glass samples with silicon dust and employing the Ocean Optics measurement equipment. This dust is selected based on results from the soil analyses. The Ocean Optics is chosen for these measurements, because it is important with a horizontal position during the measurements due to higher dust densities and gravitational forces.

This section explains the methodology used to pollute and investigate the glass samples. It aims to answer:

- Can a connection between dust density and change in transmittance be observed?
- Is there a pattern between dust densities and reduced transmittance at different angles of incidence?
- Are different wavelengths affected differently by the deposited soil?

4.5.1 Polluting the samples

Normal glass samples are polluted by letting silicon dust fall through a 6.3 cm diameter, 71.5 cm high cylindrical plastic tube. This approximates a natural and random fall, unaffected by wind circulation in the laboratory, and limits the polluted area. The pollutions are performed in the optical laboratory, to minimize movement. The polluted glass is a 10.5x10.5 cm square sample. It is a glass sample commonly used to cover PV-modules. The method is illustrated in figure 32.

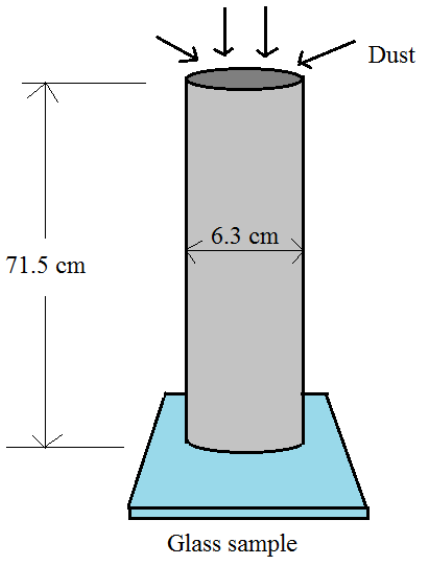

Figure 32: Polluting a glass sample with artificial dust. The dust falls through a tube to approximate a natural and random fall and to minimize the polluted area.

4.5.2 Soil density

The glass sample is weighted before the experiments are conducted, with the Mettler Toledo Excellence Plus weight. The optical equipment and the weight used during these experiments are located in different rooms in the laboratory at IFE. The amount of dust deposed at the glass sample is therefore quantified using rags, to minimize movement. Rags are weighted, soaked with Isopromanol Prima spirit and used to clean the polluted glass sample. They are dried in expanded polystyrene boxes, before they are weighted once more.

Dust density is calculated based on the mass difference measured by the rags and the cylindrical polluted surface area:

$$MD = \frac{M_{\text{after}} - M_{\text{before}}}{A_{\text{pipe}}} = \frac{\Delta M}{\pi r^2} \tag{37}$$

MD expresses the dust density, *M* is the mass of the rags (before and after they have cleaned the glass samples) and ΔM expresses the mass of the artificial dust. A_{pipe} is the circle surface area of the cylindrical tube, expressed by the inner radius, *r*.

4.5.3 Transmittance measurements

Transmittance measurements are conducted with the Ocean Optics equipment. It gives transmittance as a function of wavelength and angle of incidence. This equipment is selected because it allows the glass samples to stay in a horizontal position during measurements. This is an important property during this experiment, because accurate dust densities are important. In addition, the gravitational effect is expected to be higher than for natural accumulated soil because the dust grains and soil densities are larger.

The wavelength spectrum is set to span from 350 nm to 1100 nm, and the angle of incidence is varied between 0˚, 18˚, 36˚, 54˚ and 72˚, based on the semicircular devise in figure 26. To investigate the change in transmittance, an initial transmittance measurement on clean glass sample at the different angles of incidence, is conducted. Then, the glass sample is polluted (as explained in 4.3.1), and the transmittance is measured. Four different soil densities are investigated. These densities are higher than the natural soil deposition after one week of exposure at Kjeller. This is because the accumulated soil is expected to increase with time.

Two optical measurements employing the Ocean Optics setup were performed on a clean glass sample prior to the experiments. These initial results did not provide unequivocal results. The transmittance difference at 18˚ angle of incidence, weighted against the AM1.5G spectrum for Global Tilt (see subchapter 4.3.6), was approximately 2 %.

5 Results and discussion

This chapter presents and discusses results obtained by applying the theory given in chapter 2 and the methodology described in chapter 4. First, theoretical values for BK7-glass are presented, before initial optical measurements on the clean glass samples are given. Then, weather data, mass and optical measurements and results from the soil analyses are presented, before the experiment with artificial dust is given.

5.1 Theoretical insolation and optical values for glass

The solar spectrum outside Earth's atmosphere is attenuated by atmospheric effects. The solar intensity available for a PV-module with a tilt angle of 37° facing the equator is presented in subchapter 5.1.1.

The transmittance through glazing samples varies with factors like thickness, refractive index and absorption coefficient, and will therefore vary for different glass samples. BK7 is a glass type, which is well characterized. It is therefore used to calculate expected optical values for the glass samples. These results are given in subchapter 5.1.2.

5.1.1 Incoming radiation, based on the AM1.5G spectrum

The sum integral for AM1.5G spectrum for Global Tilt [41], for wavelengths in the interval from 350 nm to 1100 nm, is calculated based on the theory presented in chapter 4.3.6. This gives incoming solar radiation on an inclined plane at 37° tilt toward the equator, facing the sun:

$$I_{\mathrm{AM1.5G}} = 761.8\ \mathrm{W/m^2}$$

5.1.2 Theoretical optical values for BK7 glass

The theoretical transmittance, reflectance and absorbance for BK7-glass are used as a representation for normal glass. BK7-glass is selected because it is well characterized. Relevant values for the refractive index (n) and the absorption coefficient (K) are given in Appendix A, along with calculated transmittance values shown in graph 4 and 5. Recall that BK7-glass is designed to have a very low absorption.

Graph 4 shows the theoretical transmittance as a function of angle of incidence and wavelength for BK7-glass. Due to the scaling of the y-axis, the wavelength dependence is not noticeable. Therefore, graph 5 shows the transmittance for a section of incoming angles to emphasize how transmittance depends on the wavelength.

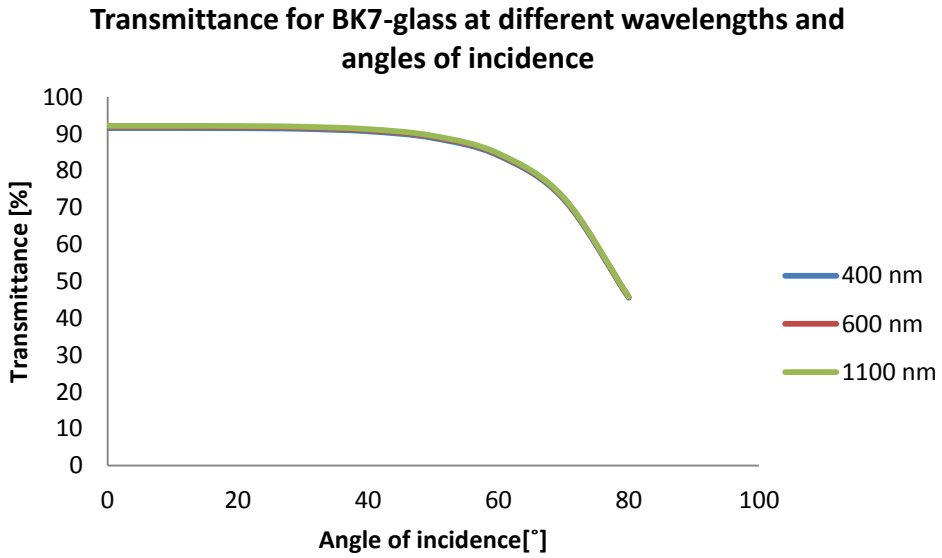

Graph 4: Calculated transmittance of BK7-glass based for different angles of incidence and wavelengths of 400 nm, 600 nm and 1100 nm. BK7-glass is considered as a glass with high transmittance.

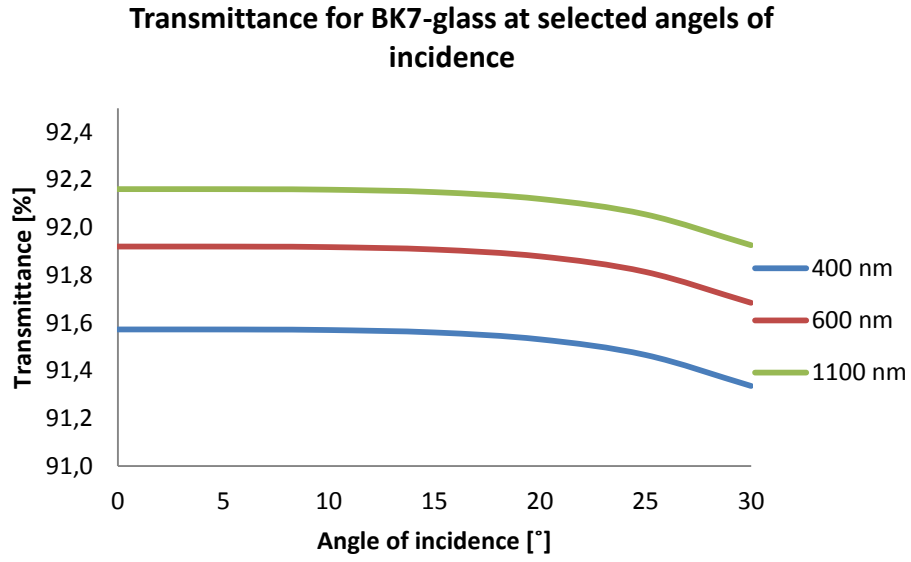

Graph 5: Calculated transmittance for BK7-glass at a section of incoming angles of incidence, to show how transmittance depends on wavelength.

The theoretical transmittance, reflectance and absorptance, as well as the amount of transmitted radiation for BK7-glass are weighted towards the AM1.5G spectrum for the wavelength spectrum 400 nm < λ < 1100 nm. Reflectance is calculated for two interfaces (front and back) of the glass. Results for 20˚ and 70˚ angles of incidence are given in table 2 below:

Glass sample	**Transmission, I_t [W/m^2]**	**Transmittance, τ [%]**	**Reflectance, $\rho_{specular}$ [%]**	**Absorptance, α [%]**
BK7-glass 20˚ incidence	700.1	91.9	8.1	0.0
BK7-glass 70˚ incidence	553.0	72.6	27.3	0.1

Table 2: Theoretical values for BK7-glass at an angle of incidence of 20˚ and 70˚.

Graphs 4 and 5 show the connection between increasing angle of incidence and decreasing transmittance, with a steeper decrease in transmittance from about 55°. In addition, graph 5 shows how transmittance depends on wavelength, and is expected to increase with increasing wavelength, in the defined wavelength interval. This statement holds for increasing wavelengths until about 1600 nm, before the transmittance decreases [42] with wavelength.

Recall that Fresnel's equations apply to smooth surfaces, and describe specular reflectance of unpolarized radiation as it interacts between media of different refractive indexes. This implies that there are no diffuse reflectance for the theoretical transmittance given in graph 4 and 5. However, any real glass surface is expected to have imperfections and some impurities on the surface, like dust. This means that reflectance consists of both specular and diffuse reflectance for most real surfaces. Optical values for any real surface are therefore expected to differ slightly from these values.

Theoretical absorptance for BK7-glass is approximately zero at all wavelengths and angles of incidence, which means that there is (theoretically) almost no absorbed light in this glass. This is because BK7-glass is designed to have these characteristics (low absorptance). This is not common for glass covering PV-cells, due to expenses. It is therefore expected that some absorptance will occur in the glass samples used during these experiments. Note that the calculations are conducted for a wavelength interval from 400-1100 nm.

5.1.3 Subchapter summary

This subchapter shows that the transmittance for BK7-glass is approximately 91.9 % at 20˚ angle of incidence, with increasing transmittance for longer wavelengths. It shows that the transmittance reduces with increasing angle of incidence, due to increasing reflectance. This reduction increases more rapidly from about 55˚.

It is likely that the absorptance is higher for the glass samples used during these experiments than the calculated values for BK7-glass. In addition, the reflectance is expected to consist of both specular and a diffuse reflectance. It is therefore reasonable to assume that the transmittance will differ.

5.2 Initial optical measurements on clean glass samples

This subchapter presents the results from measurements conducted on both normal glass and anti-soiling (TripleO) coated glass, before the samples are placed on the rooftop. It employs the methodology from subchapter 4.3. Measurements include:

- Specular reflectance from both interfaces (front and back side)
- Transmittance through the glass
- Absorptance in the glass
- Transmittance by polarized light

The measurements are conducted using the Angular Dependent Reflection and Transmission Measurement (ADRTM) setup and the ellipsometer. The equipment is described in chapter 3. Mean values are presented for the duplicated measurements.

The results from the experiment with polarized incoming radiation are found in Appendix C.

5.2.1 Initial specular reflectance measurements

The ellipsometer gives specular reflectance from both interfaces of the glass sample (front and back), as a function of wavelength, angle of incidence and polarization state. The glass samples are clean, and specular reflection is expected to represent the greatest part of the global reflection. Results for normal glass (blue tones) and anti-soiling glass (red tones) are presented in graph 6. Table 3 presents the specular reflectance weighted towards the AM1.5G spectrum for Global Tilt, for the normal and anti-soiling coated glass samples at 20° and 70°.

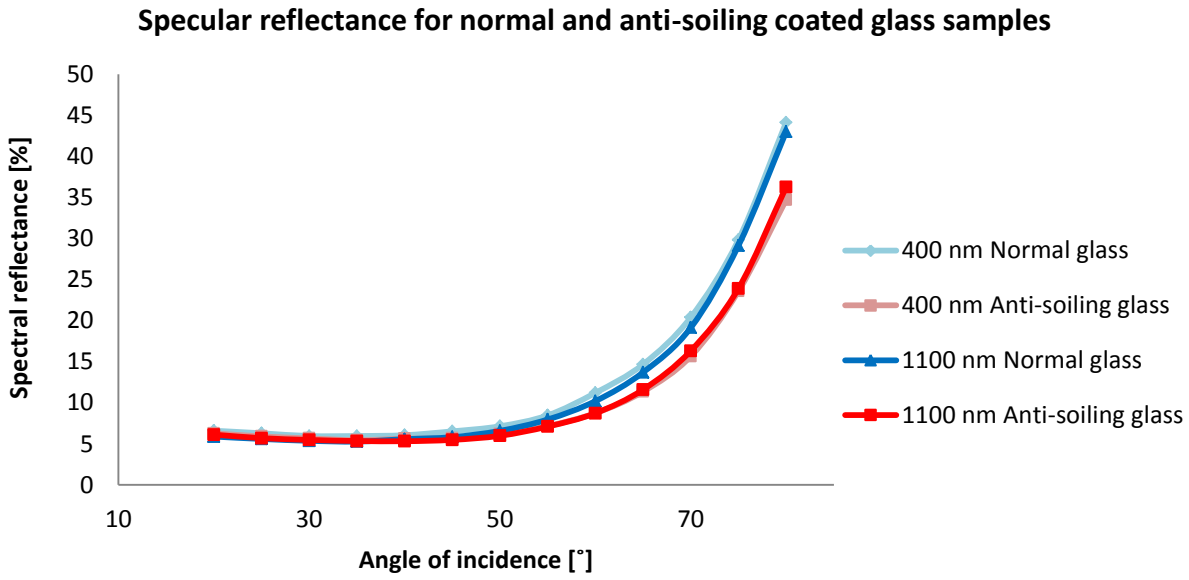

Graph 6: Measured specular reflectance for normal and anti-soiling coated glass samples employing the ellipsometer. Measurements are conducted from 20° to 80° angle of incidence.

As noticeable in graph 6 above, the specular reflectance is approximately equal for the normal and anti-soiling coated glass samples at smaller (approximately 20˚-55˚) angles on incidence. This changes at about 55˚, the same angle of incidence as the transmittance starts to decrease more rapidly (graph 4). It appears as if the anti-soiling coated glass samples have some anti-reflection function at higher angles of incidence.

A lower specular reflectance is mainly caused by either a rough surface, or differences in the refractive indexes (*n*), due to the anti-soiling coating.

A rough surface decreases the flat and smooth area, which gives specular reflectance. This reduces the portion of specular reflectance, and may increase the diffuse reflectance. A rough surface is expected to have lower specular reflectance values at all angles of incidence, but it is unknown, in this study, if the decrease in specular reflectance increases at higher angles of incidence. Lower specular reflectance is not noticed for angles below 40˚. However, it is expected that higher angles of incidence will be more sensitive to additional “bumps”, due to the larger illuminated surface area, as illustrated in figure 33. This effect increases at higher angles of incidence, because the radiation is spread at a larger surface area.

Figure 33: The incoming radiation is spread over a larger surface area at increasing angles of incidence.

Note that the diameter of the incoming beam radiation and the surface area of the detector are small. The area of interaction on the glass sample is therefore important, and hence these measurements detect variations in reflection over a very small area that may not be representative for the average surface area.

Changes in the refractive indexes affect the portion of specular reflectance differently at different angles of incidence, recall subchapter 2.3. From the measurements and theoretical considerations performed in this work. It is not possible to conclude on the nature of the anti-soiling coating.

	20˚ incidence			**70˚ incidence**		
Glass sample	BK7-glass	Normal	Anti-soiling	BK7-glass	Normal	Anti-soiling
Specular reflectance, $\rho_{specular}$ [%]	8.1	6.2	6.2	27.3	19.7	16.3

Table 3: Initial specular reflectance for the clean normal and anti-soiling coated glass samples. The table also include theoretical calculated specular transmittance for BK7-glass.

Table 3 shows that the measured specular reflectance is generally lower than the theoretical calculated specular reflectance for BK7-glass. One possible explanation is that imperfections will occur on both glass samples, reducing the specular reflectance for the normal and anti-soiling coated glass at all angles of incidence. The detector area is small, and only perfectly specular reflected radiation is detected.

The diffuse reflection has not been examined during this study, and further research is needed to investigate how the anti-soiling coating acts at higher angles of incidence. It is also suggested that the surface structure is investigated in more details.

5.2.2 Transmittance

Graph 7 presents the measured initial transmittance as a function of angle of incidence for normal and anti-soiling coated glass samples. Graph 8 presents the same measurements as a function of wavelength at 20˚ and 70˚ angles of incidence. The transmittance for normal glass samples are given by the blue curves, while the transmittance for the anti-soiling coated glass samples are given by the red curves. The methods are described in subchapter 4.3. Measured values are weighted towards the AM1.5G spectrum and presented in table 4.

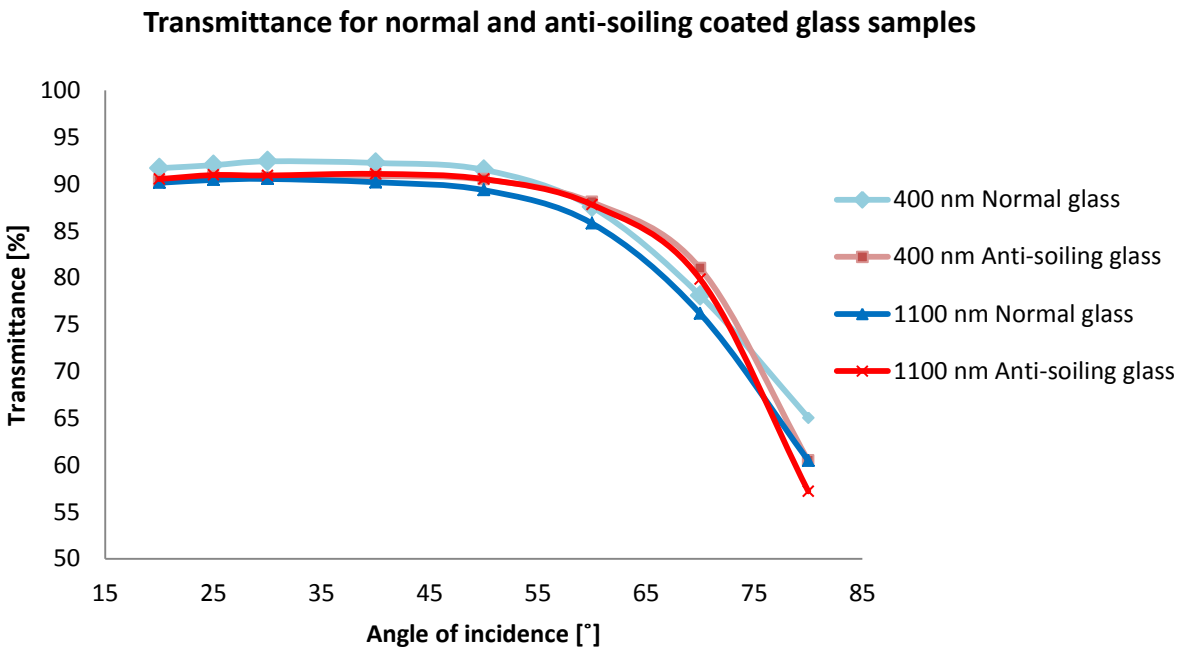

Graph 7: Measured transmittance as a function of angle of incidence for the normal and anti-soiling coated glass samples at 400 nm and 1100 nm. These measurements are conducted at clean glass samples.

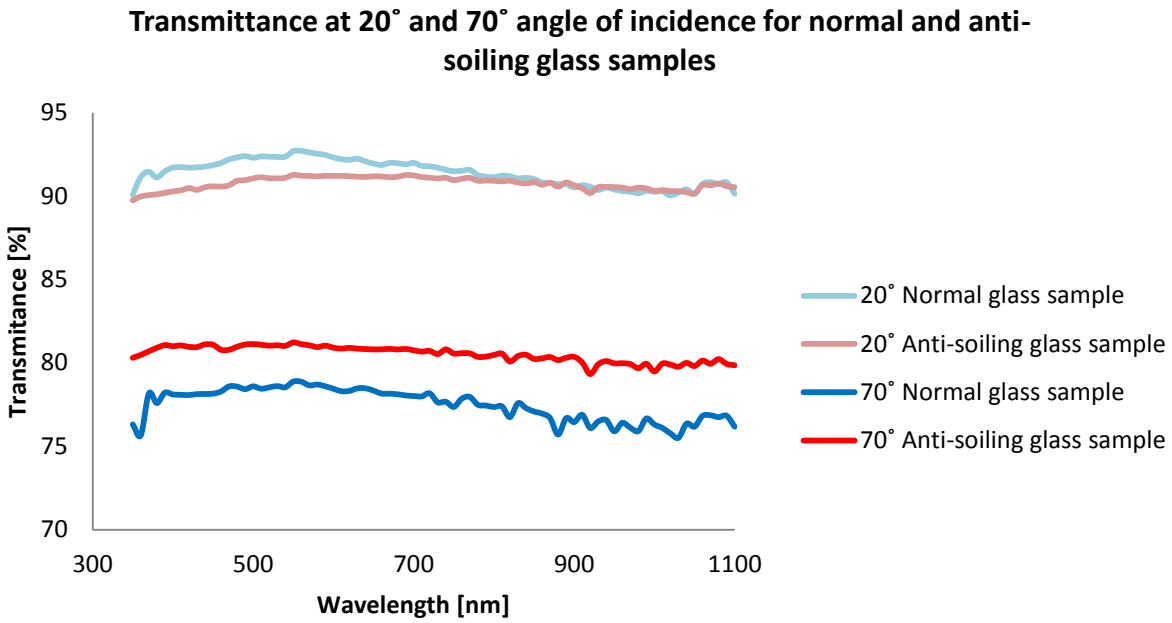

Graph 8: Measured transmittance at 20˚ and 70˚ angle of incidence, for both normal and anti-soiling glass samples. These measurements are conducted at clean glass samples.

As seen in graph 7, the measured transmittance is higher for the normal glass samples than for the anti-soiling coated glass samples at lower angles of incidence (20˚ in graph 8). This is most apparent at shorter wavelengths. One explanation is that the extra coating attenuates the amount of transmitted light, because the incoming beam radiation has to penetrate an additional coating. From table 4 below, it is seen that the absorptance is higher for the anti-soiling coated glass at lower angles of incidence.

At higher angles of incidence, from about 55˚, the transmittance is higher for the anti-soiling coated glass samples. This shift can be explained by the lower absorptance, but mostly by the reduced specular reflectance, as seen in graph 6. Recall that the transmittance measurements are based on the sum of transmittance and global reflectance from the ADRTM minus the specular reflectance from the ellipsometer, because the majority of the reflectance was assumed specular. The lower specular reflectance at higher angles of incidence for the anti-soiling coated glass will therefore result in a higher measured transmittance. The amount of diffuse reflectance is unknown and would have to be investigated before conclusions about the transmittance can be drawn. Table 4 below presents the optical values, weighted towards the AM1.5G spectrum. The difference between measured transmittance for the glass samples and BK7-glass is discussed below table 4.

It appears as if the measured transmittance is higher at shorter wavelengths. This contradicts with the theoretical calculated values for BK7-glass. This follows from the measured sum of

transmittance and global reflectance employing the ADRTM, shown in Appendix B. The same pattern is noticed throughout the experimental period, and implies that the absorptance increases with increasing wavelength. This measure uncertainty is accounted for by subtraction when changes are investigated.

	Glass sample	Transmission, I_t [W/m^2]	Transmittance, τ [%]	Specular reflectance, $\rho_{specular}$ [%]	Absorptance, α [%]
20° incidence	BK7-glass	700.1	91.9	8.1	0.0
	Normal	697.0	91.5	6.2	2.3
	Anti-soiling	691.7	90.9	6.2	2.9
70° incidence	BK7-glass	553.0	72.6	27.3	0.1
	Normal	591.2	77.6	19.7	2.7
	Anti-soiling	614.0	81.4	16.3	2.3

Table 4: Optical values for BK7, normal and anti-soiling glass at 20˚ and 70˚ angle of incidence. Measurements are conducted on clean glass samples, and include specular reflectance (ρ), absorptance (α) and transmittance (τ).

Recall that the transmittance (τ) is calculated based on the sum of transmittance and global reflectance from the ADRTM minus the spectral reflectance from the ellipsometer. As seen in table 4 and discussed in subchapter 5.2.1, the specular reflectance is lower for the normal and anti-soiling coated glass samples than for the BK7-glass. It is therefore assumed that the real transmittance values for the normal and anti-soiling coated glass samples might be lower than the values given in table 4.

However, the measured absorptance for the normal and anti-soiling coated glass samples are higher than the absorptance for BK7-glass. One explanation is that BK7-glass is designed to have low absorptance. Another explanation is that the absorptance measurements are conducted employing the center-mount configuration of the integrating sphere, and the radiation is reflected diffusely at the inner walls of the sphere before it is detected. This allows for more absorption. The higher absorptance results in a lower calculated transmittance.

The difference between the transmittance for normal and anti-soling coated glass samples and the transmittance for BK7-glass is greatest at higher angles of incidence. Recall that the transmittance due to the natural pollution of glass samples is conducted at 20˚ angle of incidence, and focuses on the change in transmittance.

5.2.3 Subchapter summary

This subchapter presents initial optical measurement for the normal glass and the anti-soiling (TripleO) coated glass samples. It appears as if the anti-soiling coating has some anti-reflection function at higher angles of incidence, likely due to changes in the refractive indexes and possibly more impurities at the surface. However, diffuse reflectance has not been detected. It has to be investigated before conclusions can be made.

The transmittance at 20° angle of incidence is about 91.5 % and 90.8 % for normal and anti-soiling coated glass, respectively. This means that the transmittance for the anti-soiling coated glass samples is about 1 % lower than the transmittance for the normal glass samples. It seems like imperfections occur on both the normal and anti-soiling coated glass samples, resulting in a lower specular reflectance than for BK7-glass.

5.3 Weather data and observations

This subchapter presents downloaded precipitation data for the experimental period and expected monthly precipitation based measurements from 1961-1990. It also presents observations made on the glass samples.

5.3.1 Weather data

The experiments in this study are carried out from the end of February to the end of April 2015, and relevant precipitation data is presented in graph 9 [43]. The weather station is located at Skedsmo, close to Kjeller. There were no wind measurements available. Graph 10 shows the mean monthly precipitation at the weather station, based on daily measurements from 1961-1990. A graph showing the mean daily precipitation for the given weeks is found in Appendix D, along with an excerpt from the research log.

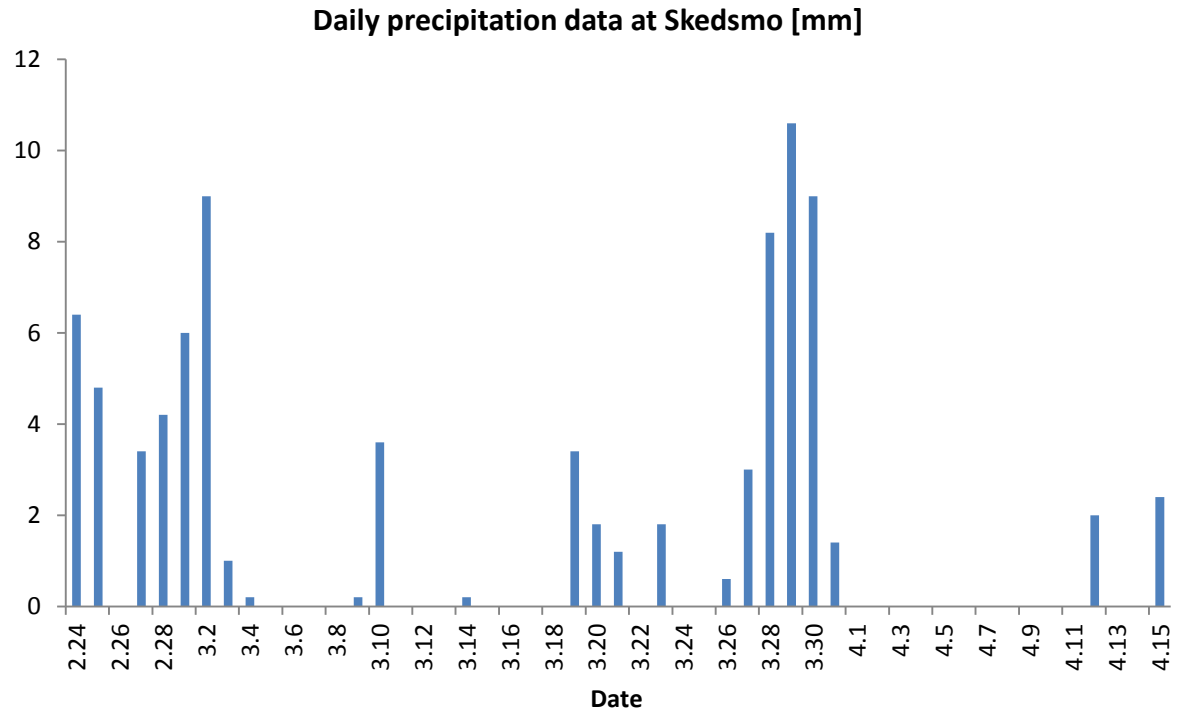

Graph 9: Daily (1 am-12 pm) precipitation [mm] from Skedsmo, Akershus. Data is downloaded from eKlima **[43]**.

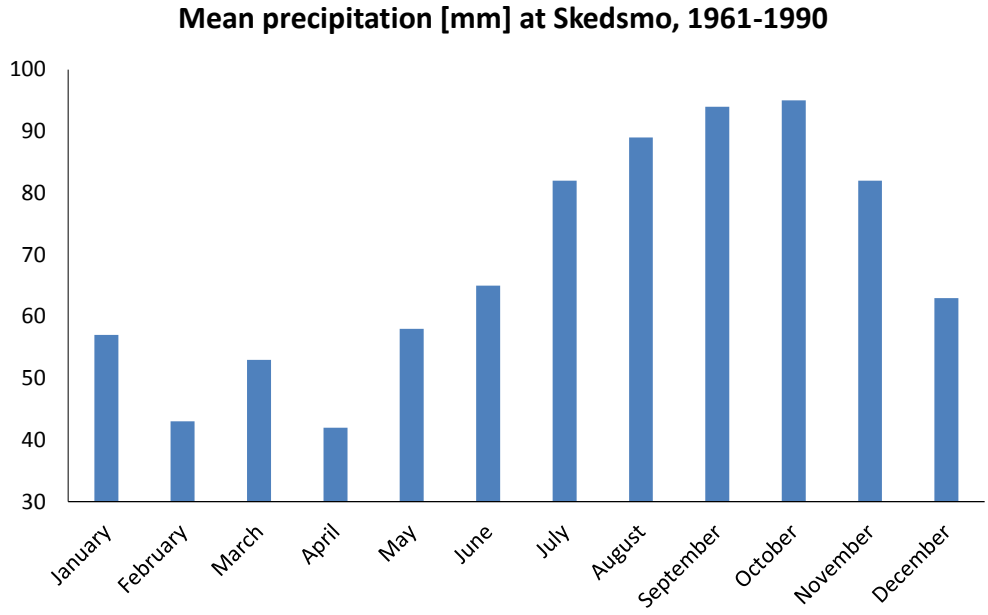

Graph 10: Mean precipitation [mm] for different months at Skedsmo. Data is based on measured daily values from 1961-1990. More recent data for Skedsmo was not available at eKlima **[44]**.

Graph 9 shows how precipitation varies throughout the experimental period. The downloaded data gives daily values, from 1 am to 12 pm. It is therefore not possible to determine the amount of precipitation that come before mass and optical measurements are conducted. Graph 10 shows the mean precipitation values for a given month, based on data from 1961-1990 at Skedsmo. More recent data are not available, but this graph is assumed to give a good representation of the expected precipitation throughout a year.

Most measurements are conducted in March. This month had approximately 61 mm of precipitation, which seems to be a representative amount of rainfall at this month for a normal year.

5.3.2 Observations

Figure 34 shows how dew forms on the surfaces of both normal (top sample) and anti-soiling (bottom sample) glass. Recall that no data sheets are available for the anti-soiling (TripleO) coating. It is noticed that more water accumulate on the coated samples, and that the water droplets are more spherically shaped. This indicates that the anti-soiling coating is a hydrophobic material. These observations were noticed for all glass samples, when dew or precipitation was present. This is described in the research log, Appendix D.

Figure 34: Two glass samples from the rooftop at IFE, Kjeller. The top sample is a normal glass sample, while the bottom sample is coated with the anti-soiling coating, TripleO.

5.4 Quantified natural soil deposition

This subchapter presents results regarding the quantified natural accumulated soil at Kjeller. Measurements are conducted on the normal and anti-soiling coated glass samples placed at the rooftop of IFE, at Kjeller. The methodologies are given in subchapter 4.2. All measurements are based on one week of soiling.

5.4.1 Quantification of the weekly accumulation of soil

This subchapter presents the results from mass measurements on the glass samples and rags. The change in soil density due to cleaning (MD_C) is presented in table 5 below. This soil density is expected to equal the amount of soil that stays on the glass samples during the optical measurements. The total accumulated soil density on the glass samples (MD_{total}) due to one week of natural soiling is given in table 6. Recall that the weight has an accuracy of 0.1 mg and that statistical uncertainties are not calculated, due to only two measurements per sample. A picture of the rags used for one cleaning event is shown in figure 35, with rag 2 being unused. More pictures are given in Appendix D.

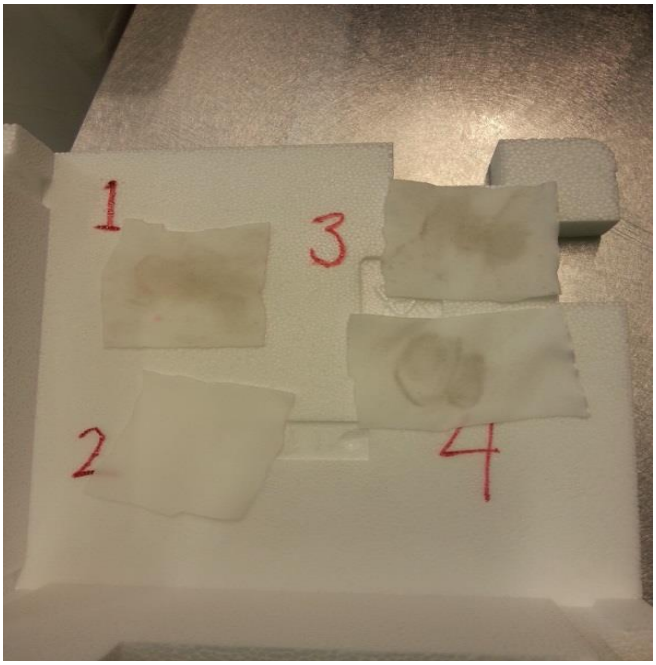

Figure 35: Rag 1, 3 and 4 after cleaning a 17x17 cm glass sample exposed to one week of soiling at Kjeller. Rag 2 is unused.

Glass sample \ Date	03.03	10.03	17.03	24.03	31.03	07.04	14.03
MD_C Normal glass [mg/m^2]	21	12	60	41	22	73	85
MD_C Anti-soiling glass [mg/m^2]	36	29	102	60	29	90	75

Table 5: The soil density that is cleaned off from the glass samples by rags, MD_C. for both normal and anti-soiling coated glass samples. This is assumed to be the amount of soil that stays on the glass samples during the optical measurements.

Glass sample \ Date	03.03	10.03	17.03	24.03	31.03	07.04	14.03
MD_{total} Normal glass [mg/m^2]	42	35	91	62	35	113	90
MD_{total} Anti-soiling glass [mg/m^2]	48	59	123	87	42	128	113

Table 6: The total accumulated soil density (MD_{total}), for both normal and anti-soiling coated glass samples, due to one week of natural soiling at Kjeller.

Table 6 above shows a higher accumulation of soil on the anti-soiling coated glass samples at all dates. The TripleO coating does not seem to work as intended at Kjeller. Recall that anti-soiling coating can be referred to as a "self-cleansing coating", meaning that it helps clean the glass samples by exploiting rainfall. Graph 11 shows daily precipitation data and the total accumulated soil density after one week of exposure. The difference between soil density for the normal and anti-soiling coated glass samples are smaller at dates associated with high precipitation. This indicates that the TripleO coating needs higher precipitation levels to clean the glass samples at Kjeller. TripleO might be more suited for areas or periods exposed to more rain, and further research is needed. Note that these results cannot be generalized, because soil composition and precipitation will vary with location and period.

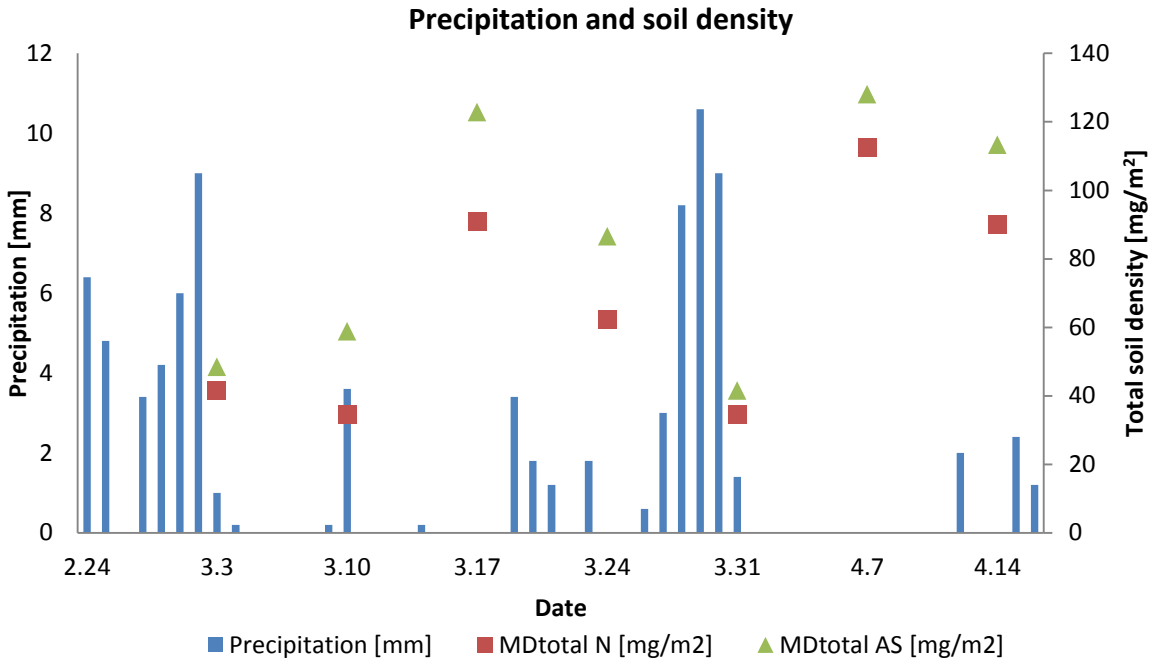

Graph 11: Daily precipitation data from eKlima and total accumulated soil density (MD_{total}) for the normal (N) and anti-soiling coated (AS) glass samples.

There are noticeable variations in weekly accumulation of soil, and a clear pattern between soil density and precipitation is noticed in graph 11. Other studies have mainly focused on the connection between efficiency, power output or transmittance reduction due to soiling and precipitation data. However, these studies seem to notice similar connections as noticed above [24] [28], that rainfall helps clean the glass samples. March 17 and April 7 follow weeks with little or no precipitation, and the soil density is greatest. March 3 and 31 follow weeks with high precipitation levels. These dates are characterized by a smaller amount of accumulated soil. However, approximately the same soil density is measured on March 10. This date follows a week with little precipitation, but with heavy rain the same day. A possible explanation is that rain above 3.6 mm is sufficient to clean the glass samples to a level of saturation at Kjeller.

Because the precipitation data are day-values, it is not possible to know the amount of rain that came before the measurements were conducted. The suggested amount of rain sufficient to clean the glass samples might therefore be less. Caron and Littmann investigated energy losses from PV-modules due to soiling in California [26]. They found that as little as 0.5 mm of rainfall is sufficient to clean a dirty module until the point of saturation in regions with lighter soiling rates. This result does not transfer directly to Kjeller. Nevertheless, it gives an indication of how little rain might be sufficient. Other results [28] give precipitation thresholds above 5 mm for more dense soiling depositions, which shows the importance of local measurements.

March 3, 10 and 31 follow, as noted above, after much precipitation, but it seems like rainfall is not sufficient to clean the glass samples completely. It appears as if the soil level is partially cleaned until a point of saturation. Research conducted on PV-modules in both California [26] and Belgium [24] states that the soil level (decrease in power production due to soiling) does not fully recover from rain alone. A suggested saturation level, for the weekly accumulation of soil on glass samples exposed to rain levels above 3.6 mm, is based on the mean value from these three weeks. This gives a soil densities for weeks exposed to rain of 37 mg/m^2 and 50 mg/m^2 for the normal and anti-soiling coated glass samples, respectively.

As noted above, March 17 and April 7 follow weeks with little or no precipitation. A mean soil density based on these two dates is suggested as the accumulated soil density due to one week of almost no rain at Kjeller. This gives soil densities of 120 mg/m^2 and 125 mg/m^2 for the normal and anti-soiling coated glass samples, respectively.

This soil density for weeks with no rain is about 275 % and 250 % of the soil density for weeks exposed to heavy rain, for the normal and anti-soiling coated glass samples, respectively. The difference underlines the cleaning effect from rainfall.

Because rain seems to have little cleaning effect on smaller dust particles (2-10 μm), but great effect on larger particles (~60 μm) [24], there is reason to believe that rainfall at Kjeller partially cleans the glass samples, leaving smaller particles on the samples. This statement needs to be investigated in a particle size analysis.

5.4.2 Weekly soil densities

Mean results for the mass change due to optical measurements ($\overline{\Delta M}_{\mathrm{OM}}$), the mass change due to the cleaning of the glass samples ($\overline{\Delta M}_{\mathrm{C}}$) and the total accumulated soil ($\overline{\Delta M}_{\mathrm{total}}$) are presented as soil densities in table 7 below.

Mean soil density	**Normal glass**	**Anti-soiling glass**
$\overline{MD}_{\mathrm{OM}}$ [mg/m^2]	21	28
$\overline{MD}_{\mathrm{C}}$ [mg/m^2]	49	66
$\overline{MD}_{\mathrm{total}}$ [mg/m^2]	67	86

Table 7: Mean results from mass measurements for both normal and anti-soiling coated glass samples. $\overline{MD}_{\mathrm{OM}}$ represents the mean soil density that falls off due to optical measurements, $\overline{MD}_{\mathrm{C}}$ represents the mean soil density that is cleaned off by the rags and $\overline{MD}_{\mathrm{total}}$ represents the mean total accumulated soil density.

These results show that about 32 % of the soil falls off due to optical measurements, for both normal and anti-soiling coated glass. It is unknown whether this soil falls off before, during or after the optical measurements are conducted, and how this might affect results from the optical measurements. Nevertheless, it is suspected that the soil falls off before the optical measurements are conducted. Hence, the amount of soil that stays on the glass samples during optical measurements is assumed to equal the amount of soil that is cleaned off (MD_C). These values are presented in table 5.

Table 7 shows that the total accumulated soil density on the anti-soiling coated glass samples is about 29 % higher than the total accumulated soil density on the normal glass samples. This again underlines how the anti-soiling coated glass samples do not seem to work as intended at Kjeller during this period.

5.4.3 Subchapter summary

The weekly accumulation of soil is greater for the glass samples coated with TripleO than for the normal glass samples. Mean values show that the total accumulated soil density on the anti-soiling coated glass samples is about 29 % higher than the total accumulated soil density on the normal glass samples. This indicates that this anti-soiling coating does not work as intended at Kjeller during this period. It is suspected that the anti-soiling coating needs higher levels of precipitation to work as planned. This is because the difference between the accumulated soil for the normal and anti-soiling coated glass samples are smaller after much rain.

A clear pattern between the accumulation of soil and precipitation is detected. These observations agree with other research results. It looks like rain cleans the glass samples until a point of saturation. This saturation point is about 37 mg/m^2 and 50 mg/m^2 per week for normal glass samples and samples coated with TripleO, respectively. 3.6 mm of rainfall seems sufficient to clean the samples until the point of saturation. Note that this precipitation level is a day-value. It is therefore unknown if parts of this rain falls before measurements were conducted.

One week of little/no rainfall resulted in a soil density of approximately 102 mg/m^2 and 125 mg/m^2 for the normal and anti-soiling coated glass samples. This is 276 % and 250 % of the soil density for weeks with heavy rain.

Mean results show that approximately 32 % of the accumulated soil falls off due to optical measurements. It is assumed that this soil falls off prior to the measurement. Hence, the amount of soil present during optical measurements is assumed to equal the amount of soil that is cleaned off.

5.5 Optical measurements on the natural polluted glass samples

This subchapter presents results from the optical measurements on the glass samples exposed to natural soiling at Kjeller. First, the weekly measurements are presented. This includes specular reflectance and transmittance. Then, results from the glass samples exposed to four and eight weeks of soiling are given. Finally, the calculated reduced efficiency is presented. The methodologies are described in subchapter 4.1 and 4.3.

5.5.1 Change in specular reflectance due to one week of soiling

The weekly specular reflectance measurements are compared to the initial measurements on the clean glass samples. The changes in specular reflectance are presented in graph 12 and 13, for normal and anti-soiling coated glass samples at 600 nm. This is a representative wavelength. Results from March 3 are not given, because ellipsometer measurements were not conducted. Changes in specular reflectance below zero imply that the measured specular reflectance is less than the initial specular reflectance measurement on clean glass samples. The specular reflectance at 20˚ and 70˚ angle of incidence is weighted towards the AM1.5G spectrum for Global Tilt, for both the normal and anti-soiling coated glass samples. The results are given in table 8.

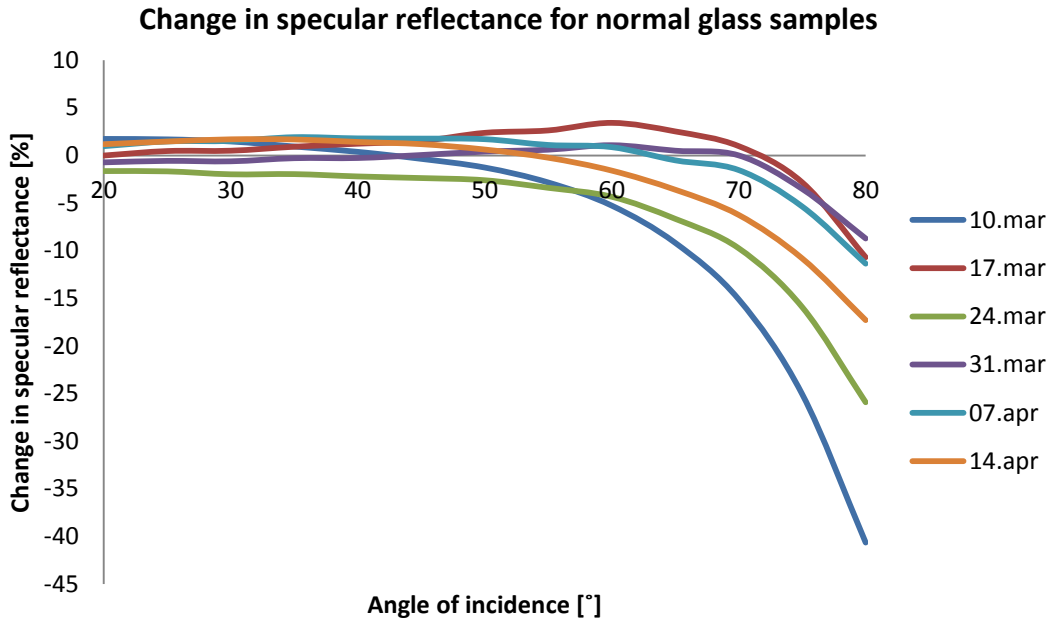

Graph 12: Change in specular reflectance at 600 nm, measured by the ellipsometer on the normal glass samples exposed to one week of soiling. Measurements are conducted at different dates.

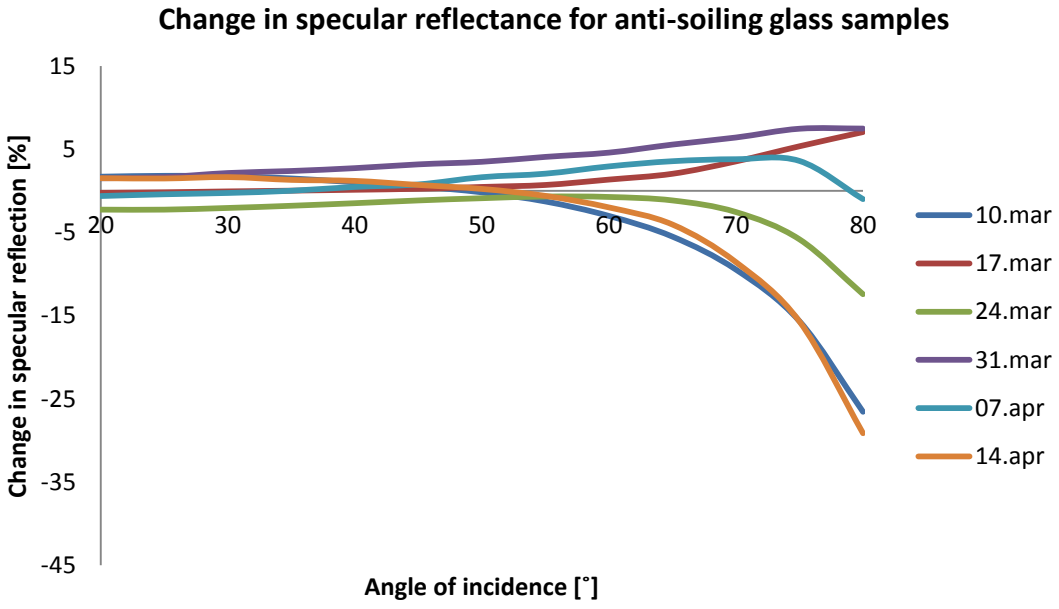

Graph 13: Change in specular reflectance at 600 nm, measured by the ellipsometer on the anti-soiling glass samples exposed to one week of soiling. Measurements are conducted at different dates.

Soil deposition on the glass samples leads to impurities on the surfaces and reduces the smooth and flat surface area, which reduces the specular reflectance. It is therefore expected that the specular reflectance decreases at all angles of incidence. This change in specular reflectance can increase at higher angles of incidence, due to the increased illuminated surface area (as discussed in subchapter 5.2.1), or due to other factors, like the unknown surface structure of the soil impurities. Graph 12 shows how the change in specular reflectance for the normal glass samples seems to fit with expectations.

As seen in graph 12 and 13, the change in specular reflectance is sometimes positive, for both glass samples, meaning that there is an increase in specular reflectance. One possible explanation is that imperfections on both the clean normal and anti-soiling coated glass samples will exist, as discussed in subchapter 5.2.1, resulting in a possibly lower initial specular reflectance measurements. Recall that the equipment is sensitive to surface variations, due to the narrow beam radiation and the small surface area of the detector.

No pattern for the change in specular reflectance for the anti-soiling coated glass samples are noticed at higher angles of incidence. The change in specular reflectance is sometimes positive (increase in specular reflectance) and sometimes negative (decrease in specular reflectance).

Date	**20˚**		**70˚**	
	$\boldsymbol{\rho_N}$ **[%]**	$\boldsymbol{\rho_{AS}}$ **[%]**	$\boldsymbol{\rho_N}$ **[%]**	$\boldsymbol{\rho_{AS}}$ **[%]**
03.03.15	-	-	-	-
10.03.15	7.9	7.8	4.7	6.8
17.03.15	6.4	6.0	20.7	19.9
24.03.15	4.7	3.9	10.0	13.6
31.03.15	5.5	7.7	19.6	22.4
07.04.15	7.4	5.7	18.3	20.3
14.04.15	7.2	7.6	13.3	7.8
MEAN	**6.5**	**6.5**	**14.4**	**15.1**

Table 8: Optical specular reflectance measurements for normal ($\boldsymbol{\rho_N}$) and anti-soiling coated ($\boldsymbol{\rho_{AS}}$) glass samples at 20° and 70° angle of incidence, after one week of soiling at Kjeller. Measurements are conducted at different dates.

The specular reflectance for the natural polluted glass samples seems to be grater for the anti-soiling coated glass at higher angles of incidence. However, no conclusions about the total reflectance can be drawn, due to the lacking measurements on diffuse reflectance.

Measured specular reflectance at 70° angle of incidence are plotted against the soil density for the glass samples during optical measurements (MD_C) and presented in graph 14 and 15 for the normal and anti-soiling coated glass samples, respectively. The red points represent the initial measured specular reflectance for the clean glass samples.

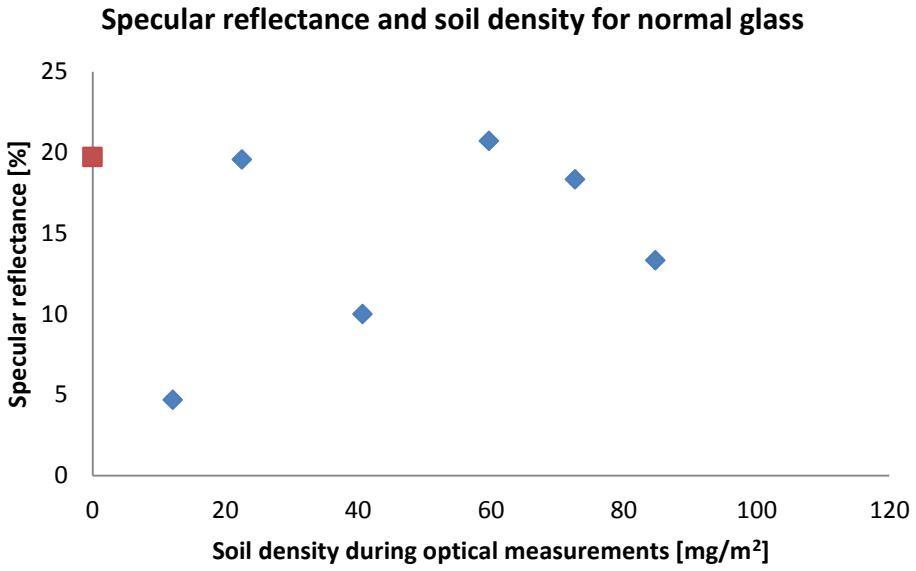

Graph 14: Measured specular reflectance at 70˚ angle of incidence and soil density present during optical measurements (MD_C) for the normal glass samples at different dates. The red point represents the initial measured specular reflectance for the clean glass samples.

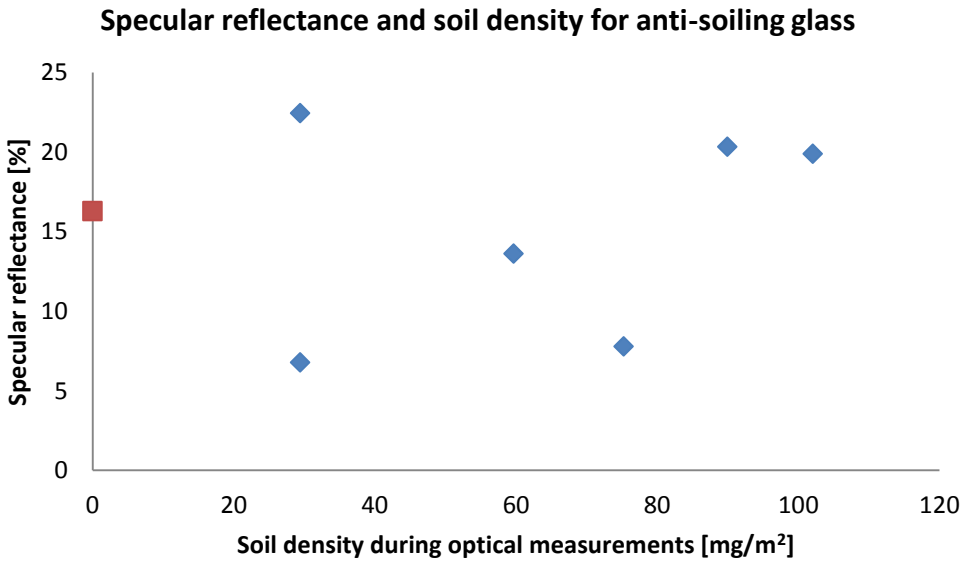

Graph 15: Measured specular reflectance at 70˚ angle of incidence and soil density present during optical measurements (MD_C) for the anti-soiling coated glass samples at different dates. The red point represents the initial measured specular reflectance for the clean glass samples.

It does not seem to be any clear relation between soil density and specular reflectance for either the normal or the anti-soiling coated glass samples. This might be due to the small diameter of the incoming beam radiation and the detector of the ellipsometer. From graph 14 and 15 above, it seems like the anti-soiling coating has some advantages at higher dust densities (about 60 mg/m^2 and 80 mg/m^2). However, no conclusions are made, because of the few measure points and great variation in measure data. In addition, the diffuse reflection and the structure of the soil grains have not been detected.

5.5.2 Change in transmittance due to one week of soiling

This subchapter presents measured changes in transmittance due to one week of soiling. Measurements are compared with soil density and precipitation.

5.5.2.1 The measured change in transmittance

The change in transmittance is measured and the transmittance is calculated by applying the methodology given in subchapter 4.3. Recall that the change in transmittance due to soiling is the main focus. Table 9 presents the measured and calculated values weighted towards the AM1.5G spectrum, and the results are discussed after the table. Graph 16 and 17 show the change in transmittance at different wavelengths. Measurements are conducted at 20° angle of incidence. Graphs showing the transmittance are given in Appendix E.

Date	τ_N **[%]**	τ_{AS} **[%]**	$\Delta\tau_N$ **[%]**	$\Delta\tau_{AS}$ **[%]**
03.03.15	90.5	90.3	-1.0	-0.5
10.03.15	90.7	90.2	-0.8	-0.6
17.03.15	90.0	89.3	-1.5	-1.5
24.03.15	90.4	89.6	-1.2	-1.2
31.03.15	90.4	90.0	-1.1	-0.9
07.04.15	90.1	89.5	-1.5	-1.4
14.04.15	90.1	90.2	-1.4	-0.6
MEAN	**90.3**	**89.9**	**-1.2**	**-1.0**

Table 9: Transmittance (τ) and change in transmittance ($\Delta\tau$) for normal and anti-soiling coated glass samples measured at 20˚ angle of incidence after one week of soiling at Kjeller. Measurements are conducted at different dates.

As seen in table 9, the change in transmittance is generally greater for the normal glass samples. However, the measured transmittance is less for the anti-soiling coated glass samples, due to the initial lower transmittance. The normal glass samples seem to be more suited at Kjeller, even though the reductions in transmittance are higher. Recall that Pettersen [22] conducted similar research with normal and TripleO coated glass samples exposed to soiling at Kjeller. This research was carried out from the end of October to the middle of November. She concluded that the measured transmittance was about 2.0 % lower for the anti-soiling coated glass samples than for the normal glass samples after five weeks of exposure. This difference between the normal and anti-soiling coated glass is greater than the difference seen in table 9. This might be due to seasonal variations, or the difference in time of exposure.

Studies conducted in Belgium (at a tilt angle of 37˚) [24] showed a decrease in transmittance at 3-4 % after five weeks of exposure. This decrease is higher than the highest (1.5 %) decrease in transmittance for the normal glass samples. The higher decrease in transmittance in Belgium might be due to the longer period of exposure, lower tilt angle and differences in geographical and weather conditions.

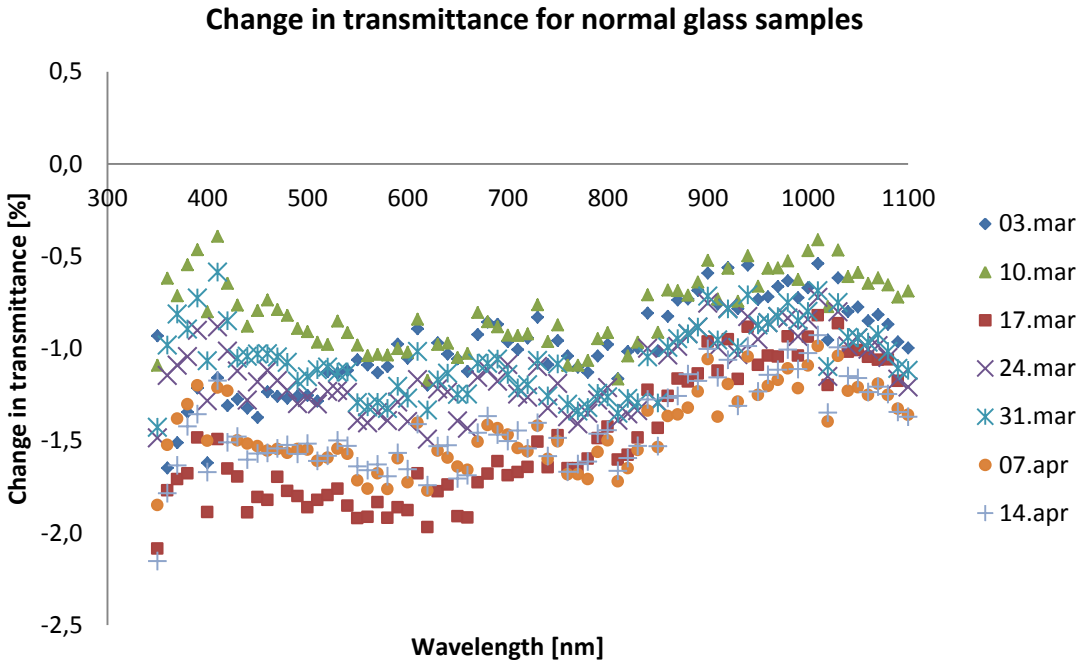

Graph 16: Change in transmittance at 20˚ angle of incidence for normal glass samples. Measurements are conducted at different dates, for glass samples exposed to one week of soiling at Kjeller.

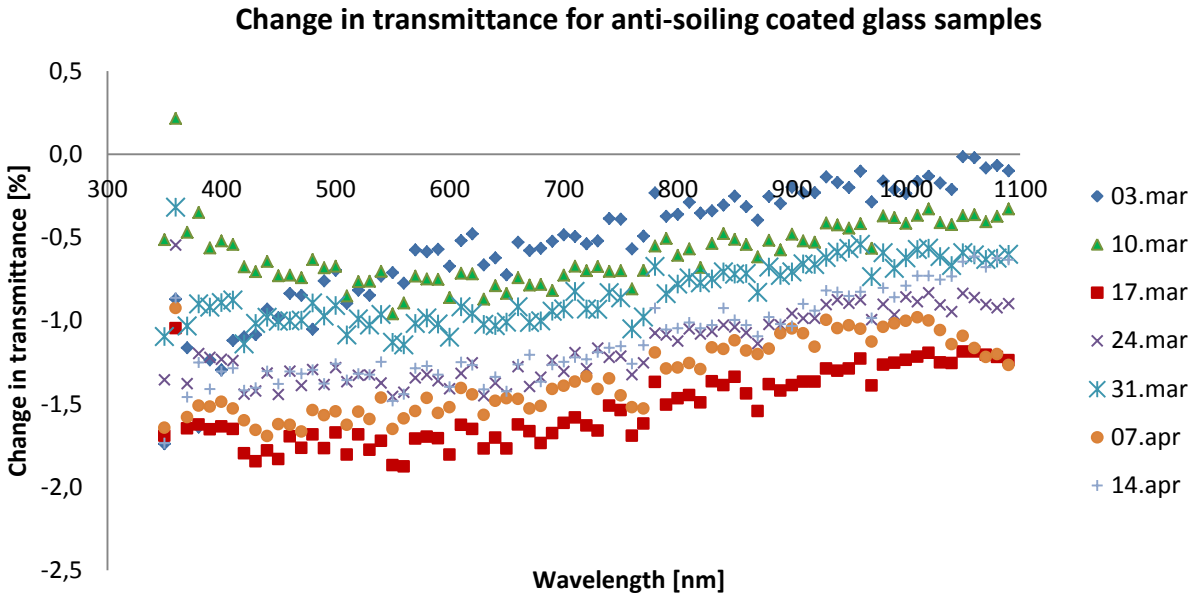

Graph 17: Change in transmittance at 20˚ angle of incidence for anti-soiling coated glass samples. Measurements are conducted at different dates, for glass samples exposed to one week of soiling at Kjeller.

As seen in graph 16 and 17, the change in transmittance seems to be greatest in the wavelength interval from about 450 nm to 800 nm for the normal glass samples and in the interval from 450 nm to 700 nm for the anti-soiling coated glass samples. This means that the amount of transmitted light decreases more in these intervals, which indicates that the shorter wavelengths are affected more than the longer wavelengths by the soil deposition.

One possible explanation is that scattering occurs at the surfaces due to the deposited soil. Recall from chapter 2.1 that both Mie and Rayleigh scattering affects the shorter wavelengths more. The different scattering models depend on the size of the dust grains and the wavelength of the radiation.

It seems likely that the larger dust grains fall off due to the vertical position during the optical measurements, leaving the smaller particles on the glass sample, because of gravitational forces. Recall that smaller dust particles affect the shorter wavelengths more [20]. However, other factors (like surface tension) may contribute, and the particle sizes have to be investigated in a particle size analysis.

Similar results were observed by Qasem [20], when he investigated artificial dust on glass samples. Qasem concluded that the measured transmittance for the deposited dust reduced more for shorter wavelengths than for longer. He also concluded that the wavelength-dependency increased with increasing soil densities. Recall that March 17, April 7 and April 14 had the highest levels of soil density present during the optical measurements. These dates measure the highest reduced transmittance, but it does not seem like these soil densities measure higher levels of wavelength-dependency. One possible explanation is that Qasem investigated higher levels of soil densities ($1.2*10^4$ mg/m^2 to $30.9*10^4$ mg/m^2).

5.5.2.2 Change in transmittance at different soil densities

The change in transmittance is plotted against the measured soil density present during the optical measurements (MD_C) in graph 18 and 19, for normal and anti-soiling glass, respectively. The reduced transmittance is given as absolute values. The different measure points represent different measure dates.

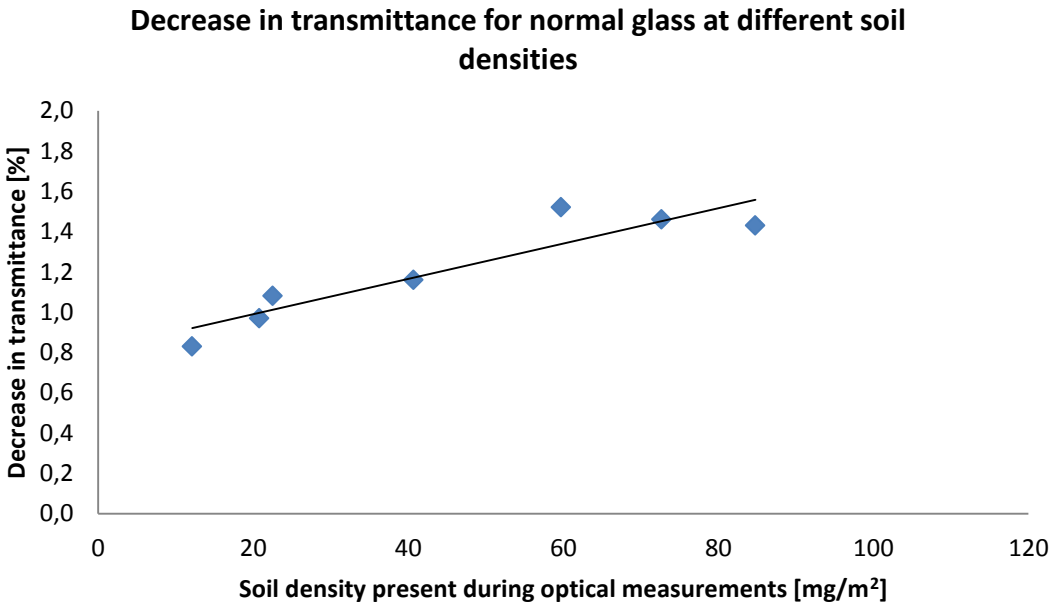

Graph 18: Measured change in transmittance at 20˚ angle of incidence for normal glass samples, at different soil densities present during the optical measurements. The different plotted points represent different measure dates.

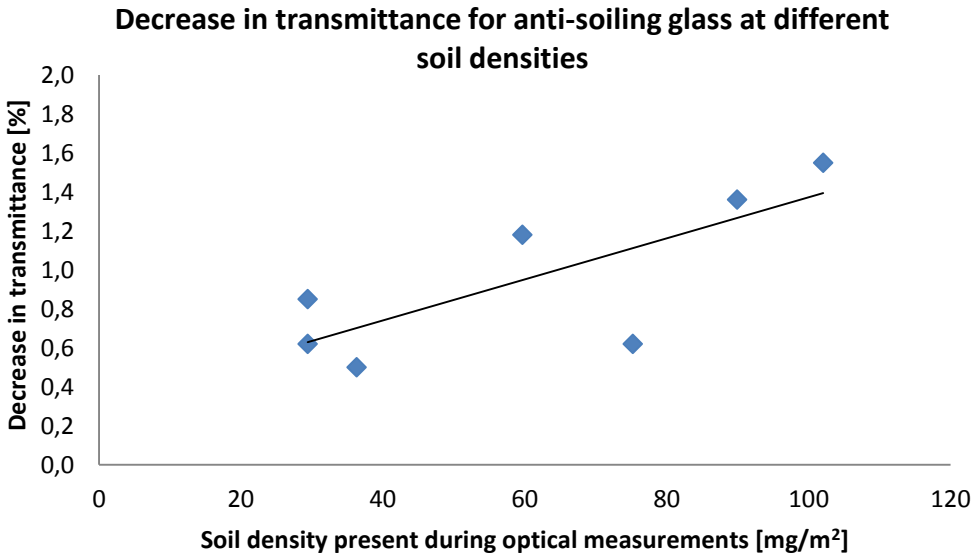

Graph 19: Measured change in transmittance at 20° angle of incidence for the anti-soiling coated glass samples, at different soil densities present during the optical measurements. The different plotted points represent different measure dates.

From graph 18 and 19, a linear connection between increasing soil density and the increasing reduction in transmittance is detected. Based on the linear connections in the two graphs, the transmittance at 20° angle of incidence is suggested to decrease with:

$$\Delta\tau_{\mathrm{N}} = 0.09\ \%\ \text{for every}\ 10\ \mathrm{mg/m^2}, \text{with}\ \mathrm{R^2} = 0.85$$

$$\Delta\tau_{\mathrm{AS}} = 0.11\ \%\ \text{for every}\ 10\ \mathrm{mg/m^2}, \text{with}\ \mathrm{R^2} = 0.59$$

for normal and anti-soiling glass respectively. R^2 is a number between 0 and 1 that indicates how well data fit a statistical model. A linear connection is most accurate when its R-squared value is close to 1. Note that this linear connection is based on relatively low soil densities.

These results show that the transmittance decreases more rapidly for the anti-soiling coated glass samples with increasing soil density. However, the reduction in transmittance is higher at lower soil densities for the normal glass samples, until the accumulated soil density reaches approximately 300 mg/m^2. Recall that the total soil densities were less than 130 mg/m^2 after one week of soiling. Soil densities after longer periods with little rain are unknown.

Based on the measure data obtained by Qasem on his research with artificial dust [20], there is a noticeable linear connection between decreasing transmittance and increasing dust density. Qasem uses dust densities in the range of 120 mg/m^2 to 3090 mg/m^2. His results show a decrease in transmittance about 2.8 % for every 10 mg/m^2 for normal glass samples. This decrease in transmittance is much higher than the decrease in transmittance measured during this study at Kjeller. One possible explanation is differences in the dust composition and size distribution. Different elements and particle sizes affect the transmittance differently [23] [20]. Another possible explanation is that the linear connection observed in graph 18 and 19 holds for smaller dust densities, but no conclusions can be made for higher dust densities.

An estimated decrease in transmittance for the total accumulated soil density (MD_{total}) is calculated by plotting the total soil density along the linear connections for the two glass samples. The results are shown in graph 20 and 21 for the normal and anti-soiling coated glass samples.

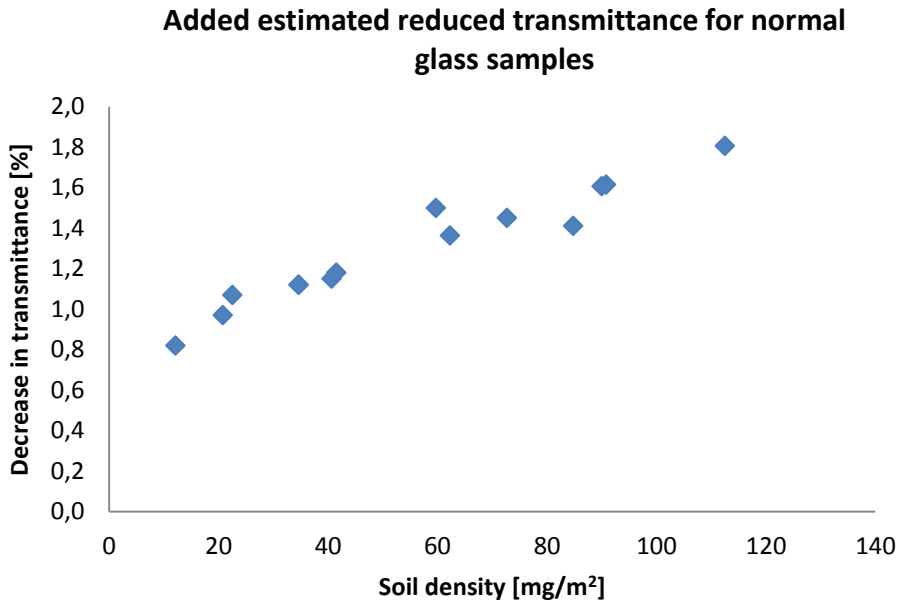

Graph 20: The estimated reduction in transmittance for the normal glass samples are based on the total accumulated soil density and the linear connection observed in graph 18. The estimates are added to graph 18.

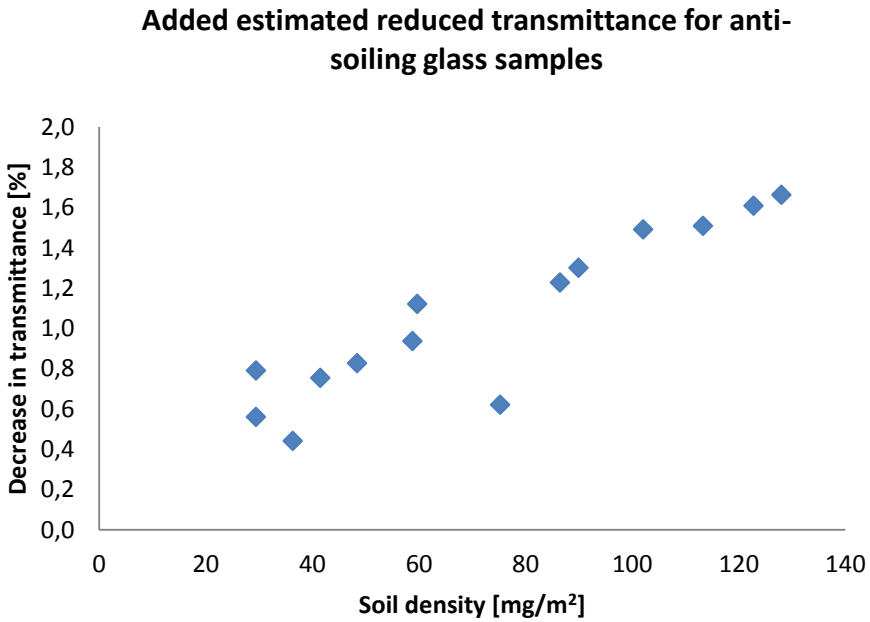

Graph 21: The estimated reduction in transmittance for the anti-soiling coated glass samples are based on the total accumulated soil density and the linear connection observed in graph 19. The estimates are added to graph 19.

The estimated reduced transmittances (based on the total accumulated soil density, MD_{total}) are presented in table 9 below, along with the measured reduced transmittance (based on the soil density present during optical measurements MD_C).

Date	$\Delta\tau_N$ **[%]**	**Estimated** $\Delta\tau_N$ **[%]**	$\Delta\tau_{AS}$ **[%]**	**Estimated** $\Delta\tau_{AS}$ **[%]**
03.03.15	-1.0	-1.2	-0.5	-0.8
10.03.15	-0.8	-1.1	-0.6	-0.9
17.03.15	-1.5	-1.6	-1.5	-1.6
24.03.15	-1.2	-1.4	-1.2	-1.2
31.03.15	-1.1	-1.1	-0.9	-0.6
07.04.15	-1.5	-1.8	-1.4	-1.7
14.04.15	-1.4	-1.6	-0.6	-1.5
MEAN	**-1.2**	**-1.4**	**-1.0**	**-1.2**

Table 10: Measures and estimated change in transmittance ($\Delta\tau$), based on the total accumulated soil density. The subscripts N and AS refers to the normal and the anti-soiling coated glass samples, respectively. The estimated changes in transmittance are based on the linear connection from graph 18 and 19.

The estimated reduced transmittance is higher for the normal glass samples, because the accumulated soil densities were less than 300 mg/m^2. It is assumed that the linear connections hold for these dust densities (MD_{total}).

The difference between the estimated and measured reduced transmittance is approximately 0.2 % and 0.3 % for the normal and anti-soiling coated glass samples, respectively. This difference equals approximately 17 % and 30 % of the measured reduced transmittance values for the normal and anti-soiling coated glass samples, respectively.

5.5.2.3 Decrease in transmittance at different levels of precipitation.

The decrease in measured transmittance for both normal and anti-soiling glass, together with precipitation data, is plotted in graph 22.

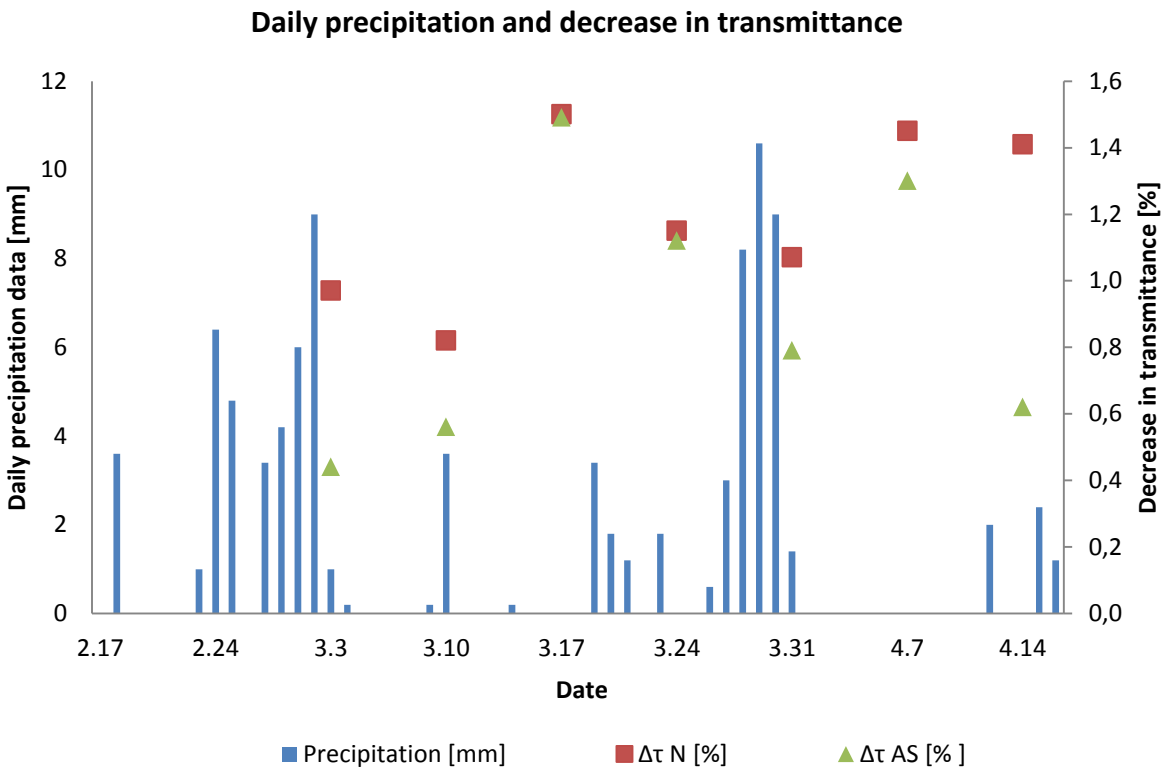

Graph 22: Daily precipitation data, and measured decrease in transmittance ($\Delta\tau$) for normal and anti-soiling glass samples at Kjeller. The letters N and AS refer to the normal and anti-soiling coated glass samples, respectively. The weather data is downloaded from eKlima, and transmittance measurements are conducted at 20˚ angle of incidence.

Graph 22 shows the connection between precipitation and decrease in transmittance. A clear pattern is observed. The graph shows higher values for the reduced transmittance after weeks of little or no rain (March 17 and April 7), and lower values for the days and weeks exposed to more rain (March 3, 10 and 31).

There are noticeably grater variations between the decrease in transmittance for the normal and anti-soiling coated glass samples on dates associated with rainfall. It was suggested in subchapter 5.4.1 that the anti-soiling coating (TripleO) needs higher levels of precipitation to work as intended. This agrees with the pattern noticed in graph 22 above.

The low values for the decrease in transmittance at March 3, 10, 24 and 31 are likely due to the precipitation. A threshold sufficient to clean the glass samples until a point of saturation was suggested to 3.6 mm (March 10), in subchapter 5.4.1. This is consistent with graph 22 above. The high level of precipitation on March 10 can explain the low change in transmittance at this date.

Even after weeks with much rain, there is a decrease in transmittance (about 1.5 % and 0.8 % for normal and anti-soiling glass on March 31). It seems like rain is not sufficient to clean the glass samples completely. This was also noticed in subchapter 5.4.1, where some accumulated soil was left at the glass samples after rainfall.

A change in transmittance after a week with high levels of precipitation is calculated as the mean change in transmittance from March 3, 10, 24 and 31. It is also calculated based on the estimated change in transmittance from table 10, based on the total accumulated soil density (MD_{total}). This gives a measured decrease in transmittance for a week with much rain at approximately 1.0 % and 0.7 % for the normal and anti-soiling coated glass samples, respectively. The estimated decrease in transmittance, due to the total accumulated soil density, after a week of much rain is about 1.2 % for the normal glass samples, and 1.0 % for the anti-soiling coated glass samples. The estimated values are about 120 % and 143 % of the measured values, for the normal and anti-soiling coated glass samples, respectively.

A change in transmittance after a week with little precipitation is calculated as the mean change in transmittance from March 17, April 7 and April 14. It is also calculated based on the estimated change in transmittance from table 10, based on the total accumulated soil density (MD_{total}). This gives a measured decrease in transmittance for a week with no rain at approximately 1.5 % and 1.2 % for the normal and anti-soiling coated glass samples, respectively. The estimated decrease in transmittance, due to the total accumulated soil density, after one week of no rain is about 1.7 % for the normal glass samples and about 1.6 % for the anti-soiling coated glass samples. The estimated values are about 113 % and 133 % of the measured values, for the normal and anti-soiling coated glass samples.

This means that the decrease in transmittance is about 42 % and 60 % higher for periods with no rain, than for periods with much rain, for the normal and anti-soiling coated glass samples, respectively. Note that these results are based on few measurement points with relative great data variations.

Recall that studies from Malaga [27] reported a mean daily irradiation loss, due to soiling, at about 4 %, but as high as 20 % after long periods without rainfall. This shows an even greater precipitation dependency. This is likely due to the short intervals without rain at Kjeller, the short exposure periods and other factors like soil composition and panel tilt angle.

5.5.3 Optical values after 4 and 8 weeks of exposure

Table 11 shows the measured change in transmittance and the calculated transmittance after four and eight weeks of exposure at Kjeller. It also shows the weekly measurement data from the prior day, exposed to one week of soiling. Graph 23 shows the decrease in transmittance for the same dates.

Weeks and date	τ_N [%]	τ_{AS} [%]	$\Delta\tau_N$ [%]	$\Delta\tau_{AS}$ [%]
1 week 17.03.15	90.0	89.3	-1.5	-1.6
4 weeks 18.03.15	90.5	89.7	-1.2	-1.1
1 week 14.04.15	90.7	90.2	-1.4	-0.6
8 weeks 15.04.15	90.2	89.7	-1.3	-1.1

Table 11: Transmittance (τ) and change in transmittance ($\Delta\tau$) for the normal and anti-soiling coated glass samples after 1, 4 and 8 weeks of exposure at Kjeller. Measurements are conducted at 20˚ angle of incidence, and the subscripts N and AS refer to the normal and the anti-soiling coated glass samples, respectively.

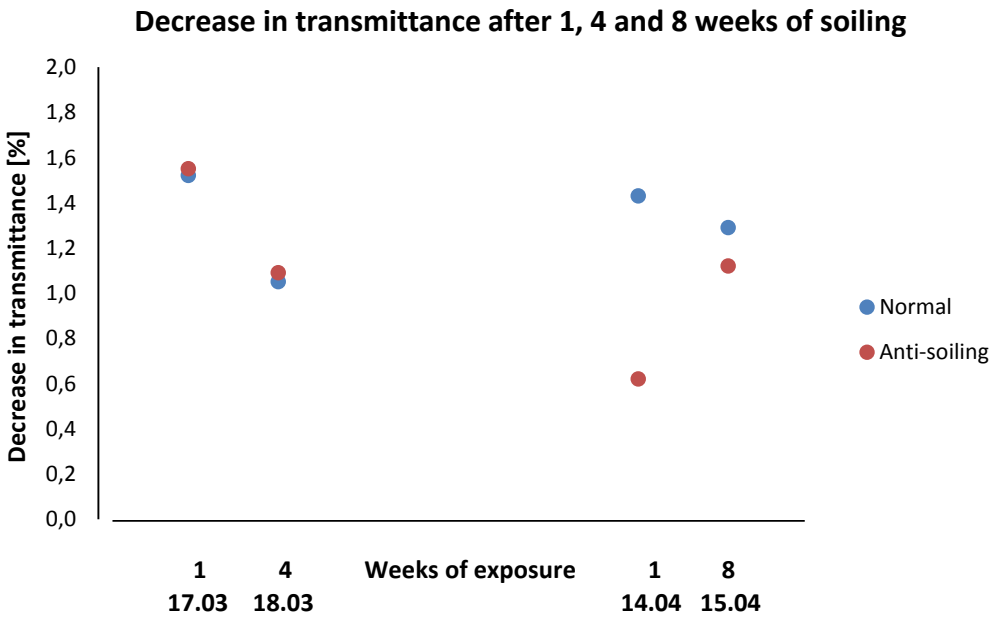

Graph 23: Decrease in transmittance for normal and anti-soiling coated glass samples after 1, 4, 1 and 8 weeks of exposure at Kjeller. The different measurement dates are given. Transmittance measurements are conducted at 20 ˚ angle of incidence.

The change in transmittance after 4 weeks of exposure (March 18) is lower than the change in transmittance after one week of soiling on March 17, as seen in graph 23. This date follows a day of no precipitation. This disagrees with expectations, because it has been observed that the

change in transmittance seems to increase in the absence of rainfall, resulting in a lower transmittance. One possible explanation is that the glass samples are permanently affected by the weekly measurements and cleaning events, even though great care is taken. Another uncertainty error is the vertical position during the optical measurements. It has been stated that approximately 32 % soil falls off due to these measurements. The lacking mass measurements after 4 and 8 weeks of exposure makes it impossible to determine if approximately the same amount, more or less soil falls off.

It does not seem like there is any clear connection between change in transmittance and time exposed to soiling. One possible explanation is precipitation. A high level of rainfall was measured one week prior to March 18, cleaning the glass sample. Rain was also measured on April 15. It therefore seems like the transmittance saturates after approximately one week of soiling at Kjeller, for periods exposed to rain. Research conducted in Belgium [24] at 37˚ tilt angle, states that the decrease in transmittance saturates after five weeks of exposure, at approximately 3-4 %. This was detected for glass samples exposed to rainfall events, but the level of precipitation is not specified. The measured decrease in transmittance in Belgium is higher than the measured decrease in transmittance after eight weeks of exposure at Kjeller (about 1.3 % for the normal glass samples). Recall that results do not transfer between different locations. Nevertheless, it seems like the problem with soiling at Kjeller is not as severe as in Belgium.

The reduced transmittance due to the total accumulated soil density has not been calculated, because no dust densities exist for the measurements on the glass samples exposed to 4 and 8 weeks of soiling.

5.5.4 Calculated reduced efficiency

The calculated change in efficiency for a representative PV-module used at IFE is found by applying the methodology given in subchapter 4.3.7. The results are presented for 20˚ angle of incidence in table 12 below. In addition, the estimated change in transmittance (based on total accumulated soil density, MD_{total}) is used to calculate an estimated change in efficiency at the defined date. This is conducted by applying:

$$\text{Estimated } \Delta\eta_{\text{N}} = \Delta\eta_{\text{N}} * \frac{\text{Estimated } \Delta\tau_{\text{N}}}{\Delta\tau_{\text{N}}}$$

Estimated $\Delta\eta_{\text{N}}$ is the estimated change in efficiency, based on the estimated change in transmittance (Estimated $\Delta\tau_{\text{N}}$) from table 10, while $\Delta\eta_{\text{N}}$ is the change in efficiency from the measured change in transmittance ($\Delta\tau_{\text{N}}$).

Date	**03.03**	**10.03**	**17.03**	**18.03** 4 weeks	**24.03**	**31.03**	**07.04**	**14.04**	**15.04** 8 weeks
$\boldsymbol{\Delta\eta_N}$ **[%]**	-0.2	-0.1	-0.3	-0.2	-0.2	-0.2	-0.2	-0.2	-0.2
Estimated $\boldsymbol{\Delta\eta_N}$ **[%]**	-0.2	-0.2	-0.3	-	-0.2	-0.2	-0.3	-0.3	-

Table 12: Calculated change in efficiency ($\Delta\eta$) for a standard PV-module with efficiency of 16.9 %, based on the measured change in transmittance ($\Delta\tau$) and the estimated change in transmittance at 20˚ angle of incidence, for the given dates. The subscript N refers to the normal glass samples.

The maximum efficiency reduction after one week of soiling at Kjeller is approximately 0.3 % for normal PV-modules. This would reduce the efficiency for this PV-module from 16.9 % to 16.6 %. The reduced transmittance after 4 and 8 weeks of exposure does not cause a higher efficiency reduction for the standard PV-module. A suggested efficiency reduction caused by soiling at Kjeller is therefore in the range from 0.2-0.3 %, based on the total accumulated soil density.

Recall that studies from California [28] detected an efficiency at 12.5 % for PV-panels, which decreased to 7.5 % after one year of soling. This decrease is much higher than the decrease noticed at Kjeller. This is likely due to the longer exposure time, which would have to be investigated at Kjeller.

The simulation and design software PVsyst suggests a power loss less than 1 % due to the accumulation of soil in a typical middle European climate [22]. The power loss is directly proportional to the loss in efficiency, and local measurements at Kjeller appear to fit with the suggested losses.

It seems like the problem with soiling at Kjeller is not as severe as in other areas where soiling on PV-modules has been investigated.

5.5.5 Subchapter summary

The specular reflectance seems to be approximately unaffected by the accumulated soil at lower angles of incidence (up until 55°). At higher angles of incidence, the specular reflectance seems to decrease more rapidly for the normal glass samples, while no pattern was noticed for the anti-soiling coated glass samples. More measurements, including diffuse reflectance, should be conducted before conclusions can be made.

There is a noticeable decrease in transmittance due to soiling. This seems to affect shorter wavelengths more, likely due to an increase in Mie and/or Rayleigh scattering.

A linear connection between increasing soil density and reduced transmittance is noticed. The transmittance is suggested to decrease with 0.09 % and 0.11 % for every 10 mg/m^2 for normal and anti-soiling coated glass at 20˚ angle of incidence.

There is a clear pattern between the changes in transmittance and precipitation data. Rainfall seems to clean the glass samples and increase the transmittance. 3.6 mm of precipitation was suggested in chapter 5.4 as a level sufficient to clean the glass samples until a point of saturation. This is confirmed by graph 22. A lower decrease in transmittance due to precipitation and a higher decrease in transmittance after weeks with little/no rain results in a valuation of approximately: 1.2 % < $\Delta\tau_N$ < 1.7 % and 1.0 % < $\Delta\tau_{AS}$ < 1.6 % for the normal and anti-soiling coated glass samples, respectively. This difference is about 42 % and 60 %, for the normal and anti-soiling coated glass.

The measured transmittance after 8 weeks of exposure is about the same as the transmittance after 4 weeks. It is suggested that the decrease in transmittance saturates for periods exposed to rainfall at Kjeller.

The transmittance losses at Kjeller after one week of soiling seem to reduce the efficiency between 0.2 % and 0.3 % for PV-modules covered with normal glass. This decrease is less than decreases detected at other locations. Is seems like the problem with soiling at Kjeller is less severe than for other areas where soiling on PV-modules has been investigated.

5.6 Soil analyses

This subchapter presents the results from soil analyses on dust from the normal glass samples exposed to soiling at Kjeller. Surface scans and point analyses were performed using the Scanning Electron Microscope (SEM) to determine particle distribution and important components in the dust. The methods are described in subchapter 4.4.

Recall that soil analyses are conducted at two selected weeks. Results will therefore only give an indication of expected soil composition and distribution at the glass samples. The surface scans on April 15 are performed after the optical measurements are conducted. Point analyses on May 4 are performed on extra glass samples from the roof, and will therefore not be affected by the vertical position during the optical measurements.

5.6.1 Size distribution

Figure 36 shows the surface of a small, normal glass sample exposed to one week of soiling at Kjeller. The picture is taken with the SEM on April 15, a date following a week of little rain. The picture is a result from a surface scan. Figure 37 shows a selected surface area, taken on May 4, after one week of soiling. It shows the largest observed dust grains.

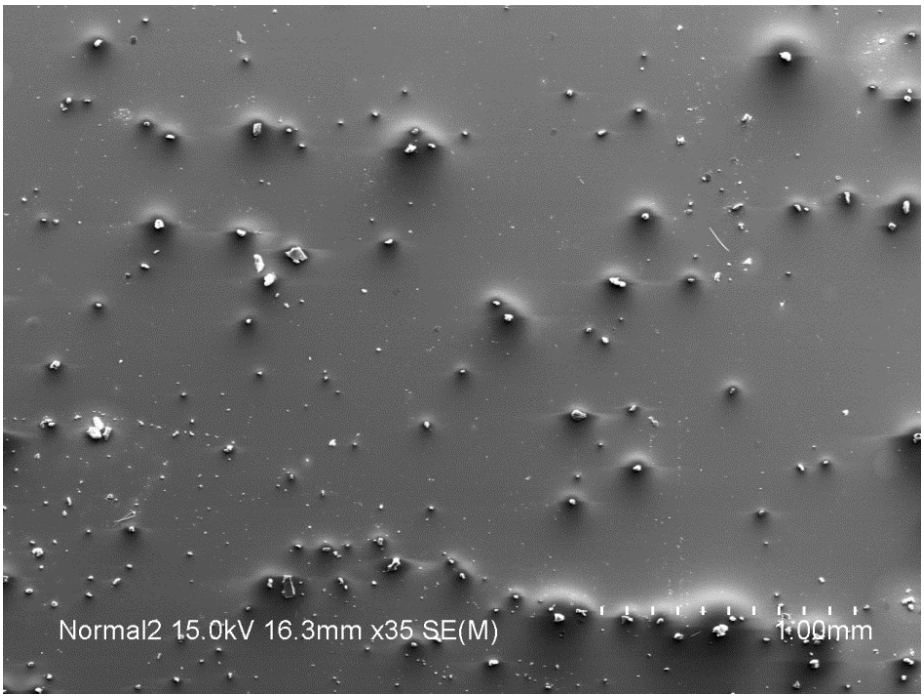

Figure 36: Surface scan of a normal glass sample from the rooftop at Kjeller, taken on April 15. This scan is taken after the optical measurements are performed, and results are therefore expected to be affected by the vertical position during those measurements. A scale in the bottom right corner shows the image resolution (total scale of 1.00 mm).

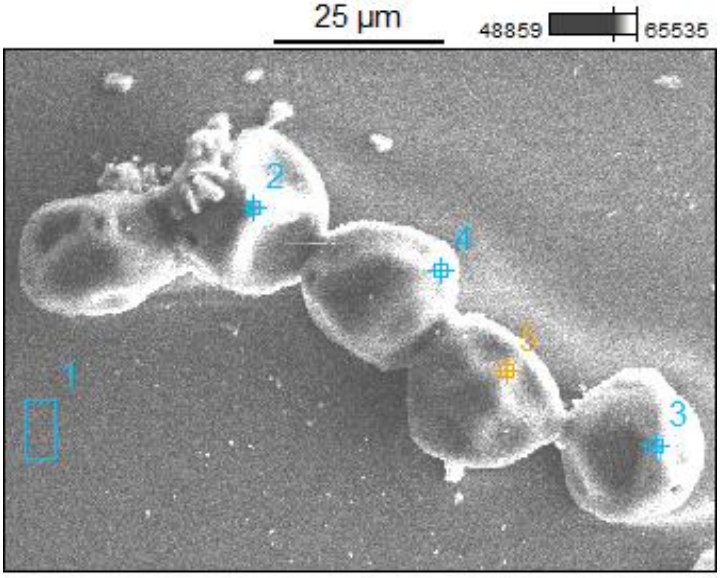

Figure 37: The largest observed dust grain from the point analyses performed at May 4. These results are not performed after optical measurements, and are therefore not affected by the vertical position during those measurements. A scale over the picture shows the image resolution.

The picture from the surface scan (figure 36) shows an approximately even dust distribution at the surfaces. It is found that the dust grains have a diameter (*d*) during optical measurements in the order of $d < 10^1$ μm.

This is based on observing pictures from the surface scans. These dust grains are the components assumed to stay on the glass sample during optical measurements. However, pictures from the point analyses on May 4 show that the largest dust grains have a diameter up to 30 μm. This strengthens the assumption made earlier, that the larger dust grains seem to fall off due to the vertical position during the optical measurements. Recall that the researchers from Belgium [24] defined dust grains in the size 2-10 μm as small dust particles, while dust grains with diameters at about 60 μm (pollen) were defined as large.

The diameters for the dust grains present during the optical measurements seem to be in the same range as the wavelength spectrum used through the optical measurements in this study. Mie scattering is therefore suggested to appear at the surface. However, the particle sizes are determined by observations, and smaller particles may occur. Recall that Rayleigh scattering occurs when the diameter of the particles are approximately 10 % of the radiation wavelength, resulting in diameters less than 0.1 μm. This means that Rayleigh scattering may occur if smaller particles are present. A more accurate size measurement is needed.

Recall from subchapter 2.1.3, that both Mie and Rayleigh scattering affect the shorter wavelength spectrum more. This agrees with results from subchapter 5.5.2, which shows how the change in transmittance is more affected at shorter wavelengths. As noted earlier, Qasem [20] looked at the wavelength-dependency of the transmittance at different dust densities. He found that the spectral effects matched the behavior that was found when dust particles were modelled with Mie scattering, mostly for particles with a diameter < 6 μm.

Particle shape has not been considered during this study. Deviations from a spherical shape will increase the scattering [20] and is therefore an interesting field for further investigations. Also, a more correct size analysis is suggested to establish a better understanding of the size distribution of the dust grains.

5.6.2 Detecting components

Surface scans on smaller areas, and areas consisting of only one dust grain are conducted on April 15. Results do not provide useful information about important soil elements, because the scan is affected by the glass surface.

One example of a point analysis conducted on May 4 is shown in figure 38 and table 12. The table gives the mass of the detected elements as a percentage of the total mass at the point. The software gives the uncertainties in the table. Results from point analyses at different surface areas are given in Appendix F.

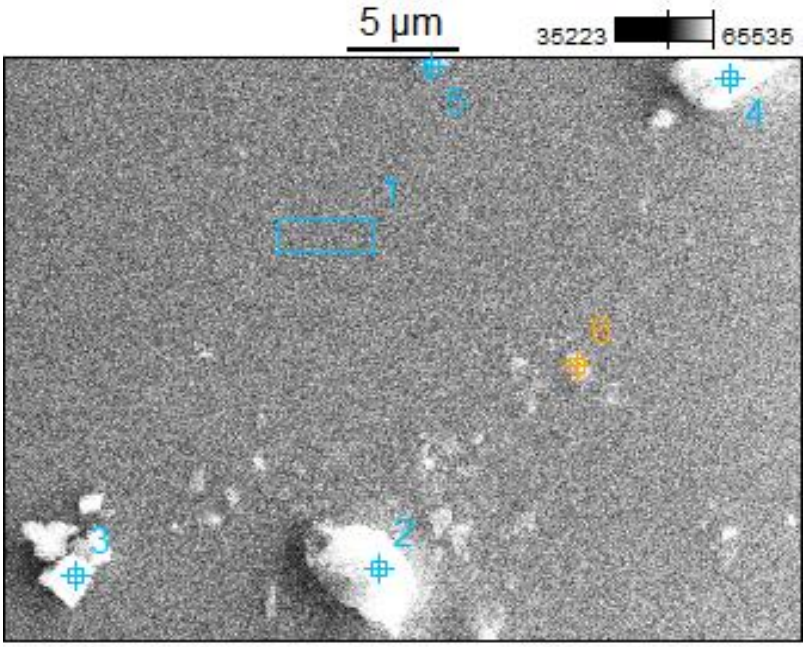

Figure 38: Picture from a point analysis conducted at May 4. Point 1 is directed at the glass surface, while the other points are directed at dust grains.

Point 1 in figure 38 is directed at the glass surface. Components that never exceeded 2.0 % are excluded from the table below and values above 10 % are highlighted with a green background. Recall from subchapter 3.4 that results from the Energy Dispersive Spectrometry (EDS) is accepted, even though uncertainties occur due to overlapping energy peaks in the X-ray emission spectrum.

	C	O	Na	Al	Si	K	Ca
Point 1	7.8 ± 0.5	48.2 ± 0.7	9.4 ± 0.2		28.7 ± 0.2		4.2 ± 0.2
Point 2	55.9 ± 0.5	30.5 ± 0.7	2.2 ± 0.1		6.8 ± 0.1		0.7 ± 0.1
Point 3	15.6 ± 0.6	47.1 ± 0.7	4.6 ± 0.2	2.7 ± 0.5	24.3 ± 0.2	2.8 ± 0.1	2.1 ± 0.2
Point 4	11.9 ± 0.5	47.3 ± 0.6	7.1 ± 0.2	7.5 ± 0.2	24.7 ± 0.2	0.7 ± 0.1	0.5 ± 0.1
Point 5	12.6 ± 0.6	46.0 ± 0.7	7.0 ± 0.1	0.2 ± 0.1	28.5 ± 0.2		4.0 ± 0.1
Point 6	15.1 ± 0.6	44.9 ± 0.7	6.8 ± 0.2	0.2 ± 0.1	27.5 ± 0.2		3.8 ± 0.2

Table 13: Results from the point analysis shown in figure 38. The table gives the mass of the detected elements as a percentage of the total mass at the point. The software gives the uncertainties in the table. Components that never exceeded 2.0 % are excluded from the table and values above 10 % are highlighted with a green background. The elements are: carbon (C), oxygen (O), sodium (Na), aluminum (Al), silicon (Si), potassium (K) and calcium (Ca).

Point 1 is directed at the glass surface and shows 48.2 % oxygen (O) and 28.7 % silicon (Si). This is consistent with expectations, because the main component in normal glass is silicon dioxide (SiO_2), but may also contain other oxides. Point 1 also detects about 9.4 % sodium (Na). This is also as expected, because sodium carbonate (Na_2CO_3) is commonly used in the manufacturing of glass. This result is consistent with other results from points directed at the glass surface at different surface areas.

Recall from subchapter 3.4 that the electron beam detects a droplet shaped excitation volume, at about 5 μm deep and 5 μm wide. From figure 38 and table 12, it is therefore likely that the point-results may be affect by the glass surface. However, both silicon and oxygen are expected components in outdoor dust. The different points cannot be compared directly, because the point-results are given as a mass percentage at the defined point. Nevertheless, aluminum (Al) and potassium (K) are detected at some dust grains and not at the glass sample, and the importance (%) of carbon seems to increase at the dust grains.

Results from a point analysis conducted at one singe dust grain are found in Appendix F. These show that only carbon and oxygen dominate at this particular dust grain, and that little silicon is present. However, this is only one dust grain and can not be used as a representation for the entire surface.

Point analyses were performed at 16 different dust grains (excluding the reference points at the glass surfaces). Graph 24 displays the number of times an element was detected with more than 5 % of the mass, while graph 25 shows the mean percentage importance for the different elements. It is important to note that the size differences have not been accounted for. Graph 24 does not account for the importance (%) of the different components, but it gives an indication of what components appear with highest frequency. Graph 25 does not account for the number of times the elements appear, but gives an indication of how important (%) an element is expected to be at a point. Elements with mean values less than 1 % are excluded from graph 25.

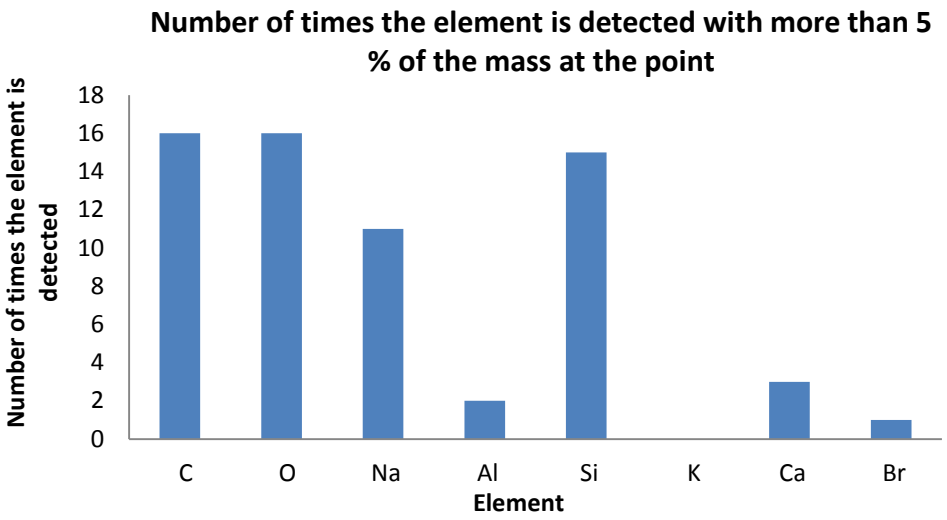

Graph 24: The number of times an element was detected with more than 5 % of the mass at a point. The illustration does not account for the size of the dust grains at the different points, or importance (%) of the element. The elements are: carbon (C), oxygen (O), sodium (Na), aluminum (Al), silicon (Si), potassium (K), calcium (Ca) and bromine (Br).

As seen in graph 24 above, the EDS detects bromine (Br). This is a seldom element, and point that detects Br are investigated in more details (Appendix F). It shows that the EDS could have detected silicon or magnesium.

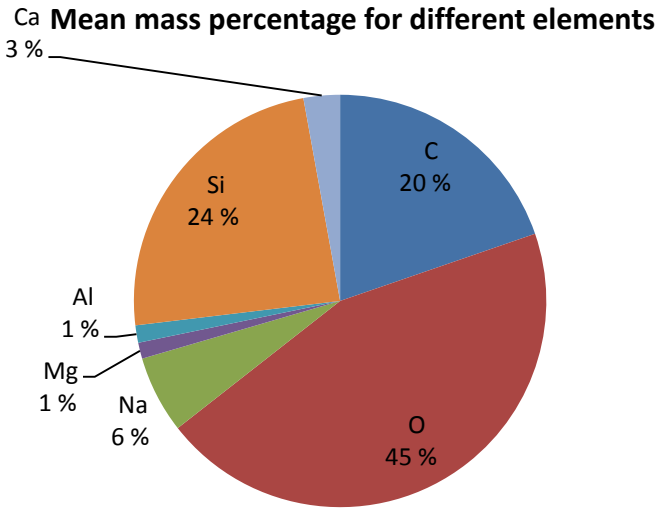

Graph 25: Mean percentage importance for the different elements. It does not account for the number of times the elements appear or the particle sizes, but gives an indication of how important (%) an element is expected to be at a point. Elements with mean values less than 1 % are excluded. The elements are: carbon (C), oxygen (O), sodium (Na), magnesium (Mg), aluminum (Al), silicon (Si) and calcium (Ca).

The dominating components from the dust at Kjeller seem to be oxygen (O), silicon (Si) and carbon (C). It is unknown how the glass surface affects the point-results. However, silicon is the second most common element in the Earth's crust, and is widely distributed in dust and sand. It is often found as silicon dioxide (SiO_2). Carbon is also a common component in the natural environment, often appearing as carbon dioxide (CO_2). Roads, industry, cities and airports are some examples of factors that can affect the amount of carbon dioxide in the airborne dust.

Sodium (Na) also seems to appear with a relative high frequency and importance (%). This element does not occur as a free metal, but sodium carbonate (Na_2CO_3) is used in the manufacturing of glass. However, sodium is also an important element for plants and is found in salts.

Recall that different dust components affect the transmittance differently. Mohammad and Farmy showed that carbon particles result in the worst deterioration of performance of PV-cells, and a higher loss in power output, among the different dusts used [23].

A better understanding of the different elements and dust components at Kjeller is therefore needed. It is suggested that the natural composition of dust is investigated at surfaces consisting of only one component that rarely exists in the natural environment. This element can be excluded from the EDS analysis.

5.6.3 Subchapter summary

It is confirmed that the larger soil particles fall off due to the optical measurements. The soil particles that stays on the glass surface during optical measurements seems to have a diameter smaller than 10 μm. This is likely to cause Mie scattering, because the diameter seems to be in the same order as the radiation wavelength. However, a more accurate size determination is needed to investigate if smaller particles are present. Bothe Mie and Rayleigh scattering affect shorter wavelengths more than longer wavelengths, which is seen in subchapter 5.5.2.

Results from the different point analyses indicate that oxygen, silicon and carbon are the most dominating components at the polluted glass sample. These are some of the most common elements in the natural environment. However, the glass sample is made of silicon dioxide, and it is difficult to know if or how much this might affect the results.

5.7 Polluting glass samples with artificial dust

This subchapter presents the results obtained by applying the methodology presented in subchapter 4.5. Four different dust densities are used to pollute a normal glass sample, and silicon is selected based on results from the particle analyses. Visibly large dust grains characterize the artificial dust, with some diameters up to approximately 1 cm.

The circular surface area of the pipe is 31.2 cm^2, and the clean glass sample has a mass of approximately 59041 mg.

Table 14 presents the four different dust densities and the corresponding change in transmittance. The change in transmittance is weighted towards the AM1.5 spectrum. The table does not provide results for 54˚ angle of incidence, because of a likely error on the initial transmittance on the clean sample. Note that the soil densities are measured in mg/cm^2, not mg/m^2 as for the experiments with natural soiling. The data are also plotted in graph 26 and 27.

Experiment	**Density [mg/cm^2]**	**0˚ $\Delta\tau$ [%]**	**18˚ $\Delta\tau$ [%]**	**38˚ $\Delta\tau$ [%]**	**72˚ $\Delta\tau$ [%]**
Dust 1	0.21	-0.9	-86.5	-9.3	-27.8
Dust 2	0.15	-0.6	-0.7	-16.0	-25.2
Dust 3	0.12	-2.3	-2.2	-10.2	-4.6
Dust 4	0.11	-0.9	-0.3	-2.6	-2.0

Table 14: Results from experiments with four different dust densities. The change in transmittance ($\Delta\tau$) is measured on normal glass samples, polluted with silicon dust.

As noted in table 14 above, there is a likely measure error at 18° angle of incidence for Dust 1. This is discussed in further details below.

Ignoring the change in transmittance for Dust 1 at 18˚ angle of incidence (because of the likely error), the decrease in transmittance is in the area of $0.3\ \% < \Delta\tau < 2.2\ \%$, for soil densities at $1090\ mg/m^2 < MD < 1540\ mg/m^2$. Recall that the natural soiling at Kjeller resulted in a mean reduced transmittance of 1.2 % with a soil density of approximately 49 mg/m^2 at 20˚, on the normal glass samples. A linear connection between increasing dust densities and reduced transmittance was observed. In addition, studies from Egypt [33] showed that dust densities at approximately $4.48*10^3\ mg/m^2$ resulted in a reduced transmittance of 12 %. This shows that the decrease in transmittance from the experiment with artificial dust is lower than expected, at the corresponding high dust densities.

One possible explanation is that the visibly large dust grains of silicon and the narrow diameter (1.5 mm) of the incoming beam radiation (noted in chapter 3.6), makes the equipment vulnerable for small surface variations. Dust deposition and the point of interaction between the beam and the surface are important factors and it is possible that the beam do not interact with the larger dust grains, only the smaller. Smaller diameters of all the particles would have resulted in a more dense cover [23], while the larger dust grains have parts of the mass centered at smaller areas and a more unevenly mass distribution. This might explain the low transmittance for Dust 1 at 18˚, if the narrow beam radiation interacts with a large dust grin.

A second possible explanation is based on the soil composition. Results from the soil analyses show that carbon is an important component in the dust at Kjeller. Recall that Mohammad and Farmy concluded that carbon results in the worst deterioration of the performance of PV-cells, and a higher loss in power output among the different dusts used (three different limestone particles with different classes, cement and carbon) [23]. Although the variation in dust elements can contribute to a lower transmittance, it is unlikely to explain the large difference in transmittance values.

5.7.1 Reduced transmittance at different wavelengths

Graph 28 shows the measured change in transmittance at 18° angle of incidence, as a function of wavelengths. Dust 1 is not presented because of the likely error at this angle.

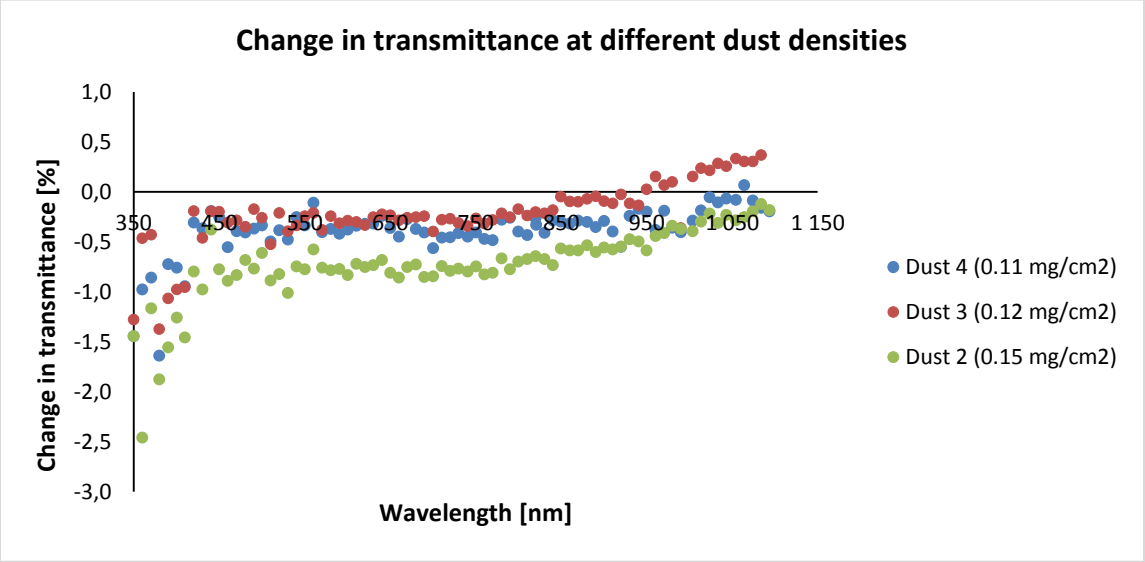

Graph 26: Change in transmittance at different dust densities. The transmittance measurements are conducted at 18° angle of incidence. Measurements are conducted on a normal glass sample, polluted with silicon dust.

As seen in graph 26 above, the change in transmittance is highest (lowest value) for Dust 2, the highest dust density. This is consistent with the results from the experiments with natural soiling. It seems like there is a positive change in transmittance for Dust 3 at wavelengths above 950 nm, which means that the transmittance increases. This is unlikely. One possible explanation is that the initial transmittance measurement on the clean glass sample is too low. Recall that two measurements were conducted on the clean glass samples prior to the experiment, and that a difference at approximately 2 % was noticed. This could indicate that all the measured decreases in transmittance should be higher (lower values in the graph).

The transmittance seems to decrease more at shorter wavelengths. This is consistent with result from the experiment with natural soiling at Kjeller (graph 16). Graph 16 showed that the wavelength-dependency varied the change in transmittance with approximately 1 % from shorter to longer wavelengths, which seems to be consistent with the wavelength-dependency in graph 26. However, recall that Qasem concluded that the wavelength-dependency for the reduced transmittance seemed to be more severe at increasing dust densities [20]. He investigated dust densities from 1.2 mg/cm^2 to 30.9 mg/cm^2. It would therefore be expected that the wavelength-dependency would be clearer during this experiment with artificial dust.

One possible explanation is the relatively low reduction in transmittance, which indicates that the soil density does not reflect the correct transmittance, as noted above.

Another possible explanation is that Mie scattering, which affects shorter wavelengths more, is more severe for smaller particles. Visibly large dust grains characterize the artificial dust, and will therefore not scatter as efficient as smaller dust particles.

5.7.2 Reduced transmittance at different angles of incidence

The change in transmittance for the different dust densities at 600 nm are plotted in graph 27 below. The value for Dust 1 at 18˚ is set to 0.9 % (based on the other dust densities) to smoothen the curve. This is because of the likely error at this measurement.

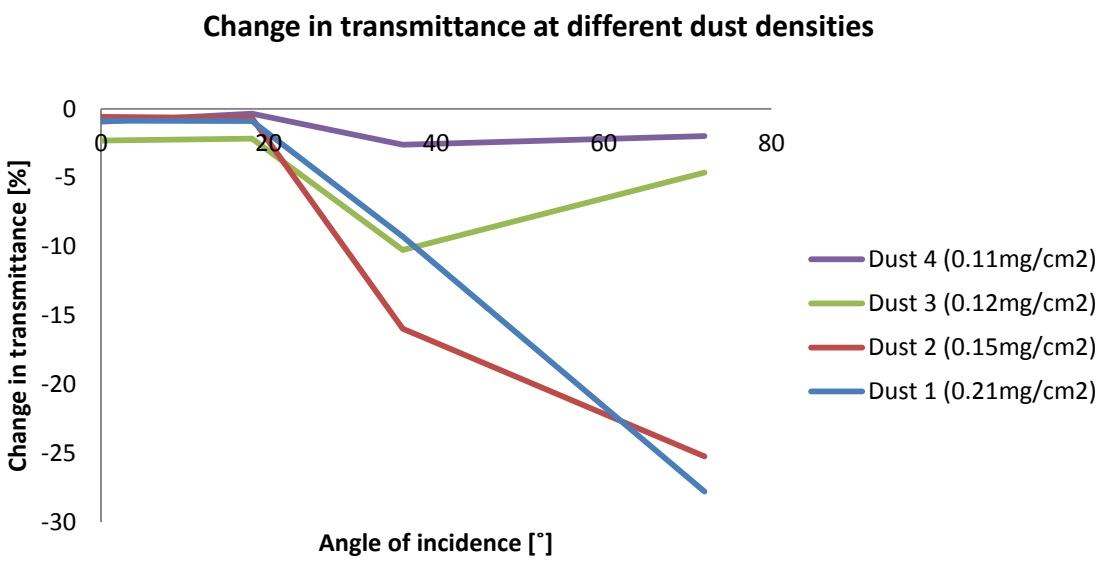

Graph 27: Plotted values from table 14 above. The graph shows the change in transmittance at different angles of incidence and different dust densities. Measurements are conducted on a normal glass sample, polluted with silicon dust.

It appears as if the measured transmittance of the polluted glass samples reduces more at increasing dust density (Dust 1 and Dust 2). This reduction seems more severe at increasing angle of incidence. However, conclusions are limited due to the missing measure data for 54˚ angle of incidence.

It is not attempted to draw any conclusions about the connection between soil density, transmittance and angle of incidence based on these measurements. This is because of the few measurement point and the great variations in measurement data. However, this is an interesting field for further investigation.

5.7.3 Subchapter summary

The transmittance reduces with increasing dust density. However, this reduction is less than expected, based on the experiment with natural soiling at Kjeller. This is likely due to the larger dust grains and the small diameter of the incoming beam radiation.

The transmittance seems to reduce more at shorter wavelengths, which is consistent with the prior experiment. However, it is expected that this wavelength-dependency would increase at higher dust densities. This is not observed, likely due to relatively high detected transmittance.

The experiment with artificial dust did not provide useful results for the relation between soil density and angle of incidence. This is because of the few measurement points and great variations in measurement data.

6 Conclusion and further work

One of the main issues with soiling on photovoltaic modules is the attenuation of the incident solar spectrum. Results regarding this issue are highly dependent on factors like the geographic location, experimental period and module setup. It is therefore important with local measurements at optimal module settings, which extend over longer periods.

Results show that the accumulated soil densities were higher for the anti-soiling (TripleO) coated glass samples than for the normal glass samples at all measurements dates. In addition, the measured transmittance appears to be lower for the anti-soiling coated glass, both before and after soil occur on the surface. The anti-soiling coating TripleO does therefore not seem to work as intended at Kjeller during this experimental conditions. However, it is suggested that the TripleO coating needs higher levels of precipitation, and could therefore be more suited for areas or periods exposed to more rain. Further research at Kjeller should involve other anti-soiling coatings, to investigate possible benefits with anti-soiling coating. It is also recommended that the TripleO coating is examined under other weather conditions at Kjeller.

A clear pattern between accumulated soil, transmittance and precipitation is observed. This observation agrees with results in other studies. Weeks with approximately no rain show soil densities that are 276 % and 250 % of the soil density measured at weeks with much rain, for the normal and anti-soiling coated glass samples respectively. A linear connection between increasing soil densities and reduced transmittance at the respective glass samples are observed. The next step is therefore suggested to involve measurements during other seasons, especially seasons with little rain. It is interesting to investigate the effect from physical cleaning, and to examine if this is necessary in a climate with much rain. One suggested method is to measure how the delivered power from PV-panels change due to rainfall, as well as after physical cleaning. This would give a better understanding of how efficient rain cleans the glass samples, and if physical cleaning is necessary in a country exposed to much rain.

The transmittance after 4 and 8 weeks of exposure at Kjeller were approximately the same as after one week of soiling. This indicates that the level of reduced transmittance saturates after approximately one week, likely due to rainfall. However, the reduced transmittance measurements after 4 and 8 weeks of exposure might be affected by the vertical position of the glass samples during the optical measurements. Results from weekly measurements show that approximately 32 % of the soil density falls off due to optical measurements. Lacking mass measurements after 4 and 8 weeks of exposure makes it difficult to determine if the same result apply to these dates. Accurate equipment with a horizontal positioned glass samples for optical measurements is therefore suggested. Another recommendation for further investigations is to study the transmittance through the glass samples “in-situ”, at the rooftop. This would exclude transportation of the glass samples and keep the samples at the correct tilt angle.

The decrease in efficiency at Kjeller (0.2-0.3 %) seems to be less severe than what other studies have reported at other locations, even when the total accumulated soil density is accounted for. This might be due to the higher tilt angle, soil compositions, weather patterns or other geographical variations. However, longer periods with little rain have not been investigated. Further research could involve direct power measurements at the PV-panel, as noted above. It should also involve longer periods of exposure.

Soiling seems to affect the shorter wavelength spectrum more than the longer wavelengths. Based on the diameter of the soil particles, observed in the soil analyses, this is likely caused by Mie scattering. A better understanding of the size distribution of the particles at Kjeller should therefore be interesting, and a particle size analysis is suggested. Other researchers have noticed the same wavelength-dependency for the transmittance, and states that this pattern increases with soil density. A better understanding of the accumulation of soil and reduced transmittance after periods with little rain are therefore recommended.

Experiments with artificial dust were conducted to investigate the relation between soil density and transmittance. However, the decreases in transmittance were lower than expected, based on the experiments with natural soiling. This is likely due to the large dust grains and the narrow diameter of the incident beam radiation, which makes the equipment vulnerable to surface variations. However, an experimental methodology is established. Improvements involve smaller dust grains, possibly from the natural soil, and a larger diameter of the incident beam radiation. Dust grains with approximately the same diameter as the natural dust are preferred.

7 References

[1] E. Viseth and V. Helljesen, “Forskerne er enige: Klima-endringene er menneskeskapte,” NRK, 16 05 2013. [Online]. Available: http://www.nrk.no/verden/klimaforskerne-er-samstemte-1.11028962. [Accessed 27 01 2015].

[2] The Shift Project, “Breakdown of Electricity Generation by Energy Sourc,” The Shift Project, 2013. [Online]. Available: http://www.tsp-data-portal.org/Breakdown-of-Electricity-Generation-by-Energy-Source#tspQvChart. [Accessed 04 02 2015].

[3] IEA - International Energy Agency, “TRENDS IN PHOTOVOLTAIC APPLICATIONS Survey report of selected IEA countries between 1992 and 2008,” SuterKeller Druck AG , 2009.

[4] International Energy Agency, IEA, “Trends 2014 in photovoltaic applications,” International Energy Agency, IEA, 2014.

[5] Green Rihno Energy, “Annual Solar Irradiance, Intermittency and Annual Variations,” Green Rihno Energy, 2013. [Online]. Available: http://www.greenrhinoenergy.com/solar/radiation/empiricalevidence.php. [Accessed 06 04 2015].

[6] Enova, “Nå gir disse ENØK-tiltakene deg rett til penger fra Enova,” Enova, 17 12 2014. [Online]. Available: http://www.mynewsdesk.com/no/enova-sf/pressreleases/naa-gir-disse-enoek-tiltakene-deg-rett-til-penger-fra-enova-1099912. [Accessed 27 01 2015].

[7] J. A. Duffie and W. A. Beckman, Solar Engineering of Thermal Processes, 2nd ed., Canada: John Wiley and Sons, Inc., 1991.

[8] J. J. Chen, Physics of Solar Energy, Hoboken, New Jersey: John Wiley and Sons, Inc., 2011.

[9] IEA, International Energy Agency, “Technology Roadmap, Solar Photovoltaic Energy,” IEA, International Energy Agency, Paris, 2014.

[10] W. Surles, A. Watrous, E. Horanyi and M. S. Zarske , “Lesson: Solar Angles and Tracking Systems,” University of Colorado, 2009. [Online]. Available: https://www.teachengineering.org/view_lesson.php?url=collection/cub_/lessons/cub_pveff/cub_pveff_lesson01.xml. [Accessed 30 04 2015].

[11] R. Watkins and J. Vallandingham, “Rayleigh Scattering,” Rowan University, 2008. [Online]. Available: http://home.comcast.net/~vinelandrobotics/. [Accessed 30 04 2015].

[12] Physics, “Why does NASA use gold foil on equipment and gold-coated visors?,” 11 02 2013. [Online]. Available: http://physics.stackexchange.com/questions/74412/why-does-nasa-use-gold-foil-on-equipment-and-gold-coated-visors. [Accessed 06 04 2015].

[13] R. Simmon, “Incoming Sunlight,” Earth Observatory, [Online]. Available: http://earthobservatory.nasa.gov/Features/EnergyBalance/page2.php. [Accessed 30 04 2015].

[14] M. Rouse , “polarization (wave polarization),” whatis, 03 2011. [Online]. Available: http://whatis.techtarget.com/definition/polarization-wave-polarization. [Accessed 30 04 2015].

[15] IEA, International Energy Agency, “TRENDS 2013 IN PHOTOVOLTAIC APPLICATIONS,” IEA-PVPS, 2013.

[16] MN Green Pages, “Solar Power, What Is Solar Power?,” MN Green Pages, 15 04 2014. [Online]. Available: http://www.mngreenpages.com/renewable-energy/solar-power/. [Accessed 30 04 2015].

[17] PV Education, “Quantum Efficiency,” PV Education, [Online]. Available: http://www.pveducation.org/pvcdrom/solar-cell-operation/quantum-efficiency. [Accessed 22 04 2015].

[18] B. Ramm, “Solceller,” Fornybar, [Online]. Available: http://www.fornybar.no/solenergi/elektrisk-energi-fra-solen/solceller. [Accessed 05 05 2015].

[19] C. Honsberg and S. Bowden , “Anti-Reflection Coating,” PV Education, [Online]. Available: http://www.pveducation.org/pvcdrom/design/anti-reflection-coatings. [Accessed 30 04 2015].

[20] H. Qasem, “Effect of accumulated dust on the performance of photovoltaic modules,” Loughborough University, Institutional Repository, Loughborough, 2013.

[21] H. P. Inc., Home Power, 2015. [Online]. Available: www.homepower.com. [Accessed 15 04 2015].

[22] A. Pettersen, “imulation and Sexperimental study of power losses due to shading and soiling on photovoltaic (PV) module,” in *Master thesis*, Ås, Norwegian University of Life Sciences, Department of Mathematical Sciences and Technology., 2015, p. 32.

[23] S. E.-S. Mohammad and M. H. Farmy, “Effect of dust with different physical properties on

the performance of photovoltaic cells," *Solar Energy*, pp. 505-511, 12 1993.

[24] R. Appels, B. Lefevre, B. Herteleer, H. Goverde, A. Beerten, R. Paesen, K. De Medts, J. Driesen and J. Poortmans, "Effect of soiling on photovoltaic modules," *Solar Energy*, pp. 283-291, 02 07 2013.

[25] D. Goossens, "Earth Surface Processes and Landforms," p. 11, 28 09 2001.

[26] J. R. Caron and B. Littmann, "Direct Monitoring of Energy Lost Due to Soiling on First Solar Modules in California," IEEE, San Francisco, 2012.

[27] J. Zorrilla-Casanova, M. Philiougine, J. Carretero, P. Bernaola-Galván, P. Carpena, L. Mora-López and M. Sidrach de Cardona, "Losses produced by soiling in the incoming radiation to photovoltaic modules," *PHOTOVOLTAICS*, pp. 790-796, 01 02 2012.

[28] A. Kimber, L. Mitchell, S. Nogradi and H. Wenger, "The Effect og Soiling on Large Grid-Conected Photovoltaic Systems in California and the Southwest Region of The United States," IEEE, Okland, 2006.

[29] R. Hammond, D. Srinivasan, A. Harris, K. Whitfield and J. Wohlgemuth, "Effects of Soiling on PV Module and Radiometer performance," IEEE, Anaheim, 1997.

[30] M. Mani and R. Pillai, "Impact of dust on solar photovoltaic (PV) performance: Research status, challenges and recommendations," *Renewable and Sustainable Energy Reviews, Volume 14, Issue 9*, p. 3124–3131, 4 8 2010.

[31] D. K. Perovich, "Light Transmission Through Snow," American Geophysical Union, San Francisco, 2002.

[32] T. Lorenz, E. Klimm and K.-A. Weiss, "Soiling and anti-soiling coatings on surfaces of solar thermal systems – featuring an economic feasibility analysis," *Energy Procedia*, p. 749 – 756, 2014.

[33] H. K. Elminir, A. E. Ghitas, R. H. Hamid, F. El-Hussainy, M. M. Beheary and K. M. Abdel-Moneim, "Effect of dust on the transparent cover of solar collectors," p. 11, 15 02 2006.

[34] H. Ahmed, S. Al-Jandal and A. Sayigh, "Dust effect on solar flat surfaces devices in Kuwait," in *Proceedings of the workshop on the physics*, Triest, ICTP, 1985, p. 353–367.

[35] J. Gjessing, "Measurement setup for angular dependent reflection and transmission," Institute for Energy Technology, Kjeller, 2011.

[36] S. L. Jacques and S. A. Prahl, “Collection by aperture of integrating sphere,” Oregon Medical Laser Center, 1998. [Online]. Available: http://omlc.org/education/ece532/class1/collect_intsphere.html. [Accessed 30 04 2015].

[37] S. Swapp, “Scanning Electron Microscopy (SEM),” [Online]. Available: http://serc.carleton.edu/research_education/geochemsheets/techniques/SEM.html. [Accessed 29 01 2015].

[38] J. Schweitzer, “Scanning Electron Microscope,” Purdue University, [Online]. Available: http://www.purdue.edu/ehps/rem/rs/sem.htm. [Accessed 29 01 2015].

[39] T. Furuseth, Interviewee, [Interview]. 05 05 2015.

[40] The University of Sheffield, “Energy Dispersive X-ray Spectrometry and X-ray Microanalysis,” [Online]. Available: http://www.web.pdx.edu/~jiaoj/phy451/Lect6.pdf. [Accessed 05 05 2015].

[41] National Renewable Energy Laboratory (NREL), “Reference Solar Spectral Irradiance: ASTM G-173,” National Renewable Energy Laboratory (NREL), [Online]. Available: http://rredc.nrel.gov/solar/spectra/am1.5/ASTMG173/ASTMG173.html. [Accessed 23 03 2015].

[42] Glass Dynamics, L.L.C., “BK-7 OPTICAL GLASS,” 2015. [Online]. Available: http://www.glassdynamicsllc.com/BK7%20Material%20Data%20Sheet.htm. [Accessed 08 04 2015].

[43] eKlima, “Døgn verdier for temperatur og nedbør ved Skjedsom, Akershus,” Meteorologisk institutt, Oslo.

[44] eKlima, “Månedsnormaler,” Meteorologisk institutt, Oslo, 2015.

[45] M. Polyanskiy, “refractiveindex.info,” 2008. [Online]. Available: http://refractiveindex.info/?shelf=glass&book=BK7&page=SCHOTT. [Accessed 12 03 2015].

[46] M. Andersen, Analysis of actual and forecasted poer production for a solar energy system in Norway, Ås: NMBU, 2014.

[47] Norsk Solenergiforening, “Solceller,” Norsk Solenergiforening, [Online]. Available: http://www.solenergi.no/om-solenergi/teknologi/solceller/. [Accessed 16 01 2015].

[48] I. L. Delphin, “Elektromagnetiske bølger,” Store Norske Leksikon, 06 11 2013. [Online]. Available: https://snl.no/elektromagnetiske_b%C3%B8lger. [Accessed 16 01 2015].

[49] A. I. Vistnes, “Refleksjon og transmisjon av elektromagnetiske bølger, polarisasjon, dobbeltbrytning,” 2014. [Online]. Available: http://folk.uio.no/arntvi/kpt9ea.pdf. [Accessed 20 01 2015].

[50] J. Zorrilla-Casanova, M. Piliougine, J. Carretero, P. Bernaola-Galvàn, P. Carpena, L. Mora-Lòpez and M. Sidrach-de-Cardona, “Losses produced by soiling in the incoming radiation to photovoltaic modules,” *Progress in Photovoltaic,* p. 7, 01 02 2012.

[51] R. Appels, B. Lefever, B. Herteleer, H. Goverde, A. Beerten, R. Paesen, K. De Medts, J. Driesen and J. Poortmans, “Effect of soiling on photovoltaic modules,” *Solar Energy,* p. 9, 02 07 2013.

[52] Norwegian Meteorological Institute, “eKlima,” [Online]. Available: http://sharki.oslo.dnmi.no/pls/portal/BATCH_ORDER.PORTLET_UTIL.Download_BLob?p_BatchId=674390&p_IntervalId=1371257. [Accessed 26 01 2015].

[53] nrk Verden, “EU enig om klimamål,” nrk, 24 10 2014. [Online]. Available: http://www.nrk.no/verden/eu-enig-om-klimamal-1.12003975. [Accessed 27 01 2015].

[54] S. L. Steven L. Jacques and S. A. Prahl, “Collection by aperture of integrating sphere,” Educational Credential Evaluators, 1998. [Online]. Available: http://omlc.org/education/ece532/class1/collect_intsphere.html. [Accessed 02 02 2015].

[55] D. K. Perovich, “Light reflection and transmission by a temperated snow cover,” *Journal of Galciology, Vol. 53, No. 181,* pp. 201-210, 19 01 2007.

[56] B. Marion, R. Schaefer, H. Caine and G. Sanchez, “Measured and modeled photovoltaic system energy losses from snow for Colorado and Wisconsin locations,” *Solar Energy,* pp. 112-121, 23 07 2013.

[57] Smart Green holding, “Analysis of the influence of dirt on PV modules,” [Online]. Available: http://www.smartgreenholding.com/imagenes/documentacion/ficheros/03B9F91F.pdf. [Accessed 02 05 2015].

[58] “BK-7 OPTICAL GLASS,” Glass Dynamics, L.L.C., 2015. [Online]. Available: http://www.glassdynamicsllc.com/BK7%20Material%20Data%20Sheet.htm. [Accessed 30 04 2015].

8 Appendix

Appendix A: Data for BK7-glass

Appendix B: Sum of transmittance and reflectance

Appendix C: Polarized incoming radiation

Appendix D: Weekly observations and mass measurements on the glass samples

Appendix E: Weekly transmittance measurements

Appendix F: Results from soil analyses

Appendix A: Data for BK7-glass

BK-7 glass is designed to have next to no absorptance. Relevant data for the refractive index (n) and the absorption coefficient (K) are given in table 15, while the theoretical calculated transmittance at different angles of incidence and wavelengths are given in table 16 below.

Wavelength [nm]	***n***	***K* [m^{-1}]**
400	1.531	0.3213
500	1.521	0.2407
600	1.516	0.2213
700	1.513	0.1603
800	1.511	0.1455
900	1.509	0.1341
1000	1.508	0.1249
1100	1.506	0.2016

Table 15: Refractive index (n) and absorption coefficient (K) for BK7-glass at various wavelengths **[45]**.

Angle of incidence [°]	**τ, 400 nm [%]**	**τ, 500 nm [%]**	**τ, 600 nm [%]**	**τ, 900 nm [%]**	**τ, 1100 nm [%]**
0	91.5	91.8	92.0	92.1	92.1
3	91.5	91.8	92.0	92.1	92.1
5	91.5	91.8	92.0	92.1	92.1
7	91.5	91.8	92.0	92.1	92.1
10	91.5	91.8	92.0	92.1	92.1
15	91.5	91.8	91.9	92.0	92.1
20	91.5	91.8	91.9	92.0	92.1
25	91.4	91.7	91.8	92.0	92.0
30	91.3	91.6	91.7	91.8	91.9
40	90.6	90.9	91.1	91.2	91.2
50	88.8	89.1	89.2	89.3	89.4
60	84.0	84.3	84.5	84.6	84.6
70	72.2	72.4	72.6	72.7	72.7
80	45.5	45.6	45.7	45.7	45.8

Table 16: Theoretical calculated transmittance (τ) at different angels of incidence, as a function of wavelength, for BK7-glass.

Appendix B: Sum of transmittance and reflectance

Graph 28 and 29 below show mean initial values for the measured sum of reflectance and transmittance for clean normal and anti-soiling coated glass samples. This is conducted employing the center-mount configuration of the integrating sphere, in the ADRTM equipment.

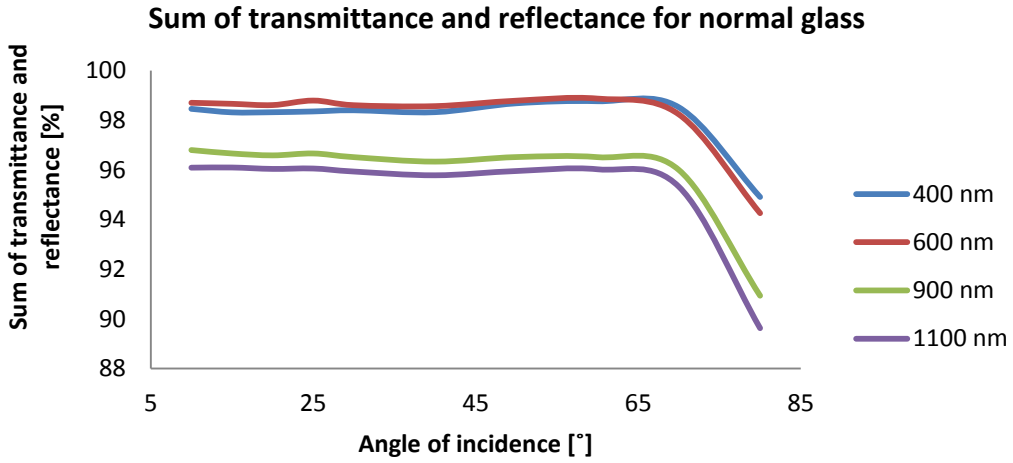

Graph 28: The sum of transmittance and global reflectance at different angles of incidence for normal glass. This is the mean values from three measurements conducted on clean glass samples.

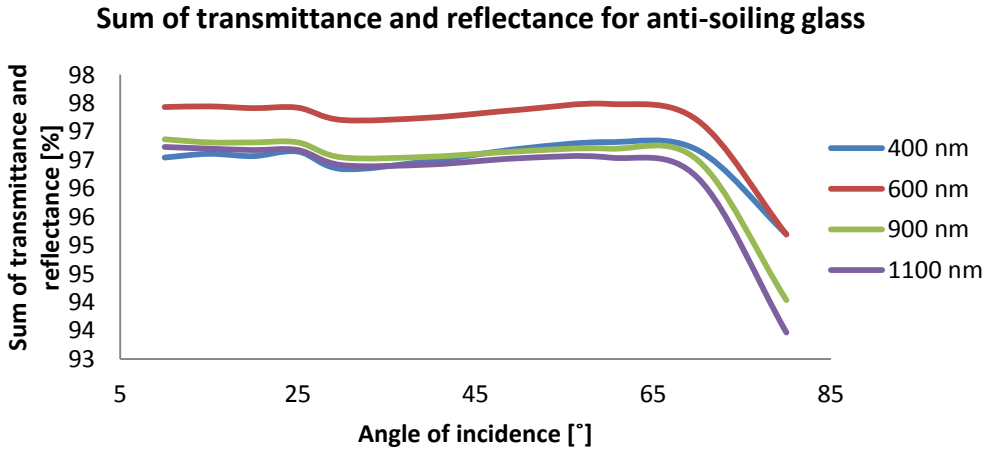

Graph 29: The sum of transmittance and global reflectance at different angles of incidence for anti-soiling glass. This is the mean values from three measurements conducted on clean glass samples.

Appendix C: Polarized incoming radiation

Polarization of incoming radiation is investigated for the normal glass samples at different angles of incidence. This is conducted employing The Angular Dependent Reflection and Transmission Measurement (ADRTM) and by selecting different polarization filters. The mean values from transmittance measurements with s- and p-polarized light are compared with results for unpolarized light. This is presented in graph 30 below.

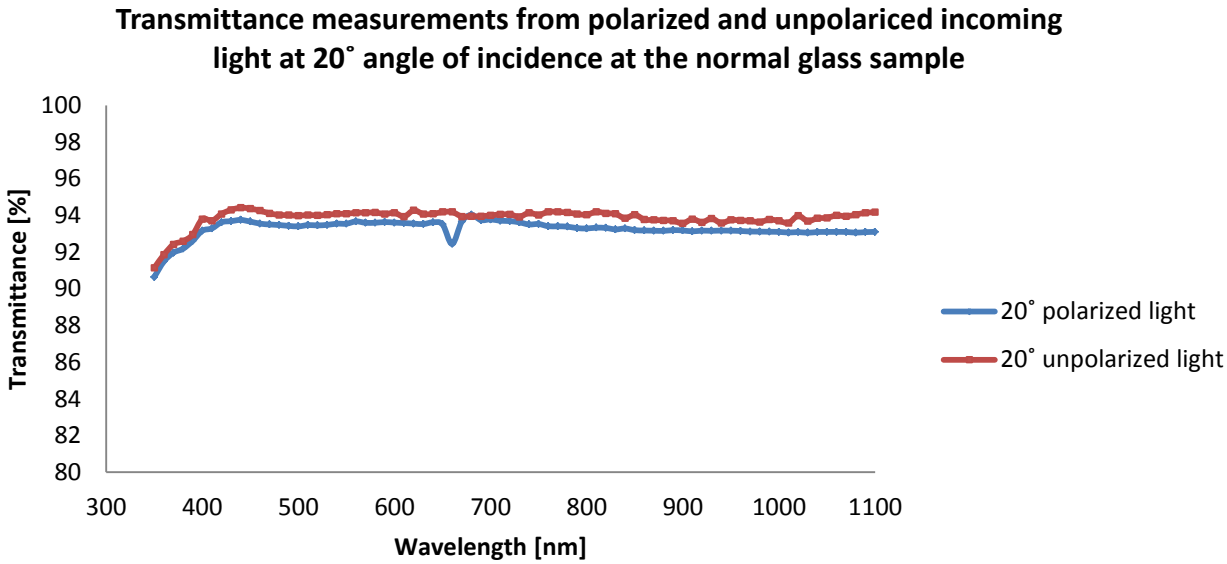

Graph 30: Correspondence between the transmittance of unpolarized and polarized light for the normal glass samples. Measurements are conducted at 20˚ angle of incidence. The polarized light has a dup at about 660 nm, due to a dup in the transmittance measurements in one of the polarization directions.

As can be seen in graph 30, there is a differences in transmission measurements with unpolarized light. By weighting the measured transmittance against the AM1.5G spectrum for Global Tilt, the difference between the polarized and unpolarized light at 20˚ angle of incidence is about 0.58 %. This difference is likely strengthened by the dup in the transmittance measurements for the polarized light at about 660 nm.

Appendix D: Weekly observations and mass measurements of the glass samples

Weekly observations of the glass samples are given in D.1, together with more pictures of the glass samples. Weekly mass measurements are given in D.2.

D.1 Weekly precipitation and observations on the glass samples

The mean daily precipitation for one week (Tuesday-Monday) is calculated based on daily precipitation data from eKlima [43], and presented in graph 31. Table 17 describes observations noted in the research log during the experimental period. Figure 39 and 40 are pictures of a normal and an anti-soiling coated glass sample exposed to rain, to underline the difference between the shapes of the droplets.

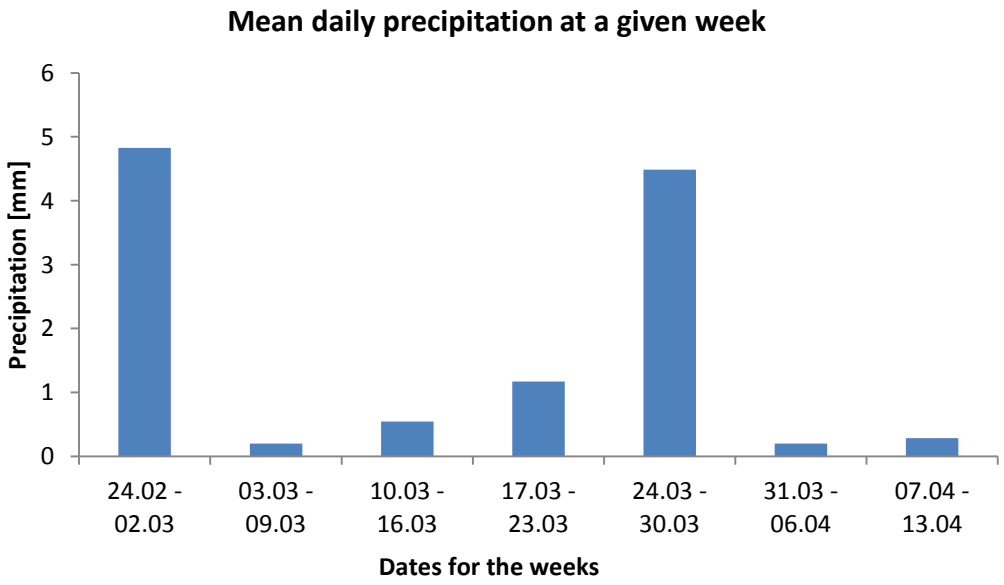

Graph 31: Mean daily precipitation data, based on downloaded data from eKlima **[43]**. One week is defined from Tuesday to Monday.

Date \ Glass sample	Normal glass	Anti-soiling glass
03.03	Dew	Much dew, very round shaped droplets
10.03	Almost dry samples Much wind	Almost dry samples Much wind
17.03	Much dew	Much dew, very round shaped droplets
18.03	Dew	Dew
24.03	Dry samples	Dry samples
31.03	Frost	Frost
07.04	Dry samples	Dry samples
14.04	Dry samples	Dry samples
15.04	Almost dry	Almost dry

Table 17: Observations made on the days the glass samples are taken down from the rooftop and investigated in laboratories. This is a section of the research log.

There is a clear difference between the shape of the droplets on the normal and the anti-soiling coated glass samples.

Figure 39: A normal glass sample.
The droplets are not as clear as in the picture to the right (of the anti-soiling coated glass).

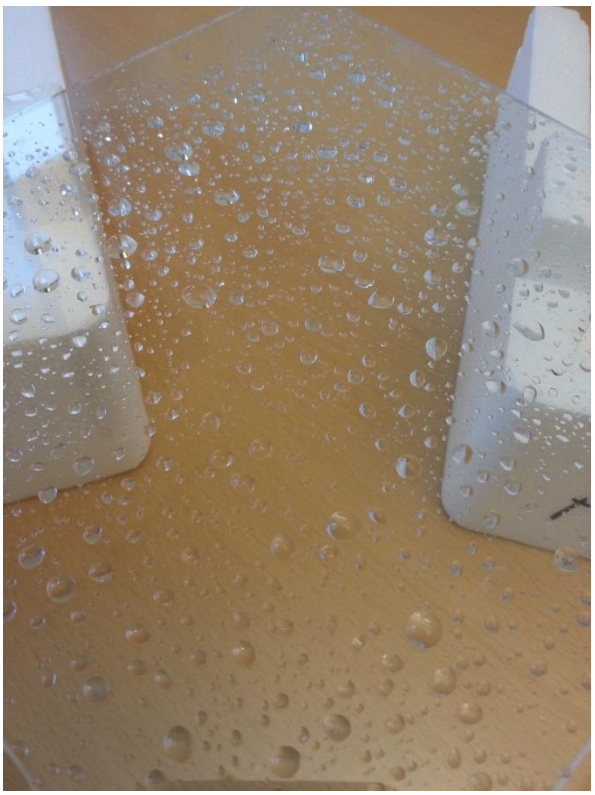

Figure 40: An anti-soiling glass sample.
The round shaped droplets are clear.

D.2 Mass measurements

The large glass samples were weighted before they were placed at the rooftop of IFE. The mass of the clean large glass samples are presented in table 18 below. N refers to the normal glass samples, while AS refers to the anti-soiling coated glass samples. The numbers 1 and 2 refer to the two different glass samples.

Glass sample	**Mass [mg]**
N1	150250.2
N2	149635.8
AS1	149918.6
AS2	148832.5

Table 18: Mass measurements on the large glass samples before they were placed at the rooftop of IFE. N and AS refer to the normal glass and anti-soiling coated glass samples, respectively. The numbers 1 and 2 refer to the two different glass samples.

The changes in mass due to optical measurements and cleaning are given in table 19, 20 and 21. Recall that the values for the large glass samples from March 3 and 10 are not used to calculate mean values. There are no available data for the change in mass due to optical measurements on March 24. Mean values are used to calculate the mass change at this date in subchapter 5.4.

Glass sample:	**03.mar**	**10.mar**	**17.mar**	**24.mar**	**31.mar**	**07.apr**	**14.apr**
$\Delta M_{OM,N1}$ [mg]	0.4	-0.9	-1.1	-	-0.2	-1.3	-0.1
$\Delta M_{OM,\ N2}$ [mg]	-0.8	0.6	-0.7	-	-0.2	-1.0	-0.1
$\Delta M_{OM,AS1}$ [mg]	-0.6	-0.3	-0.3	-	-0.5	-1.7	-0.3
$\Delta M_{OM,AS2}$ [mg]	-0.1	0.2	-0.9	-	-0.1	-1.0	-1.9

Table 19: Change in mass (ΔM_{OM}) of large glass samples due to optical measurements. The symbol N and AS refer to the normal glass and anti-soiling coated glass samples, respectively. The numbers 1 and 2 refer to the two different glass samples.

Glass sample:	**03.mar**	**10.mar**	**17.mar**	**24.mar**	**31.mar**	**07.apr**	**14.apr**
$\Delta M_{C,N1}$ [mg]	0.2	0.2	-1.3	-0.9	-0.4	-2.3	-2.4
$\Delta M_{C,N2}$ [mg]	-1.5	0.0	-1.2	-1.3	-0.5	-1.7	-1.9
$\Delta M_{C,AS1}$ [mg]	-1.1	0.3	-3.0	-2.4	-0.7	-3.0	-2.4
$\Delta M_{C,AS2}$ [mg]	-1.1	-0.8	-2.8	-0.5	-1.1	-2.1	-2.4

Table 20: Change in mass (ΔM_C) of large glass samples due to cleaning. The symbol N and AS refer to the normal glass and anti-soiling coated glass samples, respectively. The numbers 1 and 2 refer to the two different glass samples.

Rag:		**03.mar**	**10.mar**	**17.mar**	**24.mar**	**31.mar**	**07.apr**	**14.apr**
$\Delta M_{C,K1}$	[mg]	1.1	0.5	2.2	1.4	1.0	3.0	3.3
$\Delta M_{C,K2}$	[mg]	0.1	0.2	2.2	1.1	0.7	1.4	2.2
$\Delta M_{C,K3}$	[mg]	1.1	0.8	3.7	2.9	1.1	3.6	2.4
$\Delta M_{C,K4}$	[mg]	1.0	0.9	2.3	1.1	0.5	1.7	1.5

Table 21: Change in mass (ΔM) of the different rags used to clean the large glass samples. K1, K2, K3 and K4 are the four different rags, used to clean the four different large glass samples.

As noticed in the tables above, there are not always correlation between the increase in mass of the rags and the decrease in the weight of the large glass samples due to cleaning.

A picture of rags used to clean glass samples are given in figure 41. Figure 24 shows a glass sample used to measure the change in transmittance employing the integrating sphere. The soil on the glass samples can be seen in the picture.

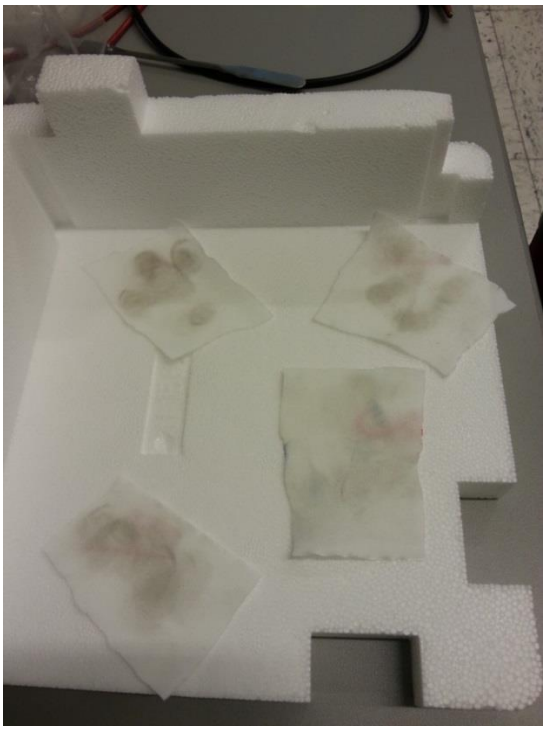

Figure 41: Rags used to clean glass samples.

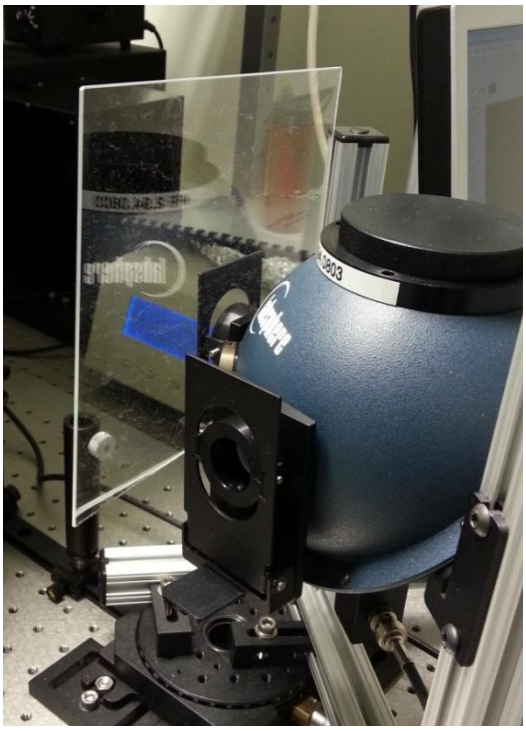

Figure 42: A large glass sample used to measure transmittance with the ADRTM.

Appendix E: Optical measurements

E.1 Weekly transmittance measurements

The weekly transmittance is plotted in graph 32 and 33 below. The calculations are based on the methodology given in subchapter 4.3.4.

The transmittance seems to decrease with increasing wavelength. This is because the same pattern is seen in the initial transmittance measurement on the clean glass samples (recall the methodology). The pattern for the initial optical measurements is discussed in subchapter 5.2.

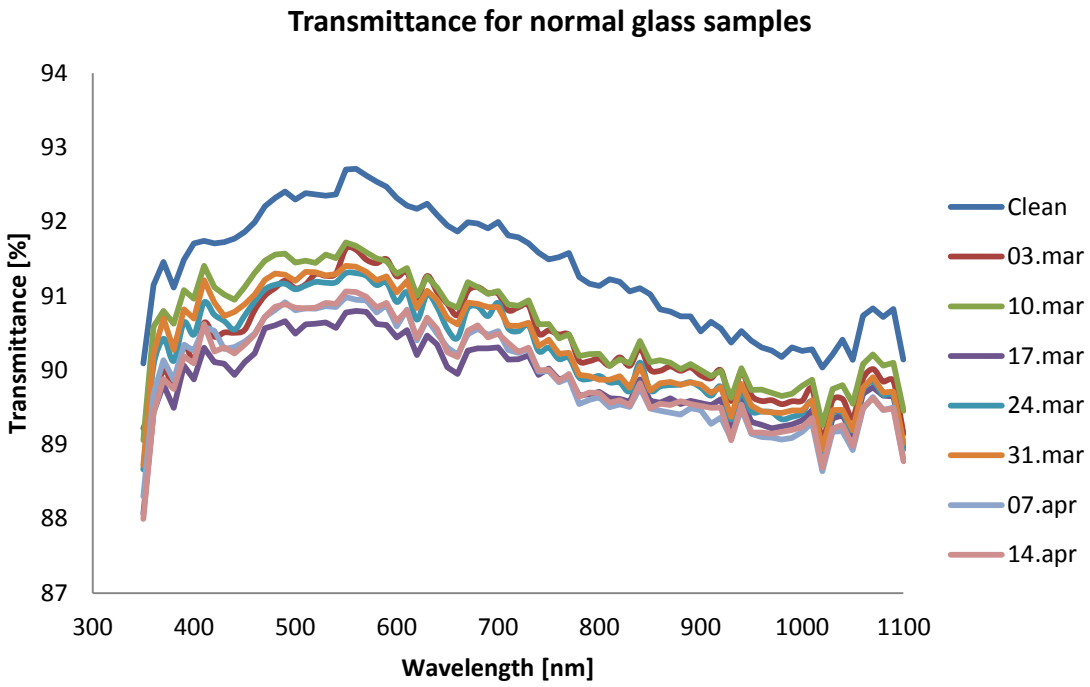

Graph 32: Measured transmittance for normal glass samples exposed to one week of soiling at Kjeller, represented by different dates. The measurement "clean" refers to the initial measurement on clean glass samples. All measurements are conducted at 20° angle of incidence.

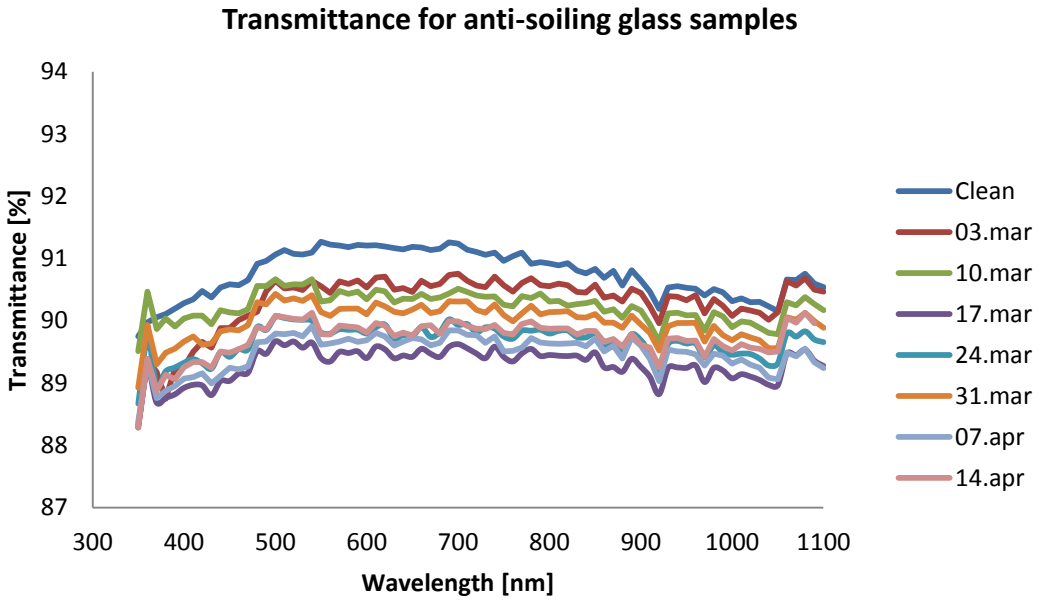

Graph 33: Measured transmittance for anti-soiling coated glass samples exposed to one week of soiling at Kjeller, represented by different dates. The measurement "clean" refers to the initial measurement on clean glass samples. All measurements are conducted at 20° angle of incidence.

As noticed, there is a higher sum of transmittance and reflectance at wavelengths from about 500-700 nm. This is discussed in subchapter 5.2. Recall that the change in transmittance is the main focus in this study, employing the Angular Dependent Reflection and Transmission Measurement (ADRTM).

Appendix F: Soil analyses

F.1 EDS picture from point 2 in the point analysis

Results from point 2 in the point analysis in subchapter 5.4 are shown in figure 43 below. The figure shows how bromine (Br) is detected. Note that the different peaks do not correspond to the amount of an element, but is a result of the amount and the likeliness that the element is correct.

Bromine is a rear element. It is therefore reason to believe that the detected element is silicon or magnesium.

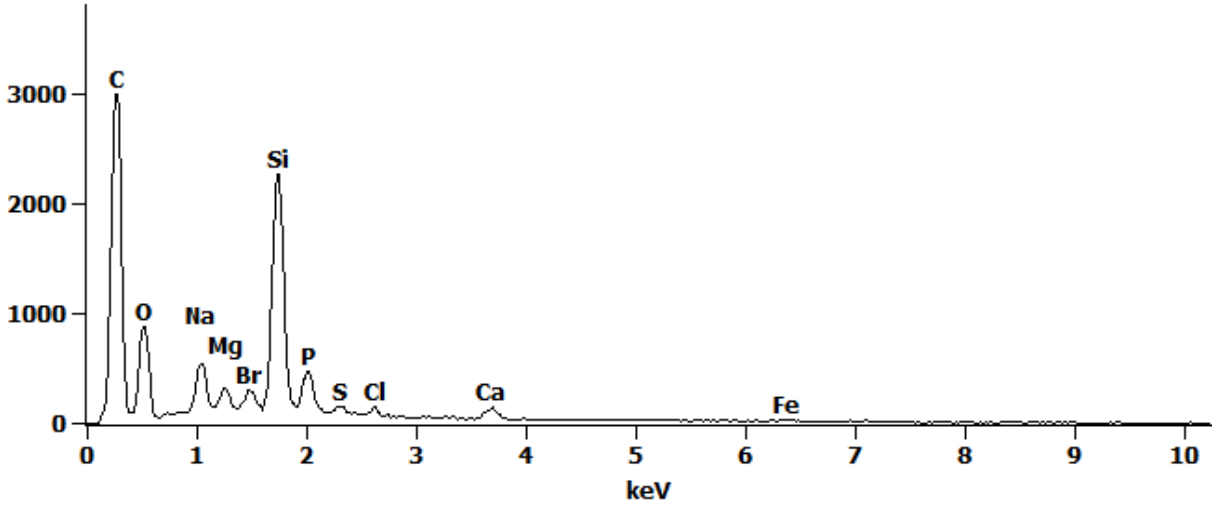

Figure 43: Results from point 2 in the point analysis from subchapter 5.4. It shows that bromine (Br) is detected. The y-axis corresponds to the number of times an element is detected and the likeliness that the element is correct. The elements are: carbon (C), oxygen (O), sodium (Na), magnesium (Mg), bromine (Br), silicon (Si), phosphorus (P), sulfur (S), chlorine (Cl), calcium (Ca) and iron (Fe).

F.2 Point analysis at a surface area

Figure 44 shows the area for a point analysis connducted at a different surface area than the table given in subchapter 5.4, and table 22 presents the results. The tabe shows the mass of an element as a percentage of the total mass at that point. No results are excluded from the table, but results at 10 % and more are highlighted with a green background.

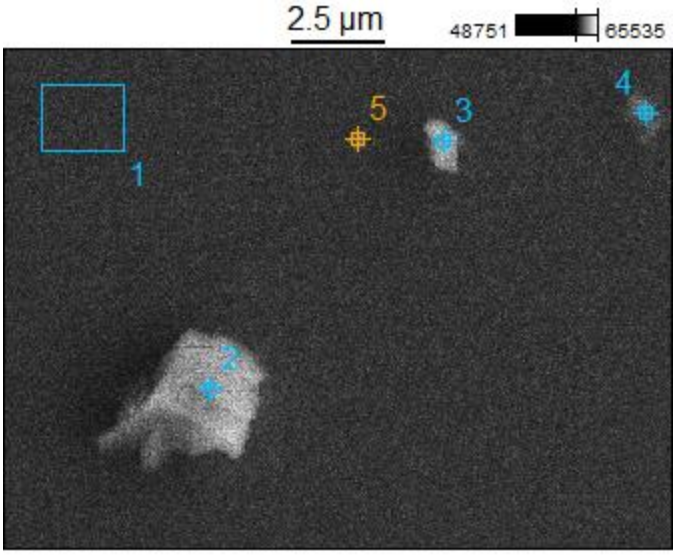

Figure 44: A point analysis at a surface area of a normal glass sample. Point 1 is directed at the glass surface, while the other points are directed at different dust grains. The picture is taken with the SEM.

	C	O	Na	Mg	Al	Si	K	Ca	Fe	Br
Point 1	7.1 ± 0.6	44.9 ± 0.7	9.6 ± 0.2	1.7 ± 0.1		31.9 ± 0.2		5.0 ± 0.2		
Point 2	9.6 ± 0.5	48.9 ± 0.8	3.70 ± 0.1	1.0 ± 0.1	5.7 ± 0.1	24.6 ± 0.2	2.7 ± 0.1	1.6 ± 0.1	2.2 ± 0.2	
Point 3	9.6 ± 0.5	48.0 ± 0.6	7.7 ± 0.2	0.8 ± 0.1		25.1 ± 0.2		2.3 ± 0.1		6.5 ± 0.2
Point 4	12.3 ± 0.6	44.5 ± 0.9	6.8 ± 0.2	2.2 ± 0.1		26.7 ± 0.2	0.2 ± 0.1	3.7 ± 0.2	0.7 ± 0.1	3.1 ± 0.2
Point 5	22.7 ± 0.6	41.4 ± 0.9	5.8 ± 0.2	1.4 ± 0.1	0.2 ± 0.1	23.8 ± 0.2		3.9 ± 0.2	0.9 ± 0.1	

Table 22: Results from the point analysis shown in figure 44 above. The elements are: carbon (C), oxygen (O), sodium (Na), magnesium (Mg), aluminum (Al), silicon (Si), potassium (K), calcium (Ca), iron (Fe) and bromine (Br). The uncertainty is given by the software.

F.3 Point analysis conducted at one dust grain

Figure 45 and table 23 show one dust grain and the results from the point analysis. Then tabe showe the mass of an element as en percentage of the total mass at that point. Results less than 1 % are excluded from the table. This particle shows much carbone and oxygen, and little silicon. Note that this is only one particle, and the results can not be used as a representation for the entire surface.

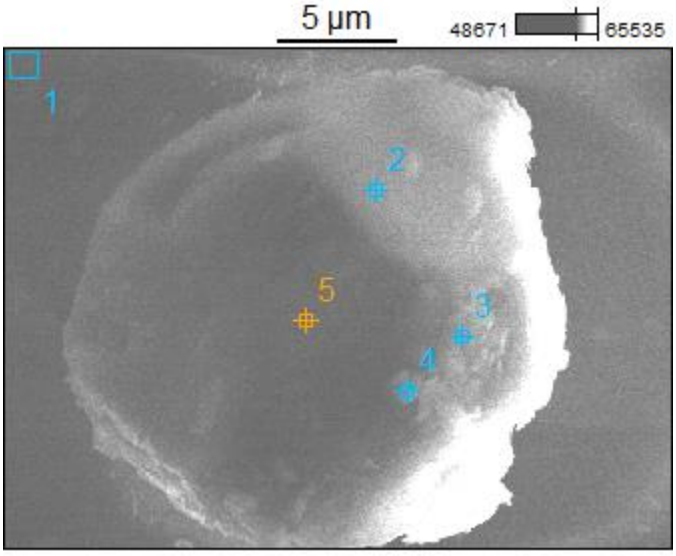

Figure 45: A dust grain at a normal glass sample. Point 1 is directed at the glass surface, while the other points are directed at different parts of the dust grain. The picture is taken with the SEM.

	C	O	Na	Mg	Al	Si	P	Ca	Fe	Mo
Point 1	9.9 ± 0.6	46.2 ± 0.7	8.9 ± 0.2	1.8 ± 0.1	0.3 ± 0.1	28.8 ± 0.2		4.1 ± 4.1		
Point 2	64.2 ± 0.4	30.3 ± 0.7	1.2 ± 0.1	0.2 ± 0.0	0.2 ± 0.0	3.0 ± 0.1	0.4 ± 0.0	0.5 ± 0.5		
Point 3	67.2 ± 0.7	21.4 ± 1.0	0.9 ± 0.1	0.4 ± 0.0	1.1 ± 0.0	3.4 ± 0.1	1.9 ± 0.1	0.7 ± 0.7	1.6 ± 0.3	
Point 4	65.2 ± 1.1	23.6 ± 1.1	1.0 ± 0.1	0.3 ± 0.0	0.7 ± 0.1	2.9 ± 0.1	2.7 ± 0.1	0.6 ± 0.1		2.9 ± 0.2
Point 5	69.6 ± 0.4	26.3 ± 0.8	0.4 ± 0.0	0.1 ± 0.0	0.3 ± 0.0	0.8 ± 0.0	1.6 ± 0.1	0.3 ± 0.0		

Table 23: Results from the point analysis on one dust grain, shown in figure 45. The elements are: carbon (C), oxygen (O), sodium (Na), magnesium (Mg), aluminum (Al), silicon (Si), phosphorus (P), calcium (Ca), iron (Fe) and bromine (Br). The uncertainty is given by the software.

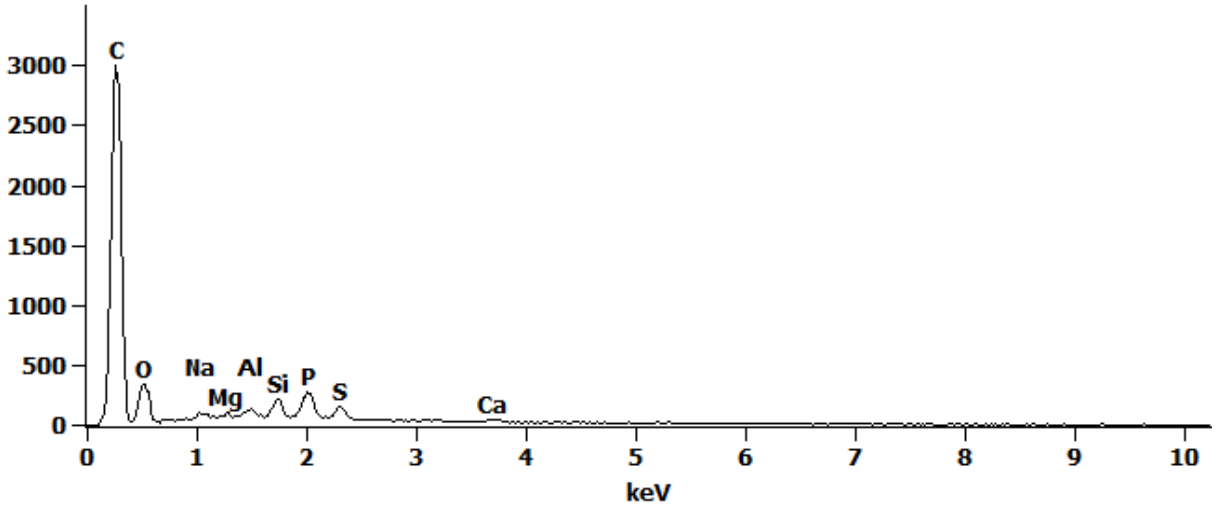

Figure 46: The results from point 5 in the point analysis shown in figure 45 and table 23above. The y-axis corresponds to the number of times an element is detected and the likeliness that the element is correct. The elements are: carbon (C), oxygen (O), sodium (Na), magnesium (Mg), aluminum (Al), silicon (Si), phosphorus (P), calcium (Ca), iron (Fe) and bromine (Br). The uncertainty is given by the software.

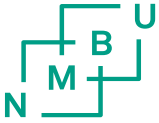

Norwegian University
of Life Sciences

Postboks 5003
NO-1432 Ås, Norway
+47 67 23 00 00
www.nmbu.no